The role of SDHA in the tissue-specific regulation of metabolism and proteomic approaches to identify novel ClpXP substrates

Inaugural-Dissertation

zur

Erlangung des Doktorgrades

der Mathematisch-Naturwissenschaftlichen Fakultät

der Universität zu Köln

vorgelegt von

Eduard Hofsetz

aus Iwanowka, Kirgisistan

Köln 2020

Berichterstatter: **Prof. Dr. Aleksandra Trifunovic**
Prof. Dr. Thomas Langer

Tag der mündlichen Prüfung: 29. November 2019

To my family and friends

Table of Contents

List of Figures

List of Tables

Abbreviations

°C	Degree Celcius
x g	Times g-force (9.81m/s^2)
A	Ampere
APS	Ammoniumperoxodisulfate
AMP	Adenosine monophosphate
AmR	Amplex Red
ADP	Adenosine diphosphate
ATP	Adenosine triphosphate
BSA	Bovine serum albumin
CAA	Chloroacetamide
Cas9	CRISPR associated protein 9
cDNA	complementary DNA
$CHCl_3$	Chloroform
CHX	Cycloheximide
CO_2	Carbon dioxide
Cre	Bacteriophage P1 derived site-specific recombinase
crRNA	CRISPR RNA
(d)dH_2O	(Double) distilled Water
DNA	Deoxyribonucleic acid
dNTP	Desoxy-ribonucleoside triphosphate
DTT	Dithiothreitol
EDTA	Ethylenediaminetetraacetic acid
EtOH	Ethanol
FA	Formic acid/Fatty acid
FAO	Fatty acid oxidation
FCCP	Carbonyl cyanide-4-(trifluoromethoxy)phenylhydrazone
fl	loxP flanked
g	Gramm
H_2O_2	Water
H&E	Hematoxylin and eosin
HCl	Hydrogen chloride

HEPES	4-(2-hydroxyethyl)-1-piperazineethanesulfonic acid
HRP	Horseradish peroxidase
IAA	Iodoacetamide
KCl	Potassium chloride
KCN	Potassium cyanide
kDa	Kilo Dalton
KO	knockout
l	Litre
m	Milli
M	Molar
MeOH	Methanol
$MgCl_2$	Magnesium chloride
(m)RNA	(Messenger) ribonucleic acid
mtDNA	Mitochondrial DNA
n	Nano
NaCl	Sodium chloride
NAD^+	Nicotinamide adenine dinucleotide (oxidised)
NADH	Nicotinamide adenine dinucleotide (reduced)
nDNA	Nuclear DNA
NADP+	Nicotinamide adenine dinucleotide phosphate (oxidised)
NADPH	Nicotinamide adenine dinucleotide phosphate (reduced)
NaF	Sodium fluoride
NaN_3	Sodium azide
NaOH	Sodium hydroxide
O_2	Molecular oxygen
OXPHOS	Oxidative phosphorylation
PAGE	Polyacrylamide gel electrophoresis
PAS	Periodic acid Schiff
PCR	Polymerase chain reaction
PBS (T)	Phosphate buffered saline (with Tween)
ROS	Reactive oxygen species
rpm	Revolutions per minute
RT	Room temperature

SD	Standard deviation
SDS	Sodium dodecyl sulfate
SOD	Superoxide dismutase
TBE	Tris borate EDTA
TEAB	Triethylammonium bicarbonate
TEM	Transmission electron microscopy
TEMED	Tetramethylethylenediamine
TES	[Tris(hydroxymethyl)methyl]-2-aminoethanesulfonic acid
tracrRNA	Trans-activating crRNA
Tris	Trisaminomethane
Tween	Polyethylene glycol sorbitan monolaurate
U	Units
UPR	Unfolded protein response
WT	Wild type
µ	Micro

Abstract

After Theodor Schwann formulated the first cell theory in 1839, another 60 years of histological advances passed by before mitochondria were discovered and the name was phrased. Yet, 120 years later, many aspects of mitochondrial biology remain enigmatic and mitochondria emerged as fundamental organelles of almost all eukaryotes far beyond the role as the powerhouses of the cell.

To contribute to the continuously growing understanding of these multifaceted organelles, the roles of succinate dehydrogenase subunit A (SDHA) and ATP-dependent Clp protease (ClpXP) in mitochondrial metabolism and proteostasis, respectively, were investigated *in vivo* and *in vitro*.

Conditional knockout of SDHA in the heart and striated muscles caused isolated complex II deficiency and ultimately organ failure. However, metabolic differences of these tissues result in varying adaptations and stress responses. This finding emphasizes the significance of the metabolic background, even if the primary defect is ATP depletion. This is particularly important for the treatment of malignant cells with SDH mutations, as the affected cell types can differ in terms of metabolic adaptations.

In order to understand the role of ClpXP in mitochondrial proteostasis, diverse proteomic approaches were employed to identify novel ClpXP targets as well as to address the mode of degradation and potentially tissue-specific activity. The combination of a classical *in vitro* substrate screen and the recently developed N-terminome quantification identified or confirmed several bona fide ClpXP substrates and a clear preference for arginine at the P1 position of the cleavage site. Furthermore, the development of an *in vivo* model for the conditional expression of CLPP in mouse hearts provided the proof of principle for tissue specific substrate screens and confirmed CLPX as the rate-limiting subunit *in vivo*.

Zusammenfassung

Nachdem Theodor Schwann die erste Zelltheorie im Jahr 1839 formulierte, benötigte es weitere 60 Jahre mit zahlriechen histologischen Fortschritten, bevor Mitochondrien entdeckt und ihr Name geprägt wurde. Erstaunlicherweise verbleiben 120 Jahre später viele ihrer Aspekte rätselhaft, während sie sich als elementare Organellen für fast alle Organismen etablierten, die weit mehr als nur die Kraftwerke der Zellen repräsentieren.

Um zu dem wachsenden Verständnis dieser faszinierenden Organellen beizutragen, wurde die Rolle der Succinat-Dehydrogenase Untereinheit A (SDHA) und der ATP-abhängigen Clp Protease ClpXP im mitochondriellen Metabolismus bzw. in der Proteostase *in vivo* und *in vitro* analysiert.

Dabei stellte sich heraus, dass der konditionelle knockout von SDHA im Herzen und in der Skelettmuskulatur eine isolierte Komplex II Insuffizienz und letztlich Organversagen auslöste. Allerdings führten metabolische Unterschiede dieser Gewebe zu abweichenden Adaptionen und Stressantworten. Dieses Ergebnis betont somit die Bedeutung des metabolischen Hintergrunds, auch wenn der primäre Defekt ATP Verlust lautet. Dies ist gerade für die Behandlung von bösartigen Zellen mit SDH Mutationen von großer Bedeutung, da diese in ihren metabolischen Grundlagen variieren können.

Um die Rolle der ClpXP Protease in der Proteostase der mitochondriellen Proteine besser zu verstehen, wurden diverse proteomische Ansätze verfolgt, die der Identifizierung neuer ClpXP Substrate, einem möglichen Degradierungsmodus, sowie einer eventuellen Gewebespezifität dienen. Die Kombination eines klassischen „Substrat-screens“ und der kürzlich entwickelten N-Terminom Quantifizierung identifizierte oder bestätigte mehrere bisher unbekannte ClpXP Substrate und zeigte eine klare Prävalenz für Arginin an der P1 Position des Hydrolysefensters. Des Weiteren eröffnet die Entwicklung eines Mausmodels für die konditionelle Expression von CLPP die Möglichkeit von gewebespezifischen Substrat-screens und bestätigt die limitierende Rolle von CLPX *in vivo.*

1 Introduction

1.1 Succinate dehydrogenase and metabolism in skeletal muscles

1.1.1 Skeletal muscles

Skeletal muscles are the sum of hundreds of individual muscles within the human body and make up about 40% of the total body weight. In contrast to smooth- or cardiac muscles, skeletal muscles are voluntarily controlled and harbour the largest protein reservoir of the human body with a protein content of more than 50%, most of which are part of the force-generating, contractile network.

Striated muscles are dynamic tissues with profound metabolic and structural plasticity that facilitate movement and posture, but also serve as a metabolic storage hub for other tissues and largely maintain the core temperature of adult humans (Wolfe 2006), indicating their usefulness for studies involving metabolism, energy and systemic regulation of thereof.

1.1.2 Skeletal muscle synthesis, composition and basic function

Early during development, mesoderm-derived somites differentiate into skeletal muscle progenitor cells (myoblasts), that express stem cell markers (*Pax3/7*) but also the first muscle specific genes such as *Myf5* and *MyoD*. These fetal progenitors further develop into myocytes that express *Acta1*, as one of the earliest markers for committed skeletal muscle cells and are morphologically distinguishable through their striated appearance. Adult muscle cells (myofibers) are multi-nucleated and elongated fibres that develop neonatally through the fusion of myocytes or through migration and fusion of muscle stem cells (satellite cells) with existing muscle fibres. These secondary fibres grow mostly through fusion with myoblasts, but stay relatively constant in numbers after birth (Chal and Pourquie 2017).

Adult muscle fibres can reach lengths of up to 1cm in humans and consist of thousands of myofibrils, the structural unit of muscle cells, which themselves contain billions of muscle filaments. The filaments are composed of thin (actin) and thick (myosin) elements that form cross-bridges to build sarcomeres and can contract the muscle fibres through ATP-dependent displacement of the myosin heads along the actin filaments (Figure 1.1). These contractions occur in parallel within the fibres of each fibre bundle within a muscle. The fibre bundles, as well as the entire muscles are

engulfed by connective tissue called the perimysium and epimysium, respectively, that prevent friction damage during contractions (Figure 1.1). In order to provide oxygen, nutrients and neuronal stimuli to all sarcomere units within a fibre, the cell membrane (sarcolemma) protrudes into the fibres as long invaginations, or T (transverse) tubules (Frontera and Ochala 2015).

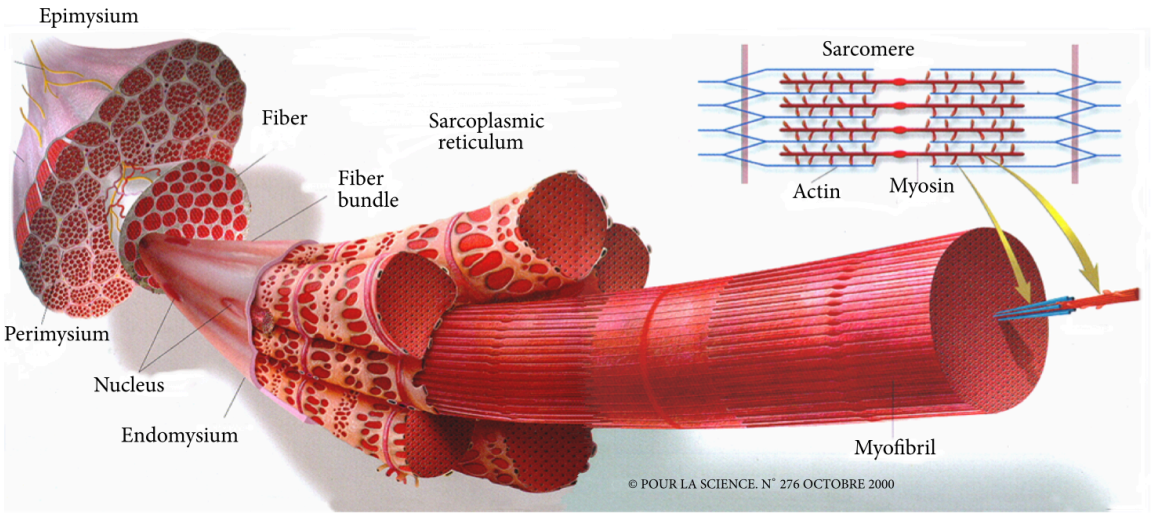

Figure 1.1 Structure of skeletal muscles
Skeletal muscle tissues consist of millions of muscle cells (muscle fibres) that are arranged in fibre bundles to build a muscle. Each fibre further consists of numerous myofibrils that are made of sarcomeres, the contractile units. The cell membrane of a muscle fibre (sarcolemma) shows invaginations (T-tubules), which are in close contact with the sarcoplasmic reticulum. Figure taken unmodified from (Listrat et al. 2016).

During a motor neuron stimulus, the arrival of an action potential at the T tubule triggers voltage-dependent channels (RYR) at the terminal cisternae of the sarcoplasmic reticulum (SR) to release calcium, which is normally kept at a nano-molar concentration within the cell (Lanner et al. 2010). The released calcium can then bind to and shift troponin at the actin filaments, allowing for myosin to bind, form cross-bridges and slide along the actin filament. The release of myosin from actin to repeat the process requires ATP and can reach up to 80% of the total energy demand within the muscle during full contraction (Barclay et al. 2007).
Historically, the first classification of muscle fibre types regarded the colour of muscles or individual fibres. Strongly innervated muscles contain more myoglobin and therefore appear morphologically red, while less innervated muscles are pale or white. Later, physiological experiments with isolated muscles and fibres marked the categories fast- and slow twitching fibres, as well as their resistance towards fatigue.

While the velocity of contraction largely correlates with the development of the SR and its surface area/volume, the resistance towards fatigue of a fibre is mainly determined by its mitochondrial content, visualised by e.g. succinate dehydrogenase (SDH) activity. The development of monoclonal antibodies against myosin heavy chain isoforms finally led to the categorization that is still widely used today (Figure 1.2): Type I slow twitching, highly oxidative fibres rich in mitochondria and myoglobin, as well as fast twitch, oxidative/glycolytic type 2A fibres and fast twitch, glycolytic type 2B fibres with highly developed SR structures. Additionally, muscles possess type 2X fibres with properties intermediate between type 2A and type 2B fibres (Schiaffino and Reggiani 2011). Notably, type 2B isoforms are not expressed in human muscles and result from miss-annotated type 2X fibres (Smerdu et al. 1994).

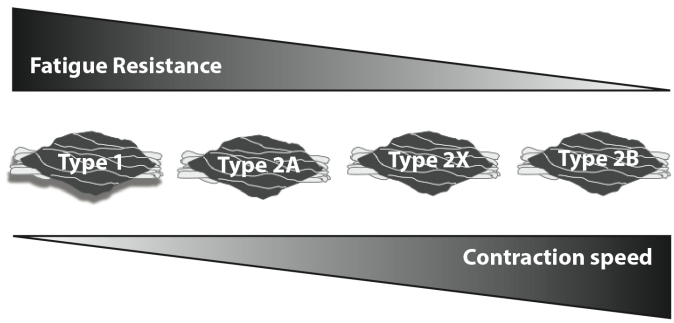

Figure 1.2 Different fibre types expressed in mouse muscles
Mouse muscles express fibre types with varying amounts of fatigue resistance and contraction speeds with type 1 fibres being the slowest and most resistant fibres and type 2B fibres being the fastest twitching fibres with the lowest resistance towards fatigue. Type 2A and 2X fibres have properties in between the other two types.

Most muscles, like for example the hind lib muscles, need to fulfil long-lasting functions such as posture maintenance, as well as short, high intensity movements like jumping. These muscles therefore have a heterogeneous composition of oxidative and glycolytic fibre types. Other, more specialised muscles such as the extensor digitorum longus (EDL) and the soleus muscle contain almost exclusively fast twitching- and slow twitching fibre types, respectively. However, fatigue resistance and therefore mitochondrial content can vary greatly between fibres of these muscles (Schiaffino et al. 1970). Similar to these mechanical and metabolic properties, different fibre types have contact to distinct motor neurons and have unique responses towards electrical stimuli. Among major differences in ion channel

composition, the high density of Na^+ channels e.g. allows for the response to high discharge rates in fast twitching fibres, to generate high-intensity, albeit short-term force.

1.1.3 Regulation of (energy-) metabolism in skeletal muscles

With great variability of mammalian muscles and muscle fibres comes profound plasticity in terms of metabolism and energy homeostasis. However, a number of factors remain in common for all fibre types and are in stark contrast to other tissues. Despite skeletal muscle's role in amino acid storage and supply, amino acids only play a minor role in ATP production and energy homeostasis, even during intense exercise (Lemon and Mullin 1980). Similarly, although an important function of glycogen in muscle function and fatigue is undisputed, this is probably independent of its utility as an energy source (Ortenblad et al. 2013). Rather, glycogen has a non-metabolic function and serves as an important factor in calcium release from the SR and fibre contraction (Ortenblad et al. 2011). This proposal is further substantiated by the fact that distinct glycogen granules can be observed close to the SR (Nielsen and Ortenblad 2013) and that muscle glycogen stores are not depleted during overnight fasting like hepatic glycogen stores (Hearris et al. 2018). At rest and during prolonged exercise, the preferred substrates for ATP production in muscles are fatty acids (Romijn et al. 1993), however, short-term and intense exercise additionally requires the oxidation of carbohydrates (mainly glucose). Therefore, glucose uptake is strongly increased during such activities and can reach 50-times the uptake at rest (Katz et al. 1986).

Skeletal muscles are already highly energy-demanding at rest (10cal/d/g muscle) (Wolfe 2006) and even more so during activity. However, resting ATP levels are comparably low at ~ 5-6mM and would be completely hydrolysed within a few seconds (Sahlin et al. 1998). Yet, during exercise with moderate intensity, ATP levels remain constant due to the breakdown of phosphocreatine (PCr) (Allen et al. 1997). At rest, mitochondrial and cytosolic creatine kinase use ATP produced by oxidative phosphorylation and glycolysis, respectively, to phosphorylate creatine. The PCr generated serves as a temporal and spatial buffer for ATP turnover (Sweeney 1994), as PCr diffuses faster than ATP (Hubley et al. 1995) and creatine kinases are located at the sites of high energy demand. Furthermore, PCr is believed to attenuate

oxidative phosphorylation and thereby protecting mitochondria from transient disturbances in ATP demand (Barclay 2017). This buffering can further extent the energy supply of active muscles to several minutes, after which only augmented vascular supply of oxygen and nutrients can further extent contractility before fatigue and exhaustion occurs.

1.1.4 Respiratory chain complexes and oxidative phosphorylation

Energy-demanding tissues such as skeletal muscles contain large amounts of mitochondria and these mitochondria are particularly dense in respiratory chain (RC) complexes to provide sufficient ATP via oxidative phosphorylation (OXPHOS).

While the respiratory chain consists of four complexes (complex I-IV), the ATP-synthase that carries out OXPHOS, is also referred to as complex V. The driving force behind oxidative phosphorylation is a proton motive force across the inner mitochondrial membrane created by complexes I, III and IV, which possess proton pumping activity. Together with the mobile electron carrier ubiquinone and cytochrome c, electrons from NADH are ultimately used to reduce O_2, which completes the respiratory chain. While the exact nature of respiratory chain complex interaction is not finally defined and may depend on the cellular environment, it is mostly agreed that these complexes can act as isolated entities, as well as arrange into higher-order structures called supercomplexes (SC). The respirasome ($I_1III_2IV_n$) is widely considered to be the standard model for respiratory chain SCs, that stabilizes individual complexes and improves electron transfer between them (Schagger and Pfeiffer 2000, Acin-Perez et al. 2008, Enriquez 2016, Wu et al. 2016). Complex II of the respiratory chain is omitted from most supercomplex models, as it is typically not observed in BN-PAGE analyses of mitochondrial SCs and behaves like an individual complex in flux control analysis experiments (Bianchi et al. 2004). However, recent near-atomical structures of human RC complexes suggested a $I_2III_2IV_2$ megacomplex in human mitochondria, that is able to incorporate complex II units between complex I and IV, resulting in $I_2II_2III_2IV_2$ complexes (Guo et al. 2017). The authors state that complex II can be modelled within the gaps of the structure and that an overall low prevalence might cause the inability to confidently map complex II into the megacomplex. In addition to technical limitations due to low stabilities, biological reasons could account for this observation. It is conceivable that complex II only

transiently attaches to the SCs in certain tissues, or under circumstances that require amplified succinate oxidation. Further, it should be noted that the structure of the megacomplex was the only reported structure obtained from human cells (HEK293), while previous structures of the respirasome were generated from mammalian heart mitochondria (Schafer et al. 2007, Althoff et al. 2011, Gu et al. 2016). A tissue-specific arrangement is therefore possible, especially since liver mitochondria were reported to have partially different arrangements that can include complex II (Acin-Perez et al. 2008).

In skeletal muscles, RC complexes also exist as both, individual complexes and in higher-order structures, such as the respirasome. Although a fibre type-specific difference was not established so far, it is nevertheless plausible, because exercise in human skeletal muscles results not only in an increased RC subunit amount, but also in the preferential assembly into supercomplex structures and increased respiration (Greggio et al. 2017).

1.1.5 Succinate dehydrogenase

Torsten Thunberg is usually credited as the discoverer of succinate dehydrogenase (SDH; complex II) in 1909, when he measured the gas exchange in frog muscles (Thunberg 1909, Hopkins and Morgan 1938) almost 50 years before the isolation of its electron acceptor ubiquinone (Crane et al. 1957, Crane 1989). 110 years of technological and intellectual milestones later, the structure (Sun et al. 2005), function and kinetic properties (Leger et al. 2001) are well described, but details about the mechanics are still debated and its implication in human diseases is continuously explored (Bezawork-Geleta et al. 2017).

SDH harbours several unique features among the RC complexes, making it a particularly interesting object to study. As the smallest RC complex, SDH consists of only four subunits (SDHA-D) that are all nuclear-encoded in almost all eukaryotes. Although it is the only complex within the respiratory chain that does not directly shuttle protons across the inner mitochondrial membrane, it is yet indirectly responsible for a large part of the proton motif force due to its second role as a TCA cycle enzyme in the oxidation of succinate.

SDH consists of two main parts: A membrane anchor made out of the alpha-helical subunits C and D and attached to it the soluble subunits SDHB and SDHA. SDHA is the flavoprotein with catalytical activity that binds and oxidises succinate to fumarate. The electrons reduce the covalently bound FAD moiety and are further transferred through three iron-sulphur clusters within SDHB. Finally, they are transferred at a heme b in the interface between SDHC and SDHD onto ubiquinone.

Currently, there are four assembly factors known, that are required for the assembly and integrity of functional SDH. SDHAF2 (Sdh5 in yeast) mediates the flavination of SDHA and its absence causes loss of SDH function (Hao et al. 2009). Flavination is the initial step during complex assembly and essential for SDHB binding to SDHA. Certain human cell types, such as triple negative breast cancer cells can contain flavinated and functional SDH even when SDHAF2 is deleted by gene editing (Bezawork-Geleta et al. 2016). However, it remains unclear whether these cells express proteins redundant to SDHAF2 or flavination occurs spontaneously. SDHAF4 (Sdh8) appears to exert chaperone activity on flavinated SDHA to prevent unintended oxidative damage before complex assembly (Van Vranken et al. 2014). Similarly, SDHAF1 and SDHAF3 (Sdh6 and Sdh7) are required for iron-sulphur cluster incorporation into SDHB and its shielding from oxidative damage (Na et al. 2014). Mutations in any of these assembly factors can lead to SDH dysfunction and the associated clinical manifestations described later.

The activity of complex II is further regulated by reversible, post-translational modifications: The tyrosine kinase FGR phosphorylates SDHA at two distinct residues, a process that is stimulated by reactive oxygen species (ROS) (Salvi et al. 2007, Acin-Perez et al. 2014). A possible physiological relevance for the phosphorylation was recently shown in cells lacking complex III activity. Impaired complex III function was associated with increased ROS levels, which in turn lead to increased complex II phosphorylation and activity (Tropeano et al. 2018). It is thus plausible that reduced respiratory chain activity mediates a compensatory activation of SDH-driven respiration. SIRT3 and SIRT5 are mitochondrial sirtuins with deacetylation and desuccinylation activity, respectively and loss of either protein is associated with increased SDH activity (Cimen et al. 2010, Park et al. 2013). However, a causal relationship between acetylation/succinylation of SDH and its activity remains to be established.

Finally, the mitochondrial chaperone TRAP1 of the HSP90 family was reported to bind SDH and limit SDH-dependent respiration, particularly in cancer cell lines. This inhibition was selective for complex II and independent of SDH protein levels (Sciacovelli et al. 2013). Surprisingly, the well-known SDH inhibitors 3-NPA and TTFA only inhibited respiration in SAOS-2 cells when TRAP1 was down-regulated, indicating that TRAP1 fully inactivates SDH-dependent maximal respiration in these cells.

1.1.6 SDH loss of function models and clinical manifestations

Mutations in any SDH subunit or its assembly factors are frequently associated with hereditary or sporadic malignancies (Laurenti and Tennant 2016, Bezawork-Geleta et al. 2017, Gill 2018). These include most commonly paraganglioma and pheochromocytoma (PGL/PHEO), gastrointestinal stromal tumours (GIST) and more rarely, renal cell carcinomas (RCC) and pituitary adenomas (PA). Additionally, (mostly) familiar germline mutations within the SDHA gene were observed in several patients with Leigh syndrome, which is sometimes accompanied by severe cardiomyopathy (Horvath et al. 2006, Ghai et al. 2011). Inactivation of both alleles of the affected SDH gene in paraganglioma usually involves at least one germline mutation and SDH mutation-derived tumours are most commonly defined by the loss of SDHB immunohistochemical staining (Gill 2018).

It is generally agreed upon that neoplasia with SDH dysfunction result from succinate accumulation within the affected cells. Increased succinate concentration can lead to the competitive inhibition of 2-oxoglutarate (2-OG)-dependent dioxygenases. With over 60 family members in humans, these enzymes are important regulators of global gene expression and cellular function. Succinate acts as a product-inhibitor of 3 major classes of dioxygenases, including over 30 JMJC histone demethylases, three known ten-eleven translocases (TETs) and two prolyl hydroxylases (PHDs) (Bezawork-Geleta et al. 2017, Bargiela et al. 2018). While succinate-mediated inhibition of the former two classes causes hypermethylation of histones and DNA, respectively, inhibition of PHDs stabilizes HIF1α even in the presence of oxygen (pseudo-hypoxic state). This hypoxic state was recognized early on as an important factor in cancer cell transformation (Warburg et al. 1927). Furthermore, other mutations leading to HIF1α stabilization can also result in the formation of PGL/PHEO and GIST like mutations in VHL (Kang et al. 2016, Rednam et al. 2017), substantiating that it is of central importance within SDH-deficient tumours.

Unfortunately, most of the research on SDH deficiency in humans is limited to samples from these patients, as there is currently no stable cell line derived from PGL/PHEO patients (Bezawork-Geleta et al. 2017).
Additionally, the analysis of mouse models with SDH deficiency created so far was limited to either neurodegeneration or specific tumour types and not expanded towards other tissues (Astuti et al. 2004, Piruat et al. 2004, Bayley et al. 2009, Ishii et al. 2011, Millan-Ucles et al. 2014, Al Khazal et al. 2019).

1.1.7 Study aim

Despite the profound knowledge about succinate dehydrogenase, its structure, function and role in multiple diseases, fundamental aspects regarding its dual function *in vivo* remain unknown. Specifically, it is still unclear how SDH function is regulated in tissues with large discrepancies regarding their ATP and metabolite demands. To address this issue, conditional mouse knockout models were developed, deleting SDHA in individual tissues. The main focus was set on metabolic and energetic changes and the stress responses as the consequences thereof. A better understanding of the tissue-specific role of SDH will ultimately also improve the knowledge about why some cell types are prone to generate neoplasia upon SDH deficiency and how these could be targeted in the future.

1.2 ClpXP protease and mitochondrial proteostasis

With over 1000 soluble and membrane-bound proteins located in different sub-compartments, mammalian as well as yeast mitochondria face the challenge to ensure the functionality and correct amount of their proteome. A varying demand for specific proteins, as well as fluctuating stress levels that can irreversibly damage proteins require high precision and plasticity of the quality control and regulatory systems within mitochondria.

1.2.1 Mitochondrial quality control and mitochondrial proteases

Quality control (QC) within a cell occurs at different levels, depending on the severity of the damage (Tatsuta and Langer 2008). On the molecular level, chaperones and proteases regulate protein abundance, folding and functionality within each organelle/compartment. If the damage exceeds this QC capacity, organellar QC systems can selectively remove non-functional organelles. With regard to mitochondria, this process is mainly regulated via fusion/fission and mitochondrial-specific autophagy (mitophagy) (Pickles et al. 2018). If this system also fails to warrant functionality, affected cells can undergo cell death in order to protect the surrounding cells within a tissue (Marino et al. 2014). In mitochondria, regulatory and QC proteostasis is mediated by ATP-dependent protease complexes that form barrel-shaped catalytic chambers to avoid unintentional activity. The membrane-bound mAAA and iAAA proteases face the matrix and intermembrane space, respectively, and are able to extract and degrade other membrane proteins. Mitochondrial matrix proteostasis on the other hand is mostly regulated by the two soluble protease complexes, ClpXP and LonP1. These proteases are structurally different and not (fully) redundant, as they cannot compensate for the loss of the other (Gispert et al. 2013, Venkatesh et al. 2019). Most of the QC within the mitochondrial matrix is performed by LonP1, particularly with regard to oxidatively damaged proteins (Bota and Davies 2002, Ngo et al. 2013, Bezawork-Geleta et al. 2015, Pinti et al. 2016), although several regulatory substrates such as TFAM or COX4I1 have been described (Fukuda et al. 2007, Matsushima et al. 2010).

Though substantial evidence for a role of ClpXP in the regulation of the mitochondrial unfolded protein response (mtUPR) exists in *C. elegans* (Haynes et al. 2007, Haynes et al. 2010), this was recently disputed in a mammalian background (Seiferling et al.

2016), indicating that ClpXP adopted different substrates and functions during evolution and may rather be a part of - than a trigger of the mtUPR in mammals. Only recently, the first substrates and *in vivo* functions were described for mammalian ClpXP and many open questions remain about other substrates, tissue-specificity and the regulation of its activity (Cole et al. 2015, Fischer et al. 2015, Szczepanowska et al. 2016, Matsushima et al. 2017, Becker et al. 2018).

1.2.2 ATP-dependent Clp protease ClpXP

ClpXP is a highly conserved protease complex found in bacteria (Baker and Sauer 2012), mitochondria (Glynn 2017) and chloroplasts (Olinares et al. 2011), consisting of a catalytic subunit (CLPP, ClpP) and an unfoldase subunit (CLPX, ClpX) (Figure 1.3).

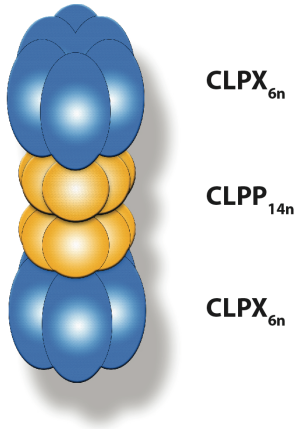

Figure 1.3 Structure of the functional ClpXP protease complex
The ClpXP protease is composed of two heptameric CLPP rings that form the catalytic core ($CLPP_{14n}$) and two hexameric CLPX rings ($CLPX_{6n}$) that attach to either site of the CLPP chamber and perform substrate recognition, unfolding and translocation.

While plants like *Arabidopsis thaliana* have multiple gene duplications for ClpP and ClpX, with partially dual DNA origin (Adam et al. 2001), bacteria and mitochondria have one gene for each subunit that is nuclear encoded. Structurally, the protease resembles the cytosolic 26S proteasome with a catalytic core consisting of two stacked CLPP heptameric rings forming a chamber. Within this chamber, 14 serine/histidine/aspartate residues form catalytic triads, which perform the peptide cleavage (Kang et al. 2005). This chamber is only stable in the presence of hexameric CLPX rings and ATP. The CLPX rings attach to the chamber and block unspecific peptide entry. In mitochondria, CLPX is the only unfoldase isoform responsible for substrate recognition, unfolding and translocation into the CLPP chamber (Lowth et al. 2012). Mitochondrial CLPX was additionally suggested to play a chaperone-like role in heme biosynthesis independent of CLPP (Kardon et al. 2015), which is also supported by the fact that the yeast strain *S. cerevisiae* possesses a homologue for CLPX but none for CLPP.

Substrate unfolding and translocation can occur at both termini and is dependent on the location of the recognition site (Olivares et al. 2017). In bacteria, known degradation motifs (degrons) such as the ssrA-tag are recognized by adaptor proteins like ClpS, SspB or TrfA (Flynn et al. 2004, Donegan et al. 2014). Fusion proteins of the ssrA-tag and fluorescent proteins are commonly used to study bacterial ClpXP activity, however this system cannot be translated to the mitochondrial homologue, as human and mouse CLPX cannot recognize the tag (Martin et al. 2008). In bacteria, ribosomes stalled on mRNAs are recycled using transfer-messenger RNAs (tmRNAs). These mRNAs are short RNA species that structurally resemble tRNAs. They are therefore able to enter stalled ribosomes, where they are translated into the ssrA-tags, resulting in fusion proteins of the aberrant protein and the tag (Janssen and Hayes 2012). The inability of human/mouse CLPX to recognize the tag might stem from the lack of known adaptors, however no tmRNA/ssrA system has yet been described in mammalian mitochondria.

1.2.3 Mammalian ClpXP substrates, interactors and tissue specificity

As mentioned before, mammalian ClpXP shows profound differences in terms of substrates in comparison to its bacterial homologue, although both proteases share strong structural and functional homology. The difference can be largely attributed to the CLPX-mediated substrate recognition, as hybrid proteases made of human CLPP and *E. coli* ClpX are able to degrade ssrA-tagged fusion proteins *in vitro* (Kang et al. 2002). The differences in substrates may have resulted during the development of multicellular organisms that demanded cell type-specific substrate regulations. The almost inevitable presence of adaptor proteins also in eukaryotic mitochondria would allow even further diversification of protease function and could account for some of the differences observed between cell types and organisms and explain why individual approaches towards the identification of mitochondrial ClpXP substrates resulted in (partially) different proposed candidates.

A particular useful model for the study of mammalian ClpXP was the *Clpp*$^{-/-}$ knockout mouse that largely recapitulates the symptoms observed in Perrault syndrome patients (Gispert et al. 2013, Szczepanowska et al. 2016). Accordingly, *Clpp*$^{-/-}$ mice show growth retardation, infertility and hearing loss. In addition to the tissue-specific phenotypes, these mice show systemic aberrations, such as augmented glucose homeostasis, impaired adaptive thermogenesis and protection from diet-induced obesity and insulin resistance (Becker et al. 2018, Bhaskaran et al. 2018).

To date, mitochondrial ClpXP substrate screens using inactive CLPP variants were performed in MEFs (Szczepanowska et al. 2016) and *Podospora anserina* (Fischer et al. 2015), and a mitochondrial ClpXP interactome screen using BioID labelling was performed in human HEK293 cells (Cole et al. 2015). While all three highlight the role of ClpXP in regulating respiratory chain subunits and metabolic enzymes, the screen in MEFs also generated ERAL1 as a potential substrate, that affects mitoribosome biogenesis, primarily in the heart. The effect was less pronounced in cells and not observed in hepatocytes (Becker et al. 2018), which strongly insinuates the importance of tissue-specific substrates and the careful consideration of any substrate screen system. Non-screen approaches with knockout or knockdown models have further suggested LRPPRC1 as a substrate in *D. melanogaster* (Matsushima et al. 2017), EFG1, VLCAD, PNPT1 and CLPX in mice (Szczepanowska et al. 2016, Becker et al. 2018), and NOA1 in mouse C2C12 cells (Al-Furoukh et al. 2014).

Notably, only NOA1 was verified in an *in vitro* degradation assay with recombinant proteins. This or other confirmation experiments lower the chances that increased steady state levels in the absence of the protease result as a secondary effect. However, negative *in vitro* degradation experiments might also arise due to the lack of mandatory adaptors.

Furthermore, C1QBP was suggested as a mitochondrial adaptor protein because of its strong binding to ClpXP and the fact that it is not degraded by ClpXP *in vitro* or *in vivo* (Lowth et al. 2012, Szczepanowska et al. 2016). However, its "promiscuous" affinity towards many proteins under standard purification conditions raises further questions as to which of the interactions have biological meaning (Ghebrehiwet et al. 1994, Mcgee and Baines 2011, Zhang et al. 2013, Szczepanowska et al. 2016, Kim et al. 2017, Hong et al. 2018). Despite this controversy and the uncertainty about the exact function of the protein, C1QBP can still be utilized as a control for non-substrate interactors in ClpXP substrate screens.

1.2.4 Study aim

The understanding of a given protease is inevitably linked to the discovery of its substrates and the regulation of their degradation. The most useful tools to identify these substrates are undoubtedly loss of function models and screens with inactive proteases in combination with proteomic quantitation approaches.

Surprisingly, only few substrates for mammalian ClpXP were confidently identified so far and it remains unclear as to why mutations in the *CLPP* gene manifest as particular tissue deficiencies in patients with the Perrault syndrome. To identify further substrates, two independent proteomic screens were employed to quantitatively address the issue. Additionally, a mouse model conditionally expressing tagged CLPP was developed to enable purification studies *in vivo* that could shed light on the tissue-specificity of the protease.

2 Materials and Methods

2.1 Materials

Table 2.1: Materials and suppliers used in the study

Name	Supplier
2-Propanol	AppliChem
^{35}S-methionine	Hartmann Analytic
Acetyl-CoA	Sigma Aldrich
40% Acrylamid (37.5:1)	Carl Roth
4-16% Acrylamide gels	Life Technologies
ADP	Sigma Aldrich
Agarose	Carl Roth
6-Aminohexanoic acid	Carl Roth
Antimycin A	Sigma Aldrich
APS	Sigma Aldrich
Bradford Reagent	Sigma Aldrich
BSA	Sigma Aldrich
BSA (FA-free)	Sigma Aldrich
Cas9 mRNA	Tebu-bio
Cas9 protein	IDT
Catalase	Sigma Aldrich
cDNA synthesis kit	Applied Biosystems
Coomassie Brillian Blue G-250	AppliChem
Cytochrome c	Sigma Aldrich
Detection screen	Fuji
Diaminobenzidine	Sigma Aldrich
Digitonin	Merck
DMEM medium	Life Technologies
Dulbeco PBS	Life Technologies
Dried milk powder	AppliChem
DTT	Sigma Aldrich
EDTA	Sigma Aldrich

EGTA	Sigma Aldrich
Ethanol	Applichem
Ethidium bromide	Sigma Aldrich
FBS Superior	Merck
FCCP	Sigma Aldrich
GoTaq polymerase/buffer	Promega
Glutamate	Sigma Aldrich
Glycine	Applichem
H_2O_2	Sigma Aldrich
HCl	VWR
HRP	Sigma Aldrich
KCl	AppliChem
KCN	Sigma Aldrich
Klenow polymerase	Invitrogen
Malate	Sigma Aldrich
Malonate	Sigma Aldrich
Mannitol	AppliChem
Mayer's hematoxylin	AppliChem
MeOH	AppliChem
$MgCl_2$	Sigma Aldrich
NaCl	Sigma Aldrich
NADH	Sigma Aldrich
NaF	AppliChem
NaOH	Sigma Aldrich
Na orthovanadat	AppliChem
Na_3PO4	AppliChem
NaN_3	Sigma Aldrich
4x native sample buffer	Life Technologies
Nucleofector electroporation kit	Lonza
Oligomycin	Sigma Aldrich
Oxaloacetate	Sigma Aldrich
Paraformaldehyde	Sigma Aldrich

PBS	Life Technologies
Penicillin/Streptomycin	Life Technologies
Periodic acid	Sigma Aldrich
2-Propanol	Aplichem
Protaese Inhibitor Cocktail	Sigma Aldrich
Proteinase K	Applichem
Pyruvate	Sigma Aldrich
Random primer mix	Invitrogen
RNase-free water	Life Technologies
Rotenone	Sigma Aldrich
Schiff reagent	Sigma Aldrich
SDS	AppliChem
Succinate	Sigma Aldrich
Sucrose	Sigma Aldrich
SYBR Green qPCR Master Mix	Agilent
TBE	AppliChem
TEMED	Sigma Aldrich
Tris	Sigma Aldrich
Triton X-100	Sigma Aldrich
Trizol	Life Technologies
0.05% Trypsin	Life Technologies
Tween20	VWR
Ubiquinone	Sigma Aldrich

2.2 Transgenic mouse models

2.2.1 *Sdha^{tm2a}*

Sdha^{tm2a} mice were obtained from the KOMP repository (Project ID: CSD48939) as cryo-conserved sperm. The *Sdha^{tm2a}* allele harbours an FRT-flanked knockout-first cassette (Skarnes et al. 2011) between exon 5 and exon 6 of the *Sdha* gene and two loxP sites surrounding exon 6 outside of the cassette.

2.2.2 *Sdha$^{fl/fl}$*

Sdha$^{fl/fl}$ were generated via intercrossing of *Sdha^{tm2a}* mice with FLP deleter mice (*ROSA26::FLPe*) that deletes the FRT-flanked sequence. Mice were further bred to *Sdha$^{fl/fl}$* homozygosity without the *ROSA26::FLPe* allele.

2.2.3 *Sdha^{MKO}*

Conditional striated muscle-specific knockout (*Sdha^{MKO}*) mice were generated via intercrossing of *Sdha$^{fl/fl}$* mice with heterozygous *ACTA-Cre* transgenic mice (provided by Prof. Dr. Thomas Langer), harbouring one *Sdha^{fl}* allele. Matings were set up in both combinations and both male and female mice were used for the experiments. Mice were sacrificed at 3 or 4 weeks of age and skeletal muscles (quadriceps, gastrocnemius, triceps and soleus) and livers were isolated for the experiments. *Sdha$^{fl/fl}$* mice of the same sex and age were used as controls.

2.2.4 *Sdha^{HKO}*

Conditional heart and skeletal muscle-specific knockout (*Sdha^{HKO}*) mice were generated via intercrossing of *Sdha$^{fl/fl}$* mice with heterozygous *Ckmm-NLS-Cre* transgenic mice (provided by Prof. Dr. Nils-Göran Larsson), harbouring one *Sdha^{fl}* allele. Matings were set up in both combinations and both male and female mice were used for the experiments. Mice were sacrificed between 11 and 21 days of age and hearts were extracted for the experiments. *Sdha$^{fl/fl}$* mice of the same age were used as controls.

2.2.5 *Sdha^{LKO}*

Conditional hepatocyte-specific knockout (*Sdha^{LKO}*) mice were intended via intercrossing of *Sdha$^{fl/fl}$* mice with heterozygous *Albumin-Cre* transgenic mice (provided by Prof. Dr. Elena Rugarli), harbouring one *Sdha^{fl}* allele. Matings were set up in both combinations and >60 pups were genotyped without positive *Sdha^{LKO}* offspring.

2.2.6 *Clpp$^{-/-}$*

The generation and breeding of *Clpp$^{-/-}$* mice was performed as previously published (Szczepanowska et al. 2016). Mice were sacrificed at the age of 15-20 weeks and hearts were extracted for further experiments. *Clpp$^{+/+}$* mice of the same sex and age were used as controls.

2.2.7 *R26-Clpp-Flag*

Conditional *Rosa26 (R26)-Clpp-Flag* knockin mice were generated as described in (Chu et al. 2016) using pR26 CAG/GFP Dest as the targeting vector. The *Clpp-Flag* sequence (Szczepanowska et al. 2016) was cloned between the attB sites of the targeting vector using gateway cloning to create pR26 CAG/CLPP/GFP Dest. crRNA (5'-ACUCCAGUCUUUCUAGAAGAGUUUUAGAGCUAUGCU-3') annealing to the *ROSA26-1* locus and tracrRNA were obtained from IDT and annealed according to the manufacturer's instructions. pR26 CAG/CLPP/GFP Dest targeting vector (20ng/µL), sgRNA (15ng/µL), *Cas9* mRNA (30ng/µL) and Cas9 protein (30ng/µL) in injection buffer (Tris-HCl 10mM, EDTA 0.1mM, pH 7.5) was injected into pro-nuclei in the transgenic core facility of the CECAD institute and the offspring was genotyped for positive insertion as described in (Chu et al. 2016) with PCRs amplifying within the targeting vector (Neo) and throughout targeting vector and locus (R26). Positive mice were back-crossed for 3 generations before analysis. Targeting with *R26-Clpp-Trap-Flag* did not result in positive offspring.

2.2.8 *R26-Clpp-Flag Ckmm-Cre*

CLPP-FLAG expression was induced in the heart by crossing *R26-Clpp-Flag* mice with *Ckmm-Cre* mice. Mice heterozygous for each allele were sacrificed at 10 weeks of age and *R26-Clpp-Flag* mice without *Ckmm-Cre* were used as controls.

2.3 Mouse housing conditions and sacrifice

All mice were kept in single-ventilated cages at 22-24°C in groups of 2-5 per cage in the CECAD animal facility. Mice were fed a ssniff chow diet (v1554-330) consisting of 10 kJ% fat, 23 kJ% protein and 67 kJ% carbohydrates, as well as drinking water ad libitum. The animals were kept under a 12h light/dark cycle starting at 6 am and killed by cervical dislocation or decapitation (pups at 11 days of age) at 12pm. All experiments were approved and permitted by the Animal Ethics Committee of North-Rhein-Westphalia (Landesamt für Natur, Umwelt und Verbraucherschutz Nordrhein-Westfalen; LANUV) following German and European Union regulations. All animal work was performed in accordance with recommendations and guidelines of the Federation of European Laboratory Animal Science Associations (FELASA).

2.4 Blood glucose measurement

Immediately following sacrifice, tail vain blood was collected and used for blood glucose measurement with an ACCU-Check Aviva (Roche) according to the manufacturer instructions.

2.5 Cell culture models

For the substrate trapping screen, previously published *Clpp*$^{-/-}$ MEFs were used (Szczepanowska et al. 2016).

2.5.1 Cell culture

Cells were grown at 37°C, 21% O_2 and 5% CO_2 conditions in full DMEM high glucose medium with 10% FBS added and split before cells reached 80% confluency for maintenance. Cells were detached from culture dishes with 1 min incubation in 0.05% trypsin solution, following quenching with 3x the volume of culture medium.

2.5.2 Transfection of CLPP-FLAG constructs

Clpp$^{-/-}$ cells were transfected with previously published constructs (Szczepanowska et al. 2016) using the Nucleofector electroporation kit (Lonza) according to the manufacturer instructions. 4 times 10^6 MEF cells were transfected per condition and replicate and transferred to 10cm culture dishes. 24h post transfection, the medium

was exchanged and 72h post transfection cells were harvested with trypsin and the four dished per condition were pooled. Cell pellets were washed twice with cold PBS and immediately used for lysis.

2.6 Biochemistry

2.6.1 Isolation of proteins from tissues

For tissue protein isolations, heart or skeletal muscle tissue was taken up in heart protein isolation buffer (50mM HEPES, 0.1M NaF, 10mM Na orthovanadate, 10mM EDTA, 100mM NaCl, 1% Triton X-100, 0.2% SDS, pH 7.4) or skeletal muscle protein isolation buffer (50mM Tris-HCl, 150mM NaCl, 1mM EDTA, 1% NP-40, pH 7.5), respectively with protease and phosphatase inhibitor cocktails and lysed with ceramic beads in a FastPrep homogenizer (MP Biomedicals, Santa Ana, CA, USA). After 30 min incubation on ice, insoluble material was removed by centrifugation at 20,000x g for 30 min and the supernatant was stored at -80°C until further use.

2.6.2 Isolation of mitochondria from skeletal muscles

Mitochondria from skeletal muscles were isolated as described previously (Frezza et al. 2007). In summary, freshly isolated muscle tissue was isolated, stripped from visible connective tissue, minced and incubated in 0.05% trypsin and 10mM EDTA for 30 min. The trypsin solution was removed and the tissue resuspended in skeletal muscle isolation buffer 1 (150mM sucrose, 10mM EDTA, 50mM KCl, 50mM Tris-HCl, 0.2% FA-free BSA pH 7.7). Using a Teflon potter at 1600 rpm, the tissue was homogenized on ice and un-lysed fragments were removed at 700x g centrifugation. The mitochondria were collected from the supernatant with 8000x g centrifugation and resuspended in skeletal muscle isolation buffer 2 (250mM sucrose, 3.3mM EGTA, 10mM Tris-HCl pH 7.7). Mitochondria were collected again with 8000x g centrifugation and resuspended in 75µL isolation buffer 2. Protein concentration was determined with Bradford reagent and mitochondria were used immediately for respiration measurement and frozen once for BN-PAGE analysis.

2.6.3 Isolation of mitochondria from hearts

To isolate mitochondria, fresh heart tissue was homogenized with a Teflon potter at 1000 rpm in 5mL heart mitochondria isolation buffer (100mM sucrose, 50mM KCl, 1mM EDTA, 20mM TES, pH 7.2) with the addition of subtilisin A (1mg/g heart) and 0.2% BSA (FA-free). Fat was removed with the supernatant after centrifugation at 8500x g at 4°C and the homogenate was resuspended in 30mL isolation buffer. Unlysed material was removed by centrifugation at 800x g and the supernatant was centrifugated at 8500x g to collect the crude mitochondrial fraction. The pellet was resuspended in 100µL isolation buffer and used immediately for respiration measurements or stored at -80°C.

2.6.4 SDS-PAGE and western blot

To separate proteins via polyacrylamide gel electrophoresis under denaturating conditions, proteins were incubated with Laemmli buffer (final: 50 mM Tris-HCl, 2% SDS, 10% Glycerol, 1% 2-mercaptoethanol, 12.5 mM EDTA, 0.02% Bromphenol Blue, pH 6.8) at 95 °C for 5 minutes. Chilled samples were than loaded on 10% or 12% Tris-Glycine acrylamide gels in a Mini-PROTEAN Tetra Cell (BioRad, München, Germany). Separation gel (10-12% acrylamide-bisacrylamide (37.5:1), 37.5 mM Tris-HCl, 0.1% SDS, pH 8.8) and stacking gel (5% acrylamide-bisacrylamide (37.5:1), 12.5 mM Tris-HCl, 0.1% SDS, pH 6.8) were casted and used when completely polymerized. To catalyse polymerization, 0.1% APS and TEMED were added to the separation gel and 0.25% APS and TEMED to the stacking gel.

Electrophoresis was performed at constant 85 V in running buffer (25 mM Tris-HCl, 250 mM Glycine, 0.1% SDS, pH 8.3) until the loading dye reached the separating gel and at constant 150 V until it reached the end of the gel. After electrophoresis, the gels were shortly washed and the transfer was assembled in a BioRad Criterion Blotter:

- Black sieve
- Sponge
- 2 layers of Whatman paper
- Gel
- Nitrocellulose membrane
- 2 layers of Whatman paper
- Sponge
- Red sieve

Proteins were transferred in transfer buffer (30 mM Tris-HCl, 240 mM Glycine, 0.037% SDS, 20% methanol) at constant 400 mA and 4 °C for 2 hours. After transfer, the membranes were shortly washed in dH_2O and successful transfer was evaluated by Ponceau S staining.

Afterwards, the Ponceau S staining was removed with PBST and membranes were blocked for 60 minutes in 5% Milk-PBST.

Primary and secondary antibody incubation has been performed according to the manufacturer's instructions, each following 3 rounds of 5 minutes washing in PBST. After the last washing, ECL solution was applied to the membranes, which were then exposed to Fujifilm Super RX films.

Table 2.2: Antibodies, suppliers and identifiers used for western blots

Name	Supplier	Cat. Nr.
4-HNE	Abcam	ab46545
AcK	Abcam	21623
ACTIN	Sigma	A5441
AKT	CST	9272
pAKT	CST	4060
ALDH18A1	Sigma	HPA01260
AMPK	CST	2532
pAMPK	CST	2535
ATF4	Proteintech	10835-1-AP
ATP5A1	Abcam	ab14748
C1QBP	Millipore	AB2991
Citrate Synthase	Santa Cruz	sc-515640
CLPP	Sigma	WH0008192M1
CLPX	Sigma	HPA040262
COXI	Molecular Probes	459600
COXIV	Molecular Probes	A21348
EIF2a	Abcam	ab26197
pEIF2a	Abcam	ab32157
pERK1/2	CST	9102
ETFDH	Santa Cruz	sc-515202
FLAG M2	Sigma	F1804
HSC70	Santa Cruz	sc-7298
HSP60	ATCC	HSP60
MCAD	Santa Cruz	sc-49047
MHC Type I	Sigma	M8421
MHC Type IIa	ATCC	sc-71
MHC Type IIb	ATCC	BF-F3
MTHFD2	Abcam	ab56772
mTOR	CST	2972
pmTOR	CST	2971
NDUFA9	Molecular Probes	459100
NDUFB8	Abcam	ab110413
OAT	Abcam	ab137679
P62	Abnova	H00008878-M01
PYCR1	Abcam	ab94780
RPS6	Biomol	A300-557A-M
pRPS6	CST	2211
SDHA	Mitosciences	MS204
SDHB	Abcam	ab110413
SHMT2	Abcam	ab224428
TOMM20	Santa Cruz	sc-17764
TUBULIN	Calbiochem	CP06
UQCRC1	Molecular Probes	459140
UQCRC2	Abcam	ab110413
VDAC1	Abcam	ab14734

2.6.5 BN-PAGE

Blue native gel electrophoresis (BN-PAGE) was performed according to the guidelines published previously (Wittig et al. 2006).

Isolated mitochondria (50-100µg) were lysed in 50µL BN-PAGE lysis buffer (50mM NaCl, 50mM imidazole, 2mM 6-aminohexanoic acid, 1mM EDTA, pH 7.0) with 6g digitonin/g mitochondrial protein for 15 min on ice. Insolubilized material was removed by centrifugation at 20,000x g for 20 min and the supernatant was mixed with 10x Loading dye (50% glycerol, 5% Coomassie) for a final detergent/dye ratio of 8g/g. 10-20µL of samples were loaded on 4-16% native acrylamide gels (Life Technologies) and electrophoresis was performed at 4°C for 30 min at 150V and 4h at 250V in an electrophoresis chamber (Invitrogen).

After completed electrophoresis, proteins were transferred onto an equilibrated PVDF membrane in western blot transfer buffer without SDS and methanol at 4°C for 16h at constant 120mA current.

After completed transfer, the membrane was shortly de-stained in methanol, blocked for 1h in 5% milk PBST and incubated with specific antibodies for 2h at room temperature. Further incubations/washes and signal detection were performed as described for SDS-PAGEs.

2.6.6 *In gel* complex IV activity assay

In-gel complex IV activity assays were performed as to the guidelines published previously (Wittig et al. 2007). After completed BN-PAGE, the gels were shortly washed and incubated in complex IV activity buffer (50mM Na_3PO_4, 25mM 3,3'-diaminobenzidine, 50µL cytochrome c, pH 7.2) for 30 min at room temperature. The gel was cleared with water and documented with a transparency scanner.

2.6.7 Whole tissue proteomics

For label-free protein quantification, tissues were harvested, frozen in liquid nitrogen and ground to fine powder. The tissue was resuspended in protein extraction buffer (Heart: 50mM HEPES, 0.1M NaF, 10mM Na orthovanadate, 10mM EDTA, 100mM NaCl, 1% Triton X-100, 0.2% SDS, pH 7.4, Skeletal muscle: 50mM Tris-HCl, 150mM NaCl, 1% NP-40, 1mM EDTA, 0.1% Na deoxycholate) with protease inhibitor cocktail and lysed for 30 min on ice with protease inhibitors present. Proteins were further

acetone-precipitated at -20°C overnight and resuspended in 8M urea (in 50mM TEAB) using a Bioruptor (Diagenode).

Protein concentration was determined using Bradford reagent and 50µg of protein was used for in-solution digestion. Protein reduction was performed with DTT at a final concentration of 5mM and incubation for 1h at room temperature. For alkylation, CAA was added to 40mM and incubated for 30 min in the dark. Lys-C protease was then added at 1:75 ratio to protein content and incubated for 4h at room temperature. Final protein digestion was achieved with trypsin at 1:75 ratio in ≤2M urea TEAB buffer at room temperature overnight.

Following protein digestion, samples were loaded onto SDB RP StageTips using standard procedure and submitted to the CECAD proteomics facility for mass-spectrometry measurement and MaxQuant analysis of the data.

2.6.8 N-terminome profiling

Terminal amine isotope labelling of substrates (TAILS) was performed at the Forschungszentrum Jülich in collaboration with Dr. Fatih Demir and Dr. Pitter F. Huesgen as described previously (Demir et al. 2017). In short, 1mg of isolated heart mitochondrial proteins were denaturated in 6M GuaHCl and purified with MeOH/$CHCl_3$ extraction. Samples were reduced with DTT (10mM) and alkylated with IAA (30mM) and labelled with light formaldehyde ($^{12}CH_2O$ for *Clpp*$^{+/+}$) and heavy formaldehyde ($^{13}CD_2O$ for *Clpp*$^{-/-}$) in 20mM cyanoborohybride overnight at 37°C. The labelling was quenched with Tris-HCl (100mM) and the pH was adjusted to 6-7. Three WT/KO pairs were pooled at equal protein amounts. Proteins were again purified with MeOH/$CHCl_3$ extraction and dissolved in 100mM HEPES pH 7.5. Trypsin digestion was performed overnight at 1:100 ratio to the protein mixtures.

Dialyzed HPG-ALD II polymer was added to bind non-labelled amines that result from trypsin digestion, which were removed through a 10 kDa cut-off spin filter column. The flow-through was collected (TAILS) and loaded onto C18 Stage-Tips as described in section 2.6.7. A small amount of collected samples was subjected to SDS-PAGE and silver staining for validation.

2.6.9 Cell lysis and co-immunoprecipitation of CLPP-FLAG fusion proteins

The transfected cells were lysed for 45 min each in 300µL IP buffer (Thermo) on ice and incubated with 30µL equilibrated α-FLAG M2 magnetic beads (Sigma) over night at 4°C on a rotating wheel. On the next day, the beads were collected with a magnetic tube rack and washed 4 times with IP buffer. Unbound proteins (flow-through, FT) and the first washing solution (W_1) were collected for the validation experiment. Proteins bound to the beads were eluted with 70µL Elution buffer (Thermo) and neutralized with 10µl 1M Tris/HCl pH 7.5. All collected samples were frozen in liquid nitrogen and stored at -80°C until further processing.

2.6.10 Co-IP eluate proteomics/verification

For the validation of the immune-purification, 1% of lysate (L), 1% of flow-through (FT), 1% of washing buffer (W_1) and 10% of the elution (E) were subjected to SDS-PAGE and western blot as described in section 2.6.4. For western blot detection, α-FLAG M2, -CLPX, -C1QBP, -TOMM20 and -ACTIN antibodies were used.

2.6.11 *In organello* translation assay

In organello translation assays were performed as described previously (Szczepanowska et al. 2016). 1.5mg freshly isolated heart mitochondria were resuspended in 1mL translation buffer (60µg/mL amino acids [Ala, Arg, Asp, Asn, Glu, Gln, Gly, His, Ile, Leu, Lys, Phe, Pro, Thr, Trp, Val], 25mM HEPES, 100mM mannitol, 10mM succinate, 80mM KCl, 5mM $MgCl_2$, 1mM KH_2PO_4, 5mM ATP, 20µM GTP, 6mM creatine phosphate, 60µg/mL creatine kinase, 60µg/mL cysteine, 60µg/mL tyrosine pH 7.4) with 7µL ^{35}S-methionine and rotated for 1h at 37°C. ^{35}S-translation buffer was removed by centrifugation at 12000x g and mitochondria were resuspended in translation buffer without ^{35}S-methionine. The samples were divided into two parts (pulse and chase) and centrifugated again. The pulse sample was resuspended in 100µL Laemmli buffer and kept for 30 min at room temperature. The chase sample was resuspended again in 500µL translation buffer and rotated for 3h at 37°C before it was resuspended in Laemmli buffer as well.

10µL of each sample was loaded on a 15cm long 15% acrylamide SDS gel and run at constant 80V in a Hofer electrophoresis chamber overnight. The gel was shortly washed, fixed in 50% methanol, 10% acetic acid for 30 min and stained with

Coomassie solution. De-staining of the background with 20% methanol, 10% acetic acid was performed until the background was clear but loaded proteins were still visible. The gel was further placed on whatman paper and dried for 2h at 80°C in a gel dryer before it was documented as the loading control of the assay. A hyper-screen film was put directly onto the gel and incubated at -80°C in a film cassette for 12h to one week with several image acquisitions in between.

2.6.12 *In vitro* enzyme activity assays

Enzyme activities were measured as described previously (Spinazzi et al. 2012). In short, frozen heart samples were homogenized in 10mM potassium phosphate buffer (pH 7.4) using a glass douncer and subjected to 3 cycles of freezing in liquid nitrogen and thawing at 37°C to break the cells and mitochondrial membranes. Protein concentration of the homogenate was determined with Bradford solution and 50µg of protein was used for the assay.

For complex I activity, the decrease in NADH absorbance (340nm) was followed. Heart homogenate in assay buffer (20mM K_2HPO_4, 0.2mM NADH, 1mM NaN3, 1mg/mL BSA, pH 8.0) was incubated at 30°C for 10 min, followed by base-line activity measurement for 2 min. Maximal complex I activity was initiated by the addition of CoQ_1 (50µM) and the absorbance was recorded for 2 min. Complex I-independent NADH oxidation was recorded after the addition of rotenone (5µM) for 2 min. Relative activity was determined by calculating the slope (10 measuring points) during maximal activity and subtracting the slope after rotenone addition.

For complex II activity, the decrease of oxidised DCPIP absorbance (600nm) was followed. DCPIP is an artificial electron acceptor, which oxidises CoQ_1H_2 and loses its blue colour when reduced. Heart homogenate was pre-incubated in assay buffer (50mM K_2HPO_4, 1.5mM KCN, 0.1mM DCPIP, pH 7.0) and succinate for 30 min. Base-line activity was recorded for 2 min at 30°C and the assay was started by the addition of CoQ_1 (50µM). Complex II-independent activity was determined with malonate (10mM). The relative activity was calculated as for complex I.

Both complex activities were further normalized to the activity of citrate synthase. Citrate synthase activity was determined by coupling the production of CoA-SH to the reduction of DTNB and recording the absorbance of the product TNB (412nm). Heart homogenate was incubated in assay buffer (75mM Tris-HCl, 0.1mM DTNB, 0.4mM Acetyl-CoA, 0.1% Triton X-100, pH 8.0) at 30°C for 2 min and the assay was started by the addition of oxaloacetate (0.5mM). The relative activity was calculated as for the complexes, except for the normalization that used the baseline activity instead of specific inhibitors.

2.6.13 Respirometry

Respiration measurements were performed as described previously (Becker et al. 2018). 50µg of freshly isolated heart mitochondria or 30µg of skeletal muscle mitochondria were added to calibrated oxygraphy chambers (OROBOROS instruments) filled with respiration medium (120mM sucrose, 50mM KCl, 20mM Tris-HCl, 1mM EGTA, 4mM KH_2PO_4, 2mM $MgCl_2$, 0.1% BSA pH 7.2). For parallel ROS measurements, 20µM AmR, 1 U/mL HRP, 5 U/mL SOD and 0.1µM H_2O_2 was added to the chambers as well. For complex I-dependent respiration, pyruvate (2mM), malate (0.8mM) and glutamate (4mM) was added to the chambers and respiration was started by the addition of ADP (2mM). Complex II-dependent respiration was started by the addition of succinate (4mM), followed by the inactivation of complex I with rotenone (0.2µM). Leak respiration was measured by the inhibition of ATP-synthase with oligomycin (1µM) and complex II-driven maximal respiration was achieved via the titration of FCCP (0.05µM increments) until no more uncoupling could be observed. Residual oxygen capacity respiration (ROX) was measured by the addition of antimycin A (1µM) and resulted in non-detectable respiration (not shown).

2.6.14 NAD^+/NADH quantification

For NAD^+/NADH quantification, the "Total NAD and NADH Assay Kit (Colorimetric)" (Abcam) was used according to manufacturer instructions. For heart and muscle tissue, 10µg of protein lysates were de-proteinized with 10kDa cut-off spin columns (Abcam) and used for the assay.

2.6.15 Amino acid quantification

Amino acid quantification of skeletal muscle samples was performed at the CECAD Lipidomics facility as described before (Murru et al. 2019). In summary, frozen tissue was lyophilized and homogenized in acetonitrile, 0.3% formic acid solution and mixed with internal standards of isotope-labelled amino acids. Amino acids were then derivatized with 6-aminoquinolyl-N-hydroxysuccinimidyl carbamate using the AccQ-Tag Ultra Derivatization kit and quantified using a Core-Shell Kinetex C18 column and a QTRAP 6500 triple quadrupole/linear ion trap mass spectrometer (SCIEX) and normalized to protein content.

2.6.16 Metabolomic quantification

Anionic metabolite quantification of skeletal muscle samples was performed at the CECAD Lipidomics facility as described in (Schwaiger et al. 2017). In summary, frozen tissue was lyophilized and homogenized in 75% MeOH, 0.2% formic acid solution mixed with internal standards (D_4-SUC, ^{13}C-ATP and ^{13}C-G6P for TCA-cycle metabolites, nucleotides and sugars, respectively). A Dionex Integrion HPIC system (Thermo Scientific) was used for anion-exchange chromatography and separation was conducted on a Dionex IonPac AS11-HC column at 30°C with a potassium hydroxide gradient. High-resolution mass spectrometry was conducted on a high field Thermo Scientific Q Exactive HF quadrupole-Orbitrap mass spectrometer and metabolite quantities were normalized to the protein content.

2.7 Molecular Biology

2.7.1 Isolation of DNA from tissues

For genotyping, ear biopsies were lysed in 500µL tail DNA lysis buffer (100mM Tris-HCl, 5mM EDTA, 200mM NaCl, 0.2% SDS, 0.2 mg/mL Proteinase K, pH 7.4) at 55°C with constant shaking until all tissue was dissolved. DNA was precipitated with 500µL 2-propanol and washed once with 70% ethanol. The DNA was resolved in 150µL dH_2O and stored at 4°C until used. For high purity DNA isolation of skeletal muscles, a small piece of tissue was lysed in 600µL DNA isolation buffer (100mM NaCl, 10mM EDTA, 20mM Tris-HCl, 0.5%SDS, 0.2 mg/mL Proteinase K pH 7.4) at 55°C with constant shaking until all tissue was dissolved. RNA was degraded with RNase A (100µg/mL) at 37°C for 30 min and phenol-chloroform extraction of DNA was performed with the

addition of 600µL PCI. The aqueous phase was collected and DNA was precipitated with 250µL of 8M ammonium acetate and 600µL 2-propanol. After centrifugation at 15000x g for 15 min at 4°C the pellet was washed with 70% ethanol and the dry pellet was resuspended in 100µL ultra-pure water. For complete dissolving, the samples were stored at 4°C overnight and the DNA concentration was adjusted to 10ng/µL.

2.7.2 Genotyping

For genotyping PCRs, the following PCR mix was prepared:

1µL DNA

1µL Fw primer (10mM)

1µL Rv primer (10mM)

1.2µL $MgCl_2$ (25mM)

2µL dNTP mix (1.25mM each)

4µL 5x Polymerase Buffer

0.05µL GoTaq Polymerase

10µL ddH_2O

All PCRs were run at the following program:

- 5 min 95°C

For 30 cycles:

- 30 sec 95°C
- 15 sec annealing [°C]
- 60 sec 72°C

Final extension:

- 10 min 72°C
- Cool-down to 4°C

The following primer were used (Cre was used independent of the driving promoter):

Table 2.3: Primer sequences and annealing temperatures for genotyping PCRs

PCR	Fw Primer [5'-3']	Rv Primer [5'-3']	Annealing
Cre	CACGACCAAGTGACAGCAAT	AGAGACGGAAATCCATCGCT	52°C
Sdha	TGAAGGACAGTAGTCACTAGATCAG	TAAAGGAACCTACTGGTGCTCTAAT	52°C
Clpp	GTGGATGATGGTCAGTAGAATCC	CCCAGACATGATTCCTAGCAC	58°C
R26	CTGCCCGAGCGGAAACGCCACTGAC	CCTGGACTACTGCGCCCTACAGA	60°C
Neo	GCTAACCATGTTCATGCCTTC	CGTTGGCTACCCGTGATATT	52°C

2.7.3 mtDNA quantification

mtDNA levels in skeletal muscles were determined as described previously (Quiros et al. 2017). In summary, RNA-free DNA from skeletal muscles was used for qPCR as described in section 2.7.5. For quantification, ND1 and 16S rRNA DNA levels were quantified and normalized to HK2 DNA levels (nDNA control).

2.7.4 Isolation of RNA from tissues and cDNA synthesis

For RNA isolation, an approximal 3 mm^3 piece of tissue was homogenized in 1mL Trizol reagent with a FastPrep homogenizer (MP Biomedicals) and ceramic beads and incubated for 5 min at room temperature. After addition of 200µL chloroform and centrifugation at 12000x g for 15 min at 4°C, the aqueous phase containing the RNA was collected and precipitated with 500µL 2-propanol. The RNA was pelleted and washed with 75% ethanol and shortly dried before resuspending it in 50µL ultra-pure water and incubation at 60°C for 10 min. The RNA concentration and purity were determined with a NanoDrop spectrophotometer and samples were stored at -80°C.

For cDNA synthesis, 10µg RNA was treated with DNase according to the manufacturers instruction and the RNA concentration was adjusted to 200ng/µL. Using the reverse transcription kit, 2µg RNA was used for cDNA synthesis in a PCR machine with the following program:

- 10 min 25°C
- 120 min 37°C
- 5 sec 85°C
- Cooldown to 4°C

The cDNA was adjusted to a final concentration of 25ng/µL and 50ng were used for a test PCR for the endogenous control HPRT (not shown).

2.7.5 mRNA quantification via qPCR

For mRNA quantification, 50ng cDNA and the Brilliant III Ultra-Fast SYBR Green qPCR Master Mix kit (Agilent technologies) were used according to the manufacturer's instruction. The following program was run on a 96well qPCR thermocycler (ABI):

- 3 min 95°C

For 40 cycles:

- 5 sec 95°C
- 15 sec 60°C

dissociation curve:

- 15 sec 95°C
- 1 min 60°C
- 15 sec 95°C

$2^{-\Delta\Delta Ct}$ was used to calculate foldchanges and mRNA levels were normalized to the endogenous controls.

Table 2.4: Primer sequences for qPCRs

PCR	Fw Primer [5'-3']	Rv Primer [5'-3']
ND1	CTAGCAGAAACAAACCGGGC	CCGGCTGCGTATTCTACGTT
16S rRNA	CCGCAAGGGAAAGATGAAAGAC	TCGTTTGGTTTCGGGGTTTC
HK2	GCCAGCCTCTCCTGATTTTAGTGT	GGGAACACAAAAGACCTCTTCTGG
4Ebp1	GGGGACTACAGCACCACTC	CTCATCGCTGGTAGGGCTA
Afg3L2	GTTGATGGGCAATACGTCTGG	GACCCGGTTCTCCCCTTCT
Atf4	GCAAGGAGGATGCCTTTTC	GTTTCCAGGTCATCCATTCG
Chop	TGCCTTTCACCTTGGAGAGACGG	CGCAGGGTCAAGAGTAGTGAAGG
Cdkn1a	CCTGGTGATGTCCGACCTG	CCATGAGCGCATCGCAATC
ClpX	CTTCGCTGTCCTAAATGTGGT	CCAACAACATACTTGTCGAGGT
Cox4i2	CTGCCCGGAGTCTGGTAATG	CAGTCAACGTAGGGGGTCATC
Fbxo32	CAGCTTCGTGAGCGACCTC	GGCAGTCGAGAAGTCCAGTC
Fgf21	GTGTCAAAGCCTCTAGGTTTCTT	GGTACACATTGTAACCGTCCTC
Fh1	GGTCATCAAAATTGGGCGAAC	CTTGCTGAACGTAACCACTGAA
Gadd45a	CCGAAAGGATGGACACGGTG	TTATCGGGGTCTACGTTGAGC
Gdf15	GAGCTACGGGGTCGCTTC	GGGACCCCAATCTCACCT
Glut1	TCAGGCGGAAGCTAAC	GGAGGAAACATGCAGTCATC
Gpd2	CACTAGATGCCGTCACCAGAG	GAAGGGCTTCTTTCACCATCC
Hprt	GCCCAAAATGGTTAAGGTT	TTGCGCTCATCTTAGGCTTT
Hsp60	GCCTTAATGCTTCAAGGTGTAGA	CCCCATCTTTTGTTACTTTGGGA
Klf15	CCATTGCCGCCAAACCTATTG	AACTCATCTGAGCGGGAAAAC
Lars	GAAAGCAGTGCTAAACCTGGA	CACTATGTCGTCATCAGAGAGC
Lias	CCTGGGGTCCCGGATATTTG	GAAGGTCTGGTCCATTATGCAA
Lonp1	ATGACCGTCCCGGATGTGT	CCTCCACGATCTTGATAAAGCG
Mthfd2	CTGAAGTGGGAATCAACAGTGAG	GTCAGGAGAAACGGCATTGC
Nars	GAGCTGTATGTATCTGACCGAGA	AAATGGTGGGAAATGGCTCTTT
Ogdh	GTTTCTTCAAACGTGGGGTTCT	GCATGATTCCAGGGGTCTCAAA
Pgc1α	TATGGAGTGACATAGAGTGTGCT	CCACTTCAATCCACCCAGAAAG
Trim63	GTGTGAGGTGCCTACTTGCTC	GCTCAGTCTTCTGTCCTTGGA
Vdac1	CCCACATACGCCGATCTTGG	GCTGCCGTTCACTTTGGTG
Vdac2	CTCCACCCTATGCTGACCTC	CCCGCTAACTTTACCAGTGTCT

2.8 Histology and Imaging

2.8.1 Formaldehyde fixation and paraffin embedding of tissues

Liver and skeletal muscle tissues were fixated overnight in 4% PBS-buffered formaldehyde solution at 4°C. Dehydration was performed automated using the following gradient: 2h 50% EtOH, 2h 75% EtOH, 1h 96% EtOH, 2x 2h 100% EtOH, 2x 2h in 100% xylol. Tissues were embedded in paraffin wax (Paraplast) for 1h, 2h and 1h.

5µm histological sections were produced using a microtome and transferred onto poly-L-lysine glass slides for the following staining procedures:

2.8.2 Hematoxylin and Eosin (H&E) staining

For morphological analysis, 5µm formaldehyde-fixated paraffin tissue sections were deparaffinized and hydrated. Sections were incubated for 4 min in Mayer's hematoxylin solution and washed for 15 min in running water. Counterstaining was performed with eosin solution for 1 min, washed with water and sections in 95% EtOH and 100% EtOH for 2 min each. Section were further cleared in xylol and mounted with Entallan.

2.8.3 PAS staining for glycogen detection

For glycogen content determination, 5µm formaldehyde-fixated paraffin tissue sections were deparaffinized and hydrated. The sections were further oxidised in 0.5% periodic acid for 5 min and incubated in Schiff reagent for 15 min. Excess solution was removed with running water for 5 min and the sections were counterstained with Mayer's hematoxylin solution for 1 min. Excess solution was again removed with running water for 5 min and sections were dehydrated and mounted as described for the H&E staining procedure.

Glycogen is stained in a deep red/purple colour, while the background is stained blue.

2.8.4 Tissue fixation and transmission electron microscopy (TEM)

Freshly isolated skeletal muscle tissue was minced into 5-10 small pieces and fixated in glutaraldehyde buffer. Sample preparation, contrasting and cutting have been performed at the CECAD imaging facility and image acquisition has been performed together with the facility.

2.9 Image processing and data analysis

Western blot films were scanned using an Epson V800 transparency scanner at 800dpi 16Bit colour depth. Histology sections were imaged with an SCN400 slide scanner (Leica) at 40x magnification and TEM images were taken with a JEOL JEM2100PLUS microscope and a OneVew (GATAN) camera. Adobe Photoshop was used to crop pictures, adjust contrast (globally to the entire scan) and remove remaining inscriptions from scanned films. Adobe Illustrator was used for figure arrangement and model illustrations.

Graphpad Prism 8 was used for graphs and charts and statistical analyses as indicated in the figures. Instant clue (University of Cologne) was used for the heatmap illustration of the hierarchical clustering.

3 Results

3.1 Role of succinate dehydrogenase in muscle metabolism

Many (mouse) models with loss of functions of mitochondrial proteins directly or indirectly affect the respiratory chain and thus ATP production. Typically, the pathological phenotype was therefore prematurely also ascribed to the lack of ATP in the past. Recently, however, it became obvious that other incidents such as the shortage of essential metabolites or an overactive stress response can substantially contribute to the progression of the phenotype or the patient outcome (Birsoy et al. 2015, Sullivan et al. 2015, Wang et al. 2018). To further elucidate the intertwined role of mitochondrial metabolism and energy homeostasis, a striated muscle-specific deletion of the catalytically active complex II subunit SDHA was developed in C57BL6N mice using ACTA-Cre-mediated recombination.

3.1.1 *SDHA^{MKO}* mice exhibit multisystemic phenotypes

SDHA was deleted in embryonic and adult myocytes and knockout mice (*Sdha^{MKO}*) survived until 4.5 weeks of age (Figure 3.1 B) with severe muscle loss and growth retardation (Figure 3.1 A and C). From 3 weeks of age, *Sdha^{MKO}* mice exhibited markedly less voluntary movement, loss of white adipose tissue, as well as clear signs of hypoglycaemia (Figure 3.1 D). Glycogen storages in muscles, evidenced by PAS staining of quadriceps sections, revealed no difference between the two genotypes, confirming that glycogen does not primarily serve as a source for ATP production *in vivo* (Figure 3.1 E) (Ortenblad et al. 2013).

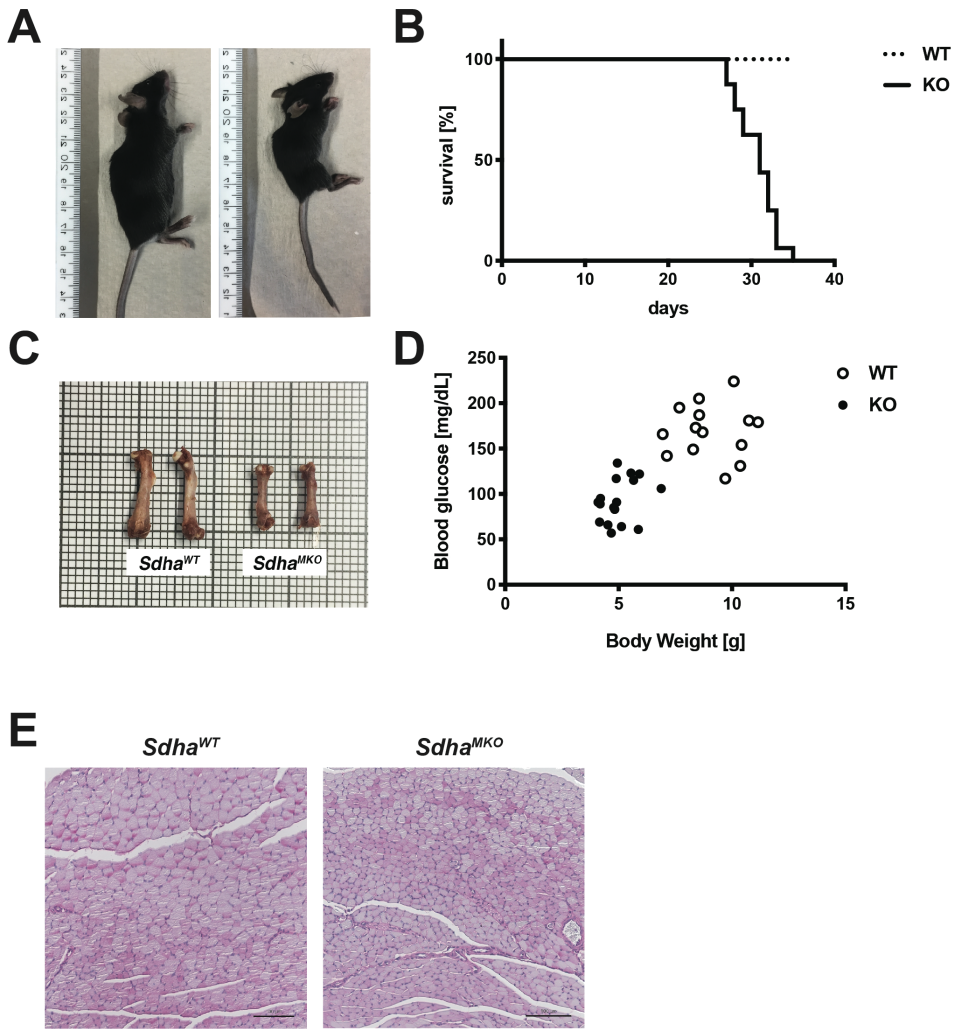

Figure 3.1 *Sdha*^{MKO} mice have reduced body and muscle mass with low blood glucose levels
(A) Photograph of wild type and *Sdha*^{MKO} mice at the age of 4 weeks. (B) Survival rate of *Sdha*^{MKO} mice. (C) Photograph of wild type and *Sdha*^{MKO} femur bones at the age of 3 weeks on 1mm² squares. (D) Blood glucose concentration and bodyweight of 3 weeks old mice. (E) PAS staining of wild type and *Sdha*^{MKO} quadriceps muscle sections at the age of 3 weeks. Data presented as individual points.

3.1.2 Loss of SDHA only affects complex II of the respiratory chain

Surprisingly, isolated muscle mitochondria had normal levels of respiratory chain proteins and complexes (Figure 3.2 A and B) and showed comparable respiratory capacity when supplemented with pyruvate, malate and glutamate in the respiration medium (Figure 3.2 C). Despite residual levels of SDHA protein in the *Sdha*^{MKO} knockout muscles (Figure 3.2 A), no SDH complexes or succinate-driven respiration (Figure 3.2 C) was detected in *Sdha*^{MKO} muscle mitochondria. In line with unaltered complex I-dependent respiratory function and normal respiratory chain subunit abundance, mtDNA levels were also comparable between wild type and *Sdha*^{MKO} muscles (Figure 3.2 D).

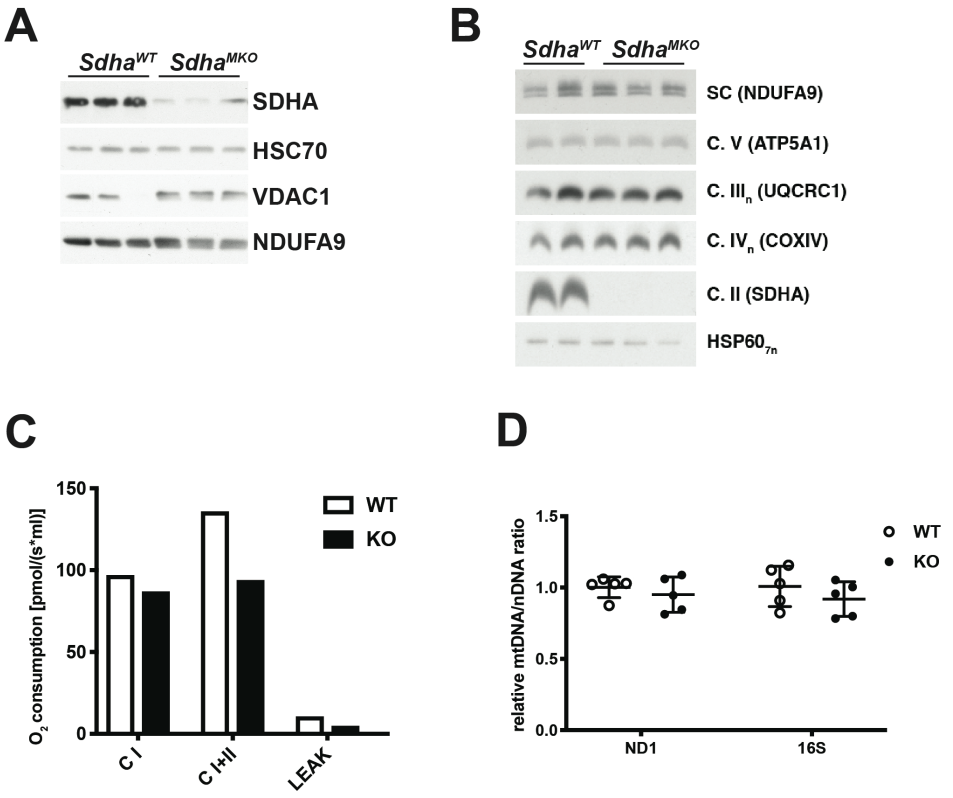

Figure 3.2 Loss of SDHA in skeletal muscle tissue only affects SDH levels and function
(A) Western blot analysis of quadriceps muscle lysates. (B) BN-PAGE analysis of muscle mitochondria. Antibodies against SDHA and respiratory chain subunits were used as indicated. HSC70, VDAC1 and $HSP60_{7n}$ were used as loading controls. (C) Respirometry of muscle mitochondria (n=1). (D) mtDNA quantification with qPCR of quadriceps muscles at the age of 4 weeks (n=5). HK2 DNA was used for normalisation. Data presented as individual bars or points with mean ± SD.

3.1.3 *SDHA^{MKO}* muscle fibres show increased atrophy at early stages

To investigate the physiological consequences of the complex II deficit in muscles in an unbiased way, label-free protein quantification of muscle lysates was performed at 3 weeks of age. Gene ontology enrichment analysis revealed a profound down regulation of processes related to cytosolic translation and an increase of (stress related) mRNA processing and extracellular matrix proteins. Additionally, lysosomal proteases and proteins associated with cell death were among the highest up-regulated proteins in *Sdha^{MKO}* quadriceps muscles (Table 3.1).

Table 3.1: GO-Term analysis of 3 weeks old quadriceps muscle proteomics

GO Term	Mean FC $log2_{(KO/WT)}$
aminoacyl-tRNA synthetase multienzyme complex	-1.02726
cytosolic large ribosomal subunit	-0.883524
polysomal ribosome	-0.821117
cytoplasmic translation	-0.816493
small ribosomal subunit	-0.677551
rRNA processing	-0.662523
cytosolic small ribosomal subunit	-0.59881
chaperonin-containing T-complex	-0.595175
endoplasmic reticulum lumen	-0.550944
structural constituent of ribosome	-0.458166
chaperone-mediated protein folding	-0.457449
translation	-0.435888
ribosome	-0.423367
ER to Golgi vesicle-mediated transport	-0.412481
endoplasmic reticulum-Golgi intermediate compartment	-0.394036
vesicle-mediated transport	-0.303095
endoplasmic reticulum membrane	-0.274995
actin cytoskeleton	0.268035
chromosome	0.274773
focal adhesion	0.309418
basolateral plasma membrane	0.34969
extracellular matrix	0.389771
cell adhesion	0.392051
mRNA processing	0.393653
catalytic step 2 spliceosome	0.399639
nuclear matrix	0.402953
caveola	0.411069
RNA splicing	0.433265
stress fiber	0.469216
spliceosomal complex	0.481776
nuclear inner membrane	0.567994
microvillus	0.616359
myosin complex	0.646945
collagen trimer	0.769881

In order to further investigate the responses elicited from affected muscles, gene expression of classical stress markers and muscle homeostasis were investigated in muscles of 3 weeks old mice. In line with an increased abundance of lysosomal proteases, *Sdha*^{MKO} muscles strongly induced the expression of ATF4- and FOXO3A-dependent atrophy markers (Figure 3.3 A), but surprisingly only increased *Atf4* mRNA expression as a stress response. Other members of the integrated stress response, such as *Chop*, *Fgf21*, *Gdf15* or *Mthfd2* were unchanged or even showed reduced expression in *Sdha*^{MKO} muscles (Figure 3.3 B). Histologically, *Sdha*^{MKO} quadriceps muscle fibres were comparable in size and did not show any signs of tissue damage (Figure 3.3 C). The absence of centralised nuclei further indicated that at least no tissue regeneration, which is commonly associated with mitochondrial defects in muscles, occurred in *Sdha*^{MKO} muscles. In line with this observation, ultrastructure of knockout muscle fibres and mitochondria was unaltered as well. The swollen and or cristae-lacking mitochondria frequently observed in e.g. complex I (Civiletto et al. 2015) or complex IV (Viscomi et al. 2011) mutant muscles could not be seen (Figure 3.3 D). While a clear fibre type switch was not observed, *Sdha*^{MKO} quadriceps muscles had increased protein levels of both, fast and slow twitching myosin heavy chain isoforms (Figure 3.3 E). This increase was not recapitulated by skeletal alpha actin (ACTA1) and the effects of this imbalance are currently unknown.

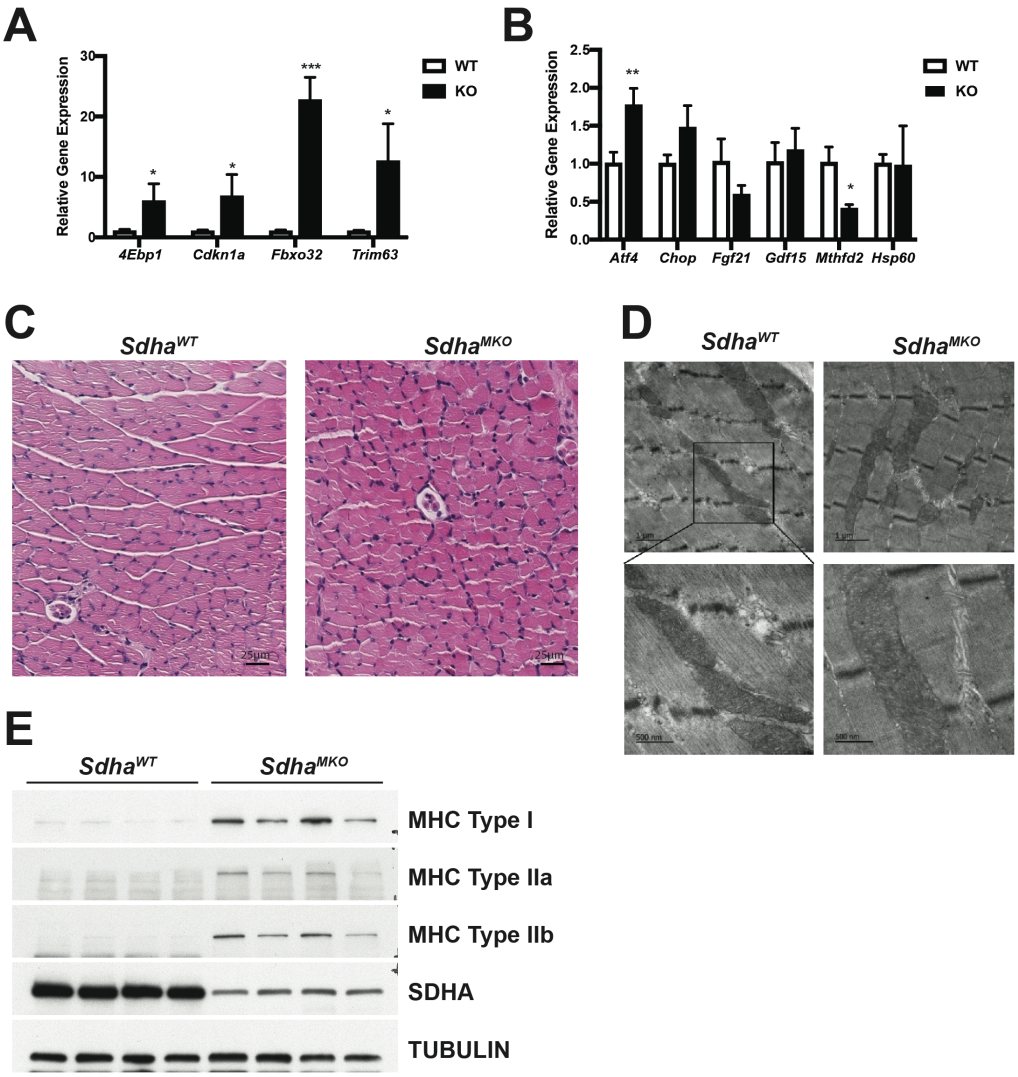

Figure 3.3 *Sdha*^{MKO} muscles display normal morphology and initiate an atrophic response at 3 weeks of age

(A) Relative expression levels of atrophy related genes with qPCR (n=5). (B) Relative expression levels of integrated stress response genes with qPCR (n=5). (C) H&E staining of 3 weeks old quadriceps muscle sections fixated in formaldehyde and embedded in paraffin. Scale bars 25µm. (D) Ultrastructure analysis of 3 weeks old quadriceps muscles using transmission electron microscopy. Scale bars: top 1µm, bottom 500nm. (E) Western blot analysis of skeletal muscle lysates for fibre type compositions. Antibodies were uses as indicated and TUBULIN was used as loading control. Data presented as mean ± SD (* P<0.05, ** P<0.01, *** P<0.001; multiple t-tests corrected with the Holm-Sidak method).

3.1.4 Increased mitobiogenesis in *SDHA^{MKO}* muscle fibres at late stages

Due to the possibility of a delayed stress response, animals were additionally analysed at 4 weeks of age, at which all animals displayed strongly reduced movement and signs of tremor as well as piloerection. Surprisingly, at this timepoint the expression of atrophy markers and *Atf4* were blunted (Figure 3.4 A). Furthermore, an isolated induction of *Chop* and *Gdf15* expression was observed at this age (Figure 3.4 B). Despite the extended time of observable phenotype, no increased expression of *Fgf21*, *Mthfd2* or *Klf15* could be detected (Figure 3.4 B). This absence of an integrated stress response was further confirmed on protein level, were also other markers such as SHMT2 or ALDH18A1 were unaltered in the *Sdha^{MKO}* knockout (Figure 3.4 C). Despite the severe muscle loss at this age, no changes in P62 levels were observed, arguing against autophagy as a main driver of atrophy. Fasting is a known trigger of autophagy-mediated muscle wasting (Bujak et al. 2015), however, muscles lacking complex IV activity were reported to have inhibited autophagy (Civiletto et al. 2018). Unlike the before mentioned markers, both MTHFD2 and PYCR1 levels were even strongly decreased compared to wild type tissue (Figure 3.4 C). To identify the main pathways affected at this age, label-free quantification of muscle proteins was again performed. While cytosolic translation was still the main overall down-regulated pathway, at this age, *Sdha^{MKO}* muscles displayed a strong accumulation of mitochondrial and peroxisomal proteins, especially regarding enzymes involved in fatty acid oxidation (FAO) (Figure 3.4 D and E). Although the sarcomere structure of muscle fibres was still not affected in *Sdha^{MKO}* muscles, the increased mitochondrial mass can be attributed to large accumulations of intermyofibrillar mitochondrial aggregations observed in *Sdha^{MKO}* muscle TEM sections (Figure 3.4 F). These clusters sporadically appeared within the fibres and seemed to be unfused congestions of mitochondrial entities that still displayed morphologically correct cristae structures. Increased mitochondrial mass was further confirmed by the accumulation of soluble and membrane bound mitochondrial proteins on western blots (Figure 3.4 G).

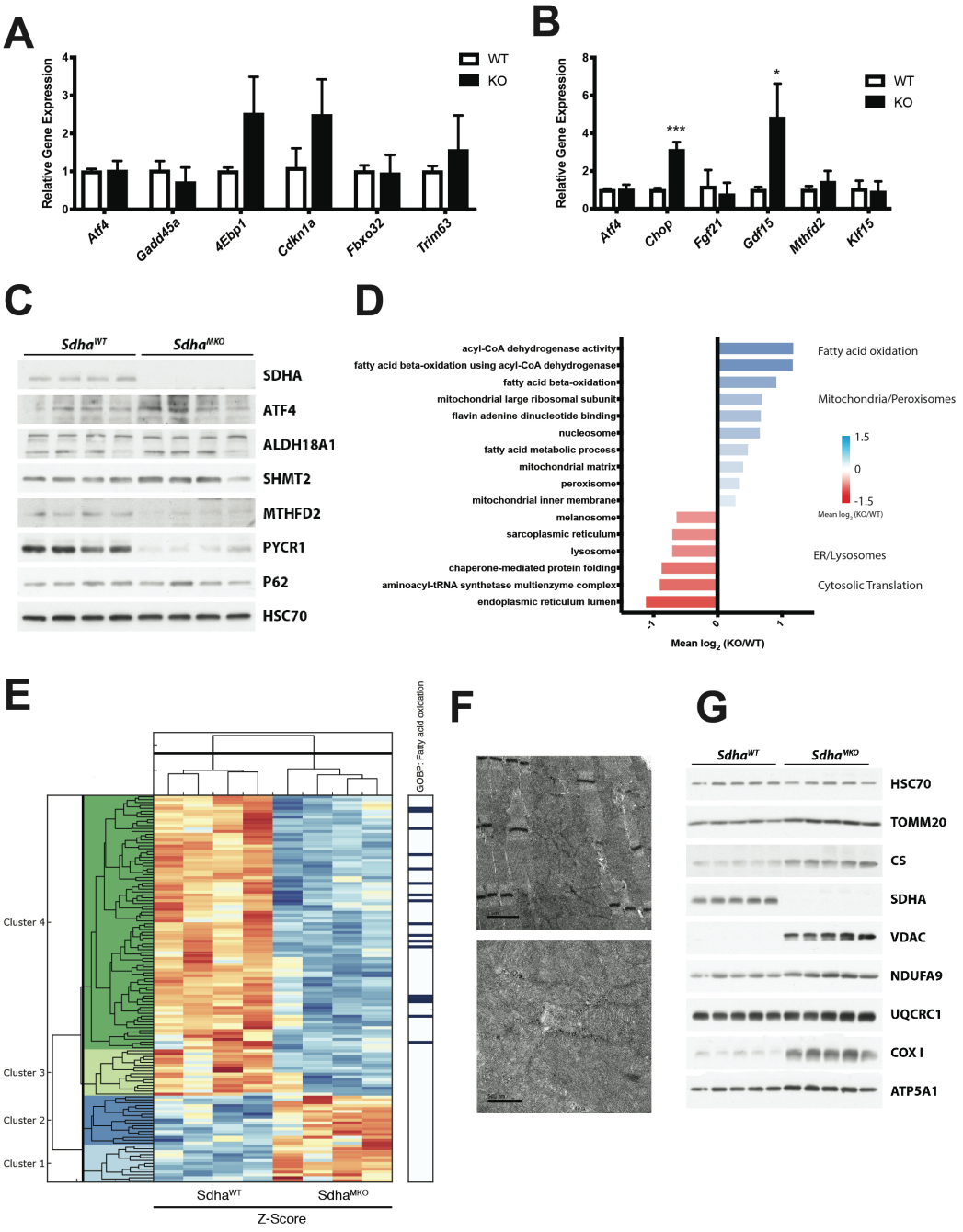

Figure 3.4 *Sdha*^{MKO} muscles have increased mitobiogenesis at 4 weeks of age
(A) Relative expression levels of atrophy related genes with qPCR (n=5). (B) Relative expression levels of integrated stress response genes and *Klf15* with qPCR (n=5). (C) Western blot analysis of skeletal muscle lysates for proteins of the integrated stress response. HSC70 was used as loading control. (D) GO-Term analysis of label-free quantifications of quadriceps lysates at 4 weeks of age. (E) Hierarchical clustering of mitochondria annotated proteins from label-free quantifications. GOBP: Fatty acid oxidation annotated proteins are depicted on the right site. (F) Ultrastructure analysis of 4 weeks old *Sdha*^{MKO} quadriceps muscles using transmission electron microscopy. Scale bars: top 1µm, bottom 500nm. (G) Western blot analysis of skeletal muscle lysates for mitochondrial proteins. HSC70 was used as loading control.

3.1.5 Metabolic changes drive AMPK-dependent NAD⁺ accumulation in *SDHA^{MKO}* muscles

To understand the underlying deficits of *Sdha^{MKO}* animals, isolated muscles were subjected to metabolic and energetic analyses. Typically, in tissues or cells with compromised respiratory chain activity, such as those of *Dars2^{HKO}* or mutator mice, NAD⁺/NADH ratios drop due to the inability to oxidise NADH via complex I of the respiratory chain (unpublished data). *Sdha^{MKO}* muscles, however, displayed increased NAD⁺ levels (Figure 3.5 A), which is in line with unaffected complex I-dependent respiration *in vitro* (Figure 3.2 C). No changes in NADH levels were detected in *Sdha^{MKO}* muscles, arguing for an increase of *de novo* synthesis or salvage of NAD⁺ rather than the inability to reduce NAD⁺. A key enzyme of the NAD⁺ synthesis pathway is nicotinamide phosphoribosyl transferase (NAMPT), which was more abundant in the knockout (3 weeks LFQ log2(KO/WT): 0.59). A well described pathway that regulates NAD⁺ synthesis via NAMPT is dependent on the activity of 5' AMP-activated protein kinase (AMPK). AMPK is an important regulator of skeletal muscle homeostasis and fully active when phosphorylated (pAMPK) and bound to AMP. *Sdha^{MKO}* animals had increased levels of pAMPK at both 3 and 4 weeks of age (Figure 3.5 B) and a decreased energy charge displayed by lower ADP and ATP levels and increased AMP content (Figure 3.5 C), indicating the induction of AMPK activity. All other detected mono-phosphorylated nucleotides were less abundant in *Sdha^{MKO}* muscles (Figure 3.5 D). *De novo* synthesis of any nucleotide is ATP-consuming and dependent on the amino acids glutamine and aspartate, which were among the most severely depleted amino acids in *Sdha^{MKO}* muscles (Figure 3.5 E). Overall amino acid abundance was decreased in *Sdha^{MKO}* muscles (Figure 3.5 E), pointing towards a change in their metabolic usage since they typically do not notably contribute to ATP production (Romijn et al. 1993).

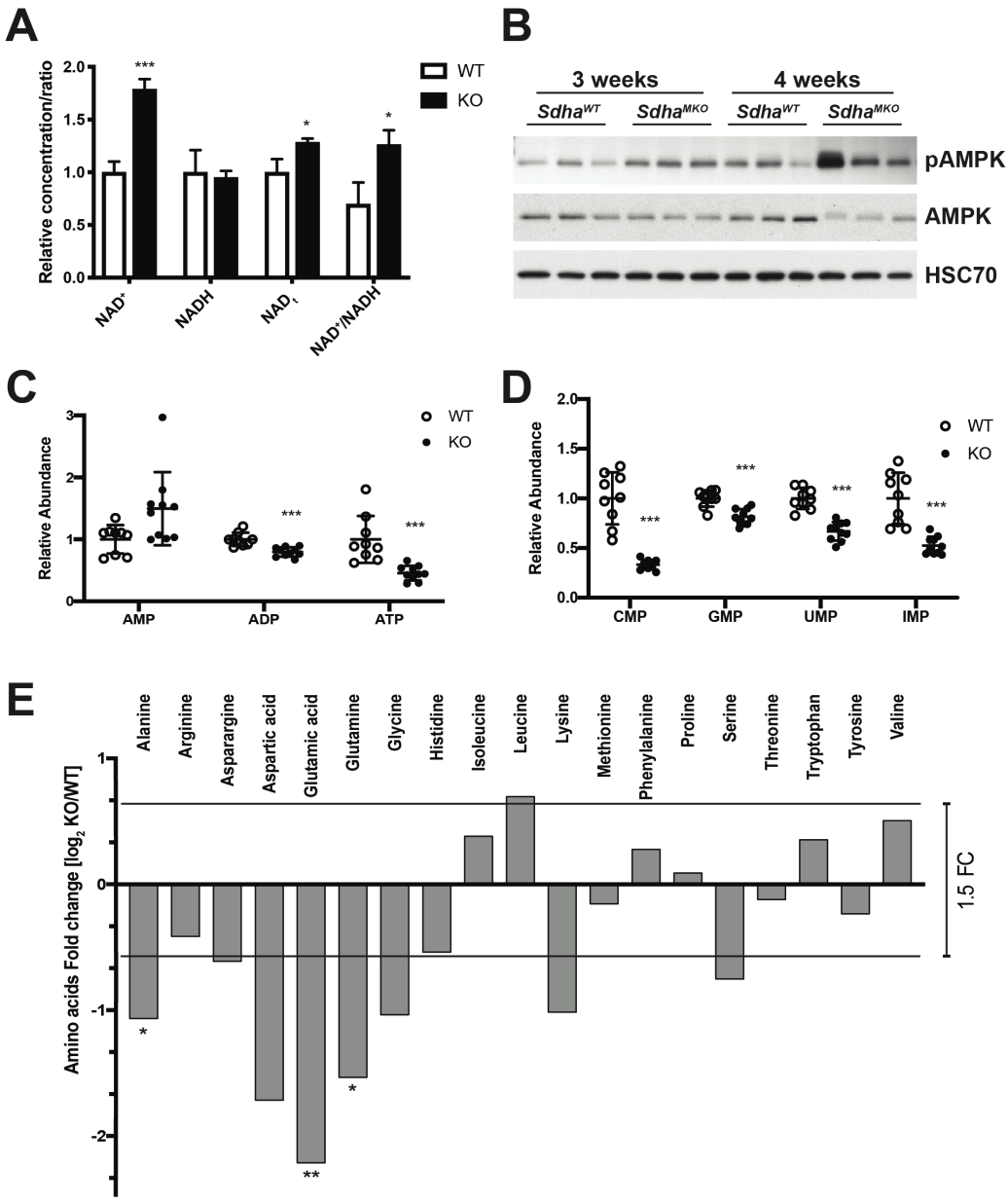

Figure 3.5 Loss of SDHA in muscles causes ATP and amino acid depletion and activates AMPK signalling

(A) Colorimetric quantification of NAD^+/NADH levels in deproteinised skeletal muscle lysates (n=4); NAD_t = total NAD^++NADH. (B) Western blot analysis of skeletal muscle lysates for AMPK and phosphorylated AMPK levels at 3 and 4 weeks. HSC70 was used as loading control. (C) Metabolomic quantification of AMP, ADP and ATP in 3 weeks old muscles (n=9-10). Protein concentration was used for normalisation. (D) Metabolomic quantification of other nucleotides in 3 weeks old muscles (n=9-10). Protein concentration was used for normalisation. (E) Quantification of amino acid levels in 4 weeks old muscles (n=4). Protein concentration was used for normalisation. Data presented as mean ± SD for nucleotides and log2 FC(KO/WT) for amino acids (* P<0.05, ** P<0.01, *** P<0.001; multiple t-tests corrected with the Holm-Sidak method).

3.1.6 AKT and ERK1/2 signalling intensifies the atrophy program in *SDHA^{MKO}* muscles

Excessive AMPK activation in skeletal muscles, such as during prolonged fasting, is a known contributor to muscle wasting due to the phosphorylation and activation of FOXO3A (Thomson 2018), which might be contributing to the atrophy observed in *Sdha^{MKO}* muscles (Figure 3.3 A). To further elaborate on the regulation of atrophy and myogenesis, other implicated kinase pathways were investigated as well. AKT (also known as protein kinase B) is a growth hormone-regulated kinase implicated in numerous biological pathways such as cell cycle/survival, protein synthesis and metabolism (Yu and Cui 2016). Phosphorylated and activated by phosphoinositide 3-kinase (PI3K), AKT phosphorylates FOXO3A, which is also one of AMPK's direct targets. Unlike AMPK, however, phosphorylation by AKT inhibits FOXO3A activity. *Sdha^{MKO}* mice displayed reduced AKT phosphorylation (Figure 3.6 A), which in turn would further strengthen FOXO3A activation by AMPK. In line with reduced AKT activity was also the lack of consistent mTOR activation (Figure 3.6 C), which has been observed in muscles of other mitochondrial dysfunction models (Khan et al. 2017). Myostatin-driven myogenesis in adult muscles is in part mediated by a mitogen-activated protein kinase (MAPK) cascade with the extracellular signal-regulated kinases ERK1/2 as the final kinases. *Sdha^{MKO}* muscles had less phosphorylated ERK1/2 (pERK1/2) independent of their age (Figure 3.6 B), indicating that additionally to increased muscle wasting, hormone induced myogenesis might be repressed. As reported before, ERK2 was the primarily expressed isoform in skeletal muscles (Figure 3.6 B). Similar to mTOR phosphorylation and signalling, eIF2α phosphorylation was unaltered in *Sdha^{MKO}* muscles (Figure 3.6 C), potentially explaining the lack of an integrated stress response signature. At both timepoints *Sdha^{MKO}* muscles had no signs of oxidative damage, however, increasingly accumulated proteins with lysine-acetylation with age (Figure 3.6 D).

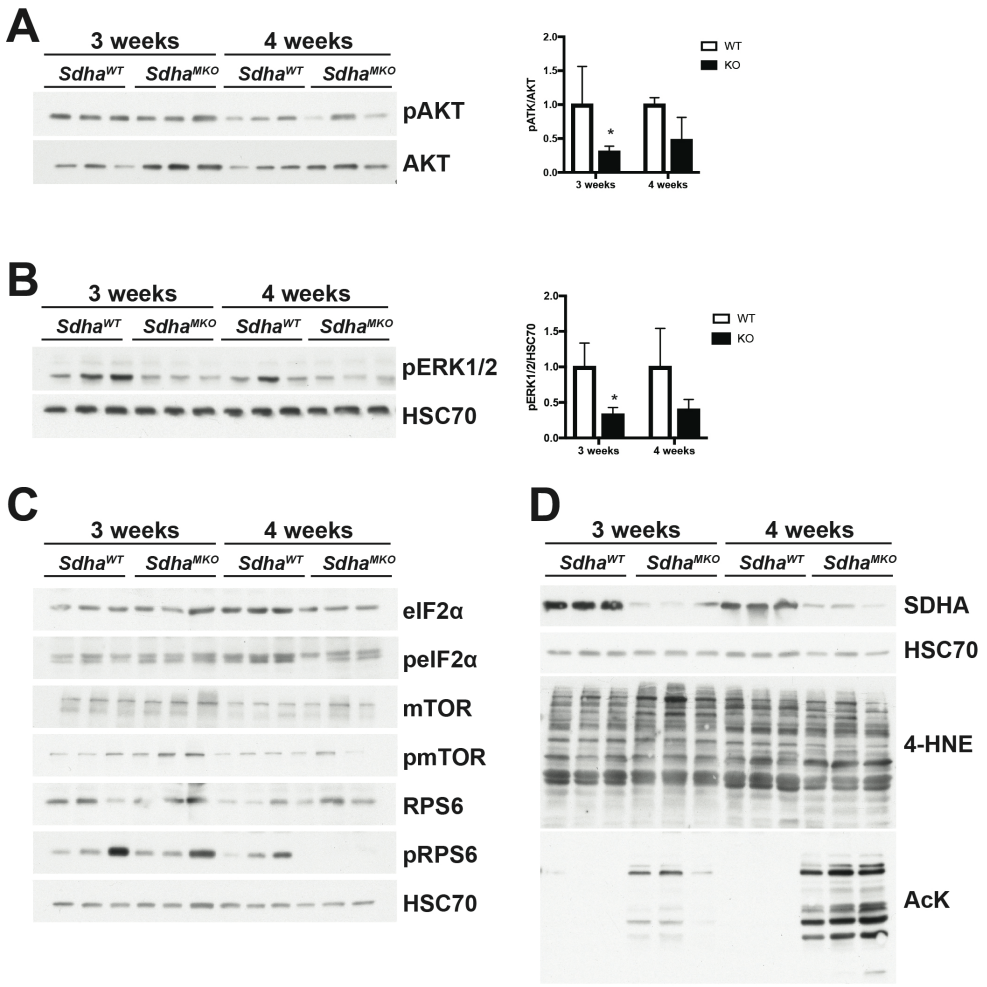

Figure 3.6 *Sdha^{MKO}* muscles have decreased ERK/AKT signalling without affecting mTOR targets
(A) Western blot analysis of skeletal muscle lysates for AKT and phosphorylated AKT levels at 3 and 4 weeks and pAKT/AKT ratio determination with densitometric quantification (n=3). (B) Western blot analysis of skeletal muscle lysates for phosphorylated ERK1/2 levels at 3 and 4 weeks and densitometric quantification (n=3). HSC70 was used as loading control. (C) Western blot analysis of skeletal muscle lysates for (phosphorylated) eIF2a, mTOR and RPS6 levels at 3 and 4 weeks of age. HSC70 was used as loading control. (D) Western blot analysis of skeletal muscle lysates for proteins with HNE modification (4-HNE) and lysine acetylation (AcK). HSC70 was used as loading control. Data presented as mean ± SD (* P<0.05, ** P<0.01, *** P<0.001; multiple t-tests corrected with the Holm-Sidak method).

3.1.7 *SDHA^{MKO}* muscles have no hypoxic response despite succinate accumulation

Most SDHx mutation-derived tumours, as well as cultured cells with impaired SDH function display succinate accumulation due to the inability to actively export the metabolite from the cells. In 3 weeks old *Sdha^{MKO}* muscles, succinate accumulated to around 800 times the wild type level (Figure 3.7 A), whereas most other detected TCA cycle metabolites were unchanged (Figure 3.7 C). Reportedly, increased succinate concentrations inhibit 2-oxoglutarate (2-OG)-dependent dioxygenases such as prolyl hydroxylases (PHDs) that regulate HIF1α stability or the activity of DNA methyl transferases (Bargiela et al. 2018). Therefore, SDHx mutations are commonly associated with a "pseudo-hypoxic" state and hyper-methylated DNA. However, the HIF1α target genes most commonly induced during hypoxia *LonP1*, *Glut1* and *Cox4i2* were all expressed to lesser extend *Sdha^{MKO}* muscles (Figure 3.7 B).

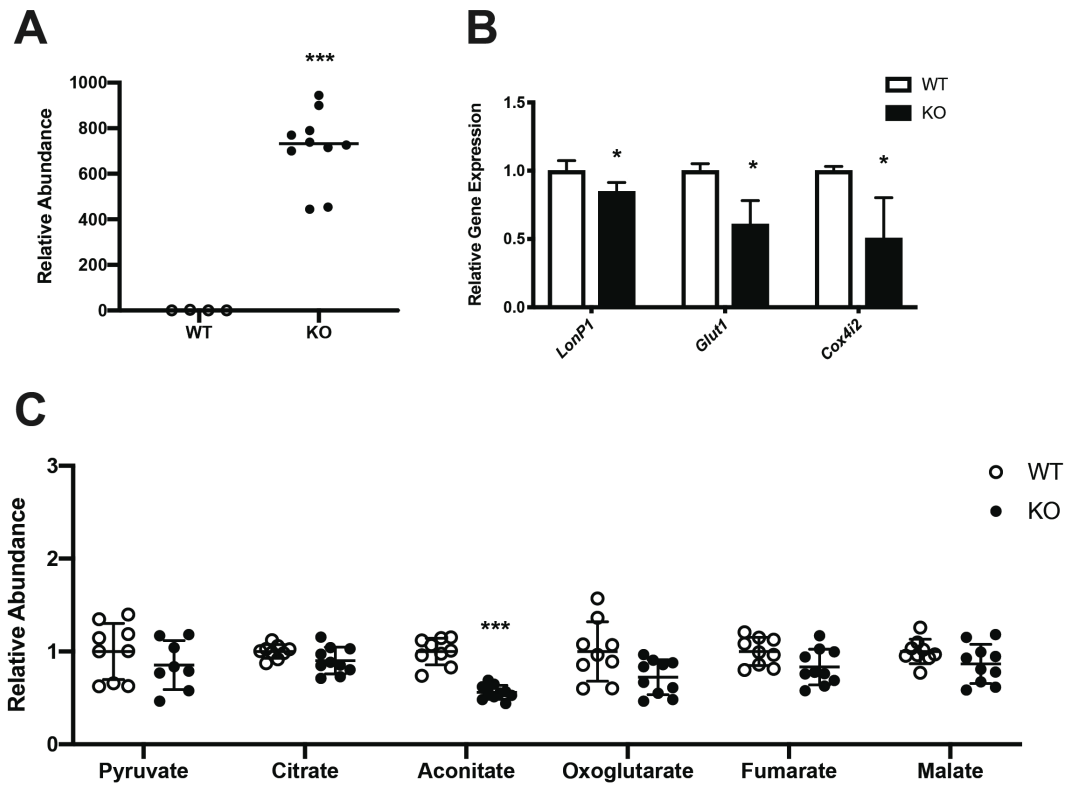

Figure 3.7 Loss of SDHA in muscles causes succinate accumulation without affecting HIF1α targets
(A) Metabolomic quantification of succinate levels in 3 weeks old muscles (n=9-10). (B) Relative expression levels of HIF1α target genes with qPCR (n=5). Metabolomic quantification of TCA cycle metabolite levels in 3 weeks old muscles (n=9-10). Data presented as mean ± SD (* P<0.05, ** P<0.01, *** P<0.001; multiple t-tests corrected with the Holm-Sidak method).

3.1.8 *SDHA^{MKO}* livers are depleted of glycogen storages

During starvation or an energetic crisis, the glucose demand of muscles is initially supplied by the liver and after prolonged time further amended by fatty acid complementation from adipose tissue. To investigate how a skeletal muscle-specific loss of SDHA affects whole body metabolism, liver sections from knockout and control animals were analysed. Similar to muscle fibres, hepatocytes from *Sdha^{MKO}* livers were comparable in size with the overall tissue size being much smaller (Figure 3.8 A). Additionally, these hepatocytes contained less glycogen, indicated by the fainter PAS staining (Figure 3.8 B). Together with the severe loss of white adipose tissue mass, it is apparent that *Sdha^{MKO}* animals show systemic adaptations to supply the compromised muscles with available energy carriers.

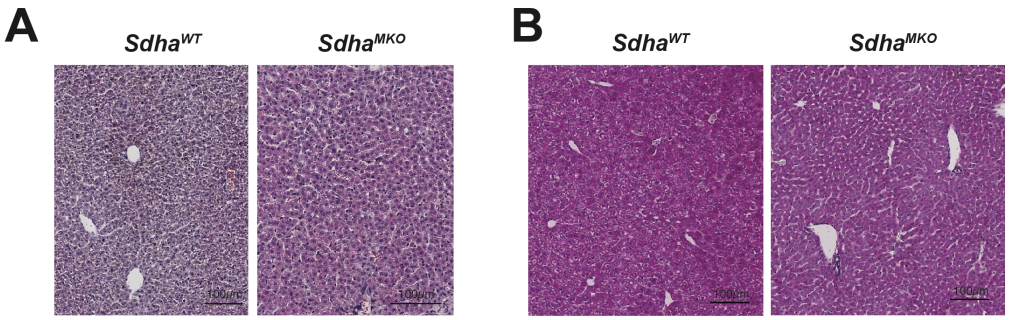

Figure 3.8 Loss of SDHA in skeletal muscles systemically affects hepatic glycogen storage
(A) H&E staining of 3 weeks old liver sections fixated in formaldehyde and embedded in paraffin. Scale bars 100µm. PAS staining of 3 weeks old liver sections fixated in formaldehyde and embedded in paraffin. Scale bars 100µm.

In summary, loss of skeletal muscle SDHA had a profound impact on local ATP production, which triggered a cascade of responses to alleviate the energy crisis, peaking in the complete depletion of all fat reserves. Additionally, systemic alterations of glucose homeostasis and body size, as well as a unique stress response signature could be observed in *Sdha^{MKO}* animals.

3.1.9 *SDHA^{HKO}* hearts lose complex II early in life and develop cardiomyopathy

Although the physiological consequences of a succinate dehydrogenase defect in striated muscles was in part comparable to those caused by other respiratory chain deficiencies, the metabolic and molecular consequences were repeatedly different or in the opposite direction. To understand whether these discrepancies stem from a difference in the investigated tissue, the affected protein, or the combination of both, SDHA was also deleted specifically in heart and skeletal muscles with Ckmm-NLS-Cre-mediated recombination. Using the Ckmm promoter, the primary and eventually fatal defect originates from the heart, allowing it to be used as a model for cardiomyocyte specific gene deletions. Deletion of SDHA in the heart (*Sdha^{HKO}*) caused lethality between 16 and 21 days of age (Figure 3.9 A) with a suddenly occurring, severe cardiomyopathy. *Sdha^{HKO}* animals had increased heart to bodyweight ratios early on (Figure 3.9 B and C) but did not exhibit hypoglycaemia as it was observed in the *Sdha^{MKO}* line (Figure 3.9 D). By the age of 11 days, animals almost completely lost succinate dehydrogenase activity, whereas complex I activity was not affected in the heart (Figure 3.9 F). This loss occurred although SDHA protein levels remained at around 50% of control animals, possibly due to a faster loss of the anchoring subunit SDHB (Figure 3.9 E).

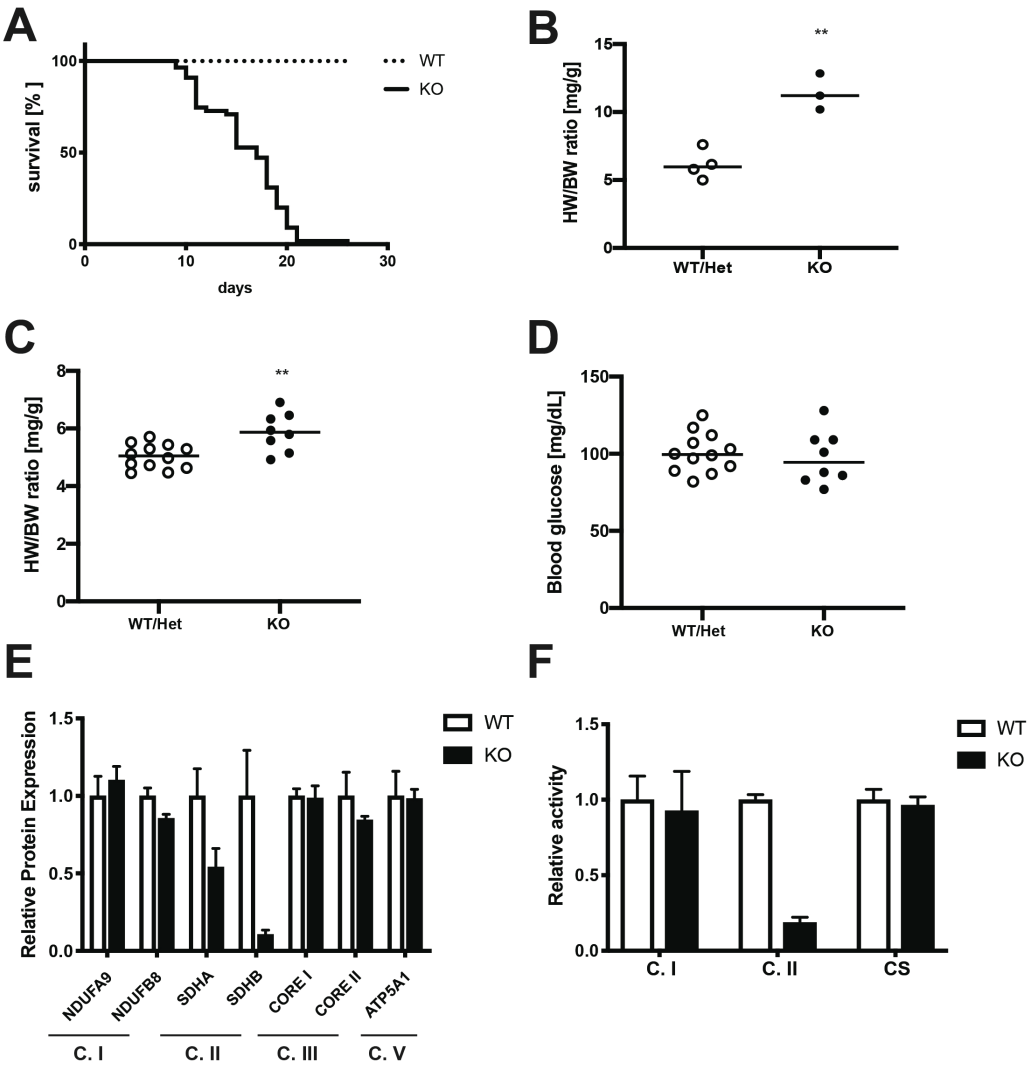

Figure 3.9 Loss of SDHA in cardiomyocytes abolishes SDH levels and function
(A) Survival rate of *Sdha*^{HKO} mice. (B) Heart to body weight ratio of 20 days old *Sdha*^{HKO} mice. (C) Heart to body weight ratio of 11 days old *Sdha*^{HKO} mice. (D) Blood glucose concentration of 20 days old *Sdha*^{HKO} mice. (E) Densiometric quantification of respiratory chain subunits (n=3). Enzyme activities of respiratory chain complex I, complex II and citrate synthase (CS) (n=4). Data presented as individual points or mean ± SD (* P<0.05, ** P<0.01, *** P<0.001; multiple t-tests corrected with the Holm-Sidak method).

3.1.10 *SDHA*^{HKO} heart mitochondria lack complex II activity and lose complex IV at late stages

Similar to muscle mitochondria, mitochondria isolated from *Sdha*^{HKO} hearts showed normal complex I-dependent respiration, whereas succinate driven respiration was largely abolished (Figure 3.10 A). Accompanied with lower respiration levels was also a reduced ROS production during the respiration measurements (Figure 3.10 B). Surprisingly, some *Sdha*^{HKO} hearts at 21 days lost complex IV subunits, complexes and complex activity (Figure 3.10 C-E), an effect that could not be observed in younger animals, even when the cardiomyopathy has progressed severely.

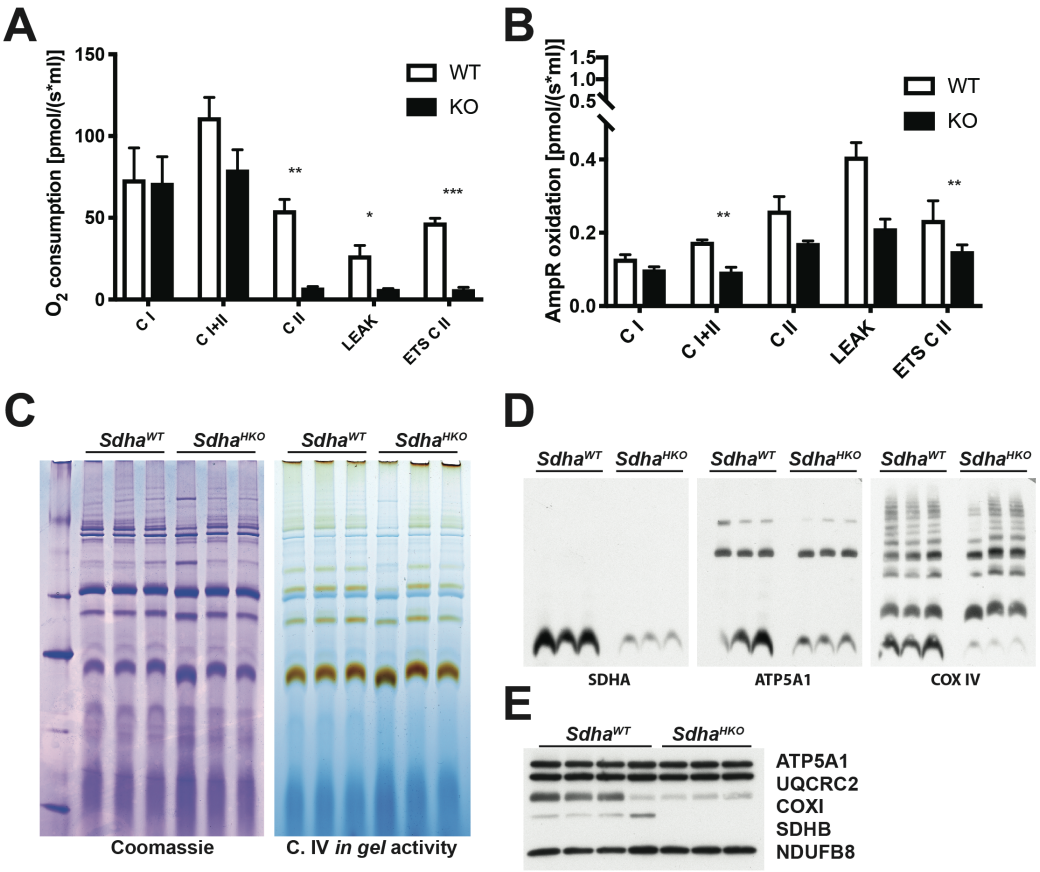

Figure 3.10 *Sdha*^{HKO} heart mitochondria show normal respiration but sporadically lose complex IV at late stages
(A) Respirometry of 19 days old heart mitochondria (n=3). (B) ROS production of 19 days old heart mitochondria determined by AmpR oxidation (n=3). (C) BN-PAGE analysis of 19 days old heart mitochondria with Coomassie staining (left) and complex IV *in gel* activity staining (right). (D) BN-PAGE analysis of heart mitochondria. (E) Western blot analysis of 21 days old heart mitochondria for respiratory chain subunits. Antibodies were used as indicated. Data presented as mean ± SD (* P<0.05, ** P<0.01, *** P<0.001; multiple t-tests corrected with the Holm-Sidak method).

This loss of complex IV subunits was also confirmed with label-free protein quantifications, that showed a clear loss of almost all detected subunits (Figure 3.11 A). Loss of complex IV and the other complex II subunits likely resulted from changes in protein stability or proteolysis, as their mRNA levels were not affected (Figure 3.11 B).

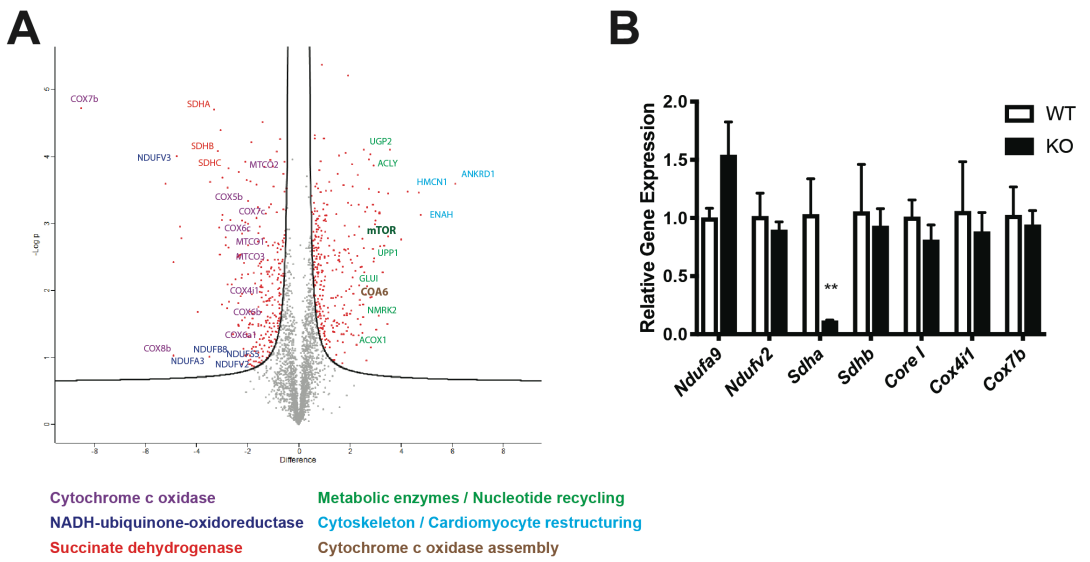

Figure 3.11 *Sdha*^{HKO} heart proteomics and respiratory chain gene expression
(A) Volcano plot of label-free quantification of 21 days old heart lysates. Individual proteins are annotated and the implicated function is noted (bottom) in the same colour. (B) Relative expression levels of respiratory chain subunits with qPCR (n=5). Data presented as mean ± SD (* P<0.05, ** P<0.01, *** P<0.001; multiple t-tests corrected with the Holm-Sidak method).

To exclude a potential role of mitochondrial translation in the loss of complex IV subunits, freshly isolated heart mitochondria were used for *in organello* translation assays, that revealed a mild reduction of translation rates in *Sdha*^{HKO} heart mitochondria for all mitochondria-encoded peptides (Figure 3.12).

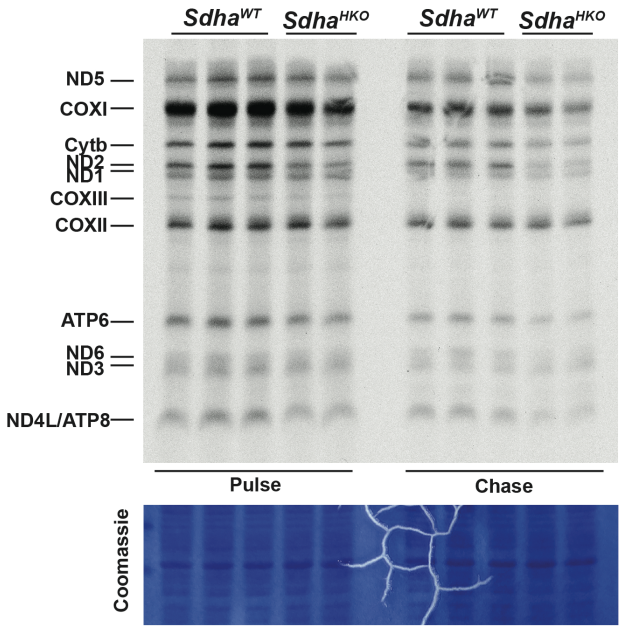

Figure 3.12 Loss of SDHA in the heart mildly disturbs mitochondrial translation
In organello analysis of heart mitochondrial translation from 20 days old wild type and *Sdha*^{HKO} mice. 30 min pulse labelling and 2h chase are presented on an autoradiography screen (top). Mitochondrial encoded peptides run as indicated. Photograph of the Coomassie stained gel as loading control (bottom).

3.1.11 *SDHA*^{HKO} hearts exhibit the classical integrated stress response

Since *Sdha*^{HKO} mice also developed cardiomyopathy when only complex II of the respiratory chain was affected, those animals were also analysed regarding their mitochondrial stress response. Unlike *Sdha*^{MKO} muscles, *Sdha*^{HKO} hearts elicited a clear integrated stress response with *Fgf21*, *Gdf15* and *Mthfd2* being among the highest up-regulated genes analysed in the *Sdha*^{HKO} hearts (Figure 3.13 A). No changes in gene expression were observed for other genes related to mitochondrial membrane-, translation- or metabolism-associated proteins (Figure 3.13 B). These changes were also reflected on the protein level, where MTHFD2/PYCR1 levels increased in *Sdha*^{HKO} hearts (Figure 3.13 C) but enzymes related to fatty acid oxidation (MCAD/ETFDH) remained unchanged (Figure 3.13 D).

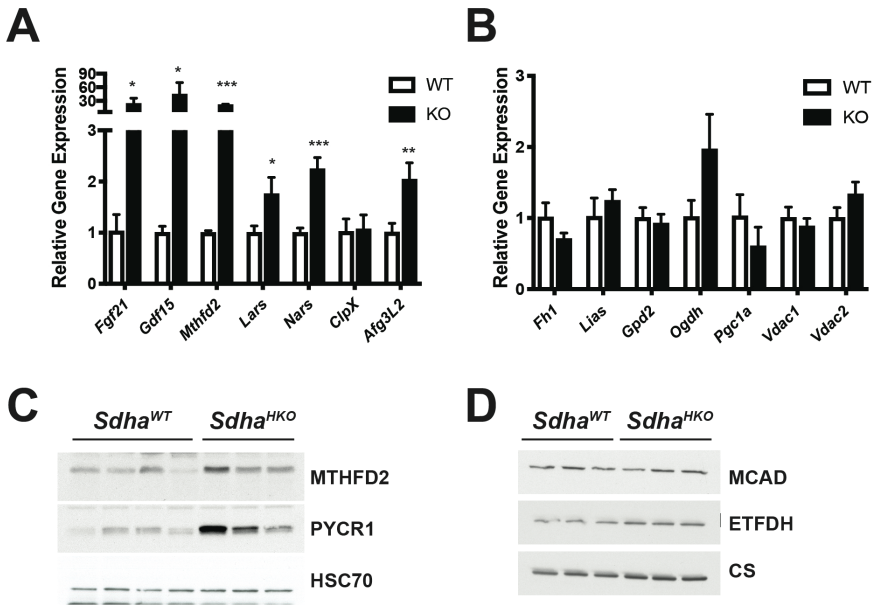

Figure 3.13 *Sdha^{HKO}* hearts exhibit canonical ISR gene expression
(A) Relative expression levels of atrophy related genes with qPCR (n=5) in 20 days old hearts. (B) Relative expression levels of metabolic genes with qPCR (n=5) in 20 days old hearts. (C) Western blot analysis of 20 days old heart lysates for proteins of the integrated stress response. HSC70 was used as loading control. (D) Western blot analysis of 20 days old heart lysates for metabolic proteins. Data presented as mean ± SD (* P<0.05, ** P<0.01, *** P<0.001; multiple t-tests corrected with the Holm-Sidak method).

3.1.12 *SDHA^{HKO}* hearts do not display AMPK-dependent accumulation of NAD$^+$

One of the most striking molecular changes within *Sdha^{MKO}* muscles was the increased NAD$^+$/NADH ratio. To determine if this ratio might influence the observed differences in stress response gene expression, *Sdha^{HKO}* hearts were also analysed for these metabolites. Indeed, no increase in NAD$^+$ levels could be observed in *Sdha^{HKO}* hearts (Figure 3.14 A), in line with unchanged AMPK phosphorylation (Figure 3.14 B). Thus, the AMPK-dependent increase in NAD$^+$ levels is potentially a modulator of the integrated stress response and only the loss of SDHA in skeletal muscles elicited the combination of the physiological phenotype and the non-canonical stress response. Furthermore, unlike *Sdha^{MKO}* skeletal muscles, *Sdha^{HKO}* hearts had increased expression of HIF1α target genes (Figure 3.14 C), indicating a pseudo-hypoxic state.

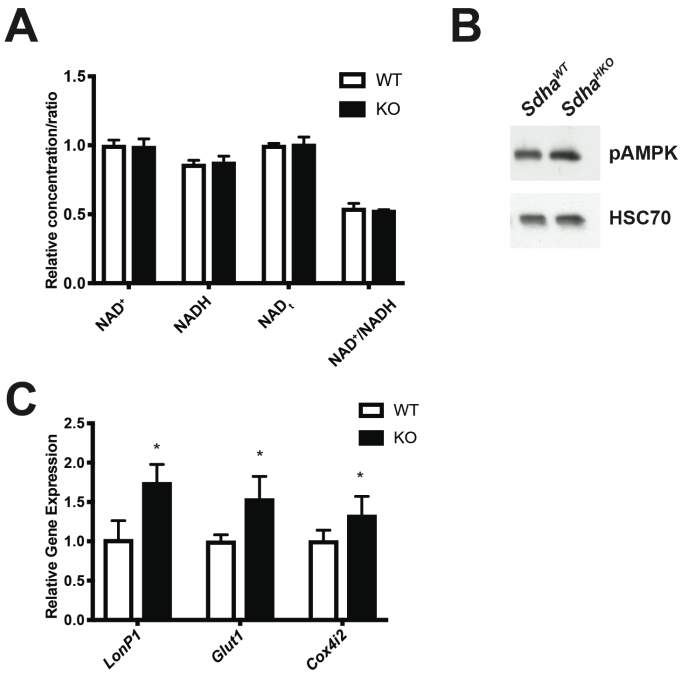

Figure 3.14 Loss of SDHA in the heart does not affect AMPK phosphorylation and NAD⁺/NADH ratios
(A) Colorimetric quantification of NAD⁺/NADH levels in deproteinised heart lysates (n=4). (B) Western blot analysis of heart lysates for phosphorylated AMPK levels at 20 days of age. (C) Relative expression levels of HIF1α target genes (n=5). Data presented as mean ± SD (* P<0.05, ** P<0.01, *** P<0.001; multiple t-tests corrected with the Holm-Sidak method).

Despite the similarity between heart and skeletal muscle tissue, the adaptations to the loss of SDHA, as well as the resulting stress responses were markedly different. Whereas the increased AMP/ATP and NAD⁺/NADH ratios crystalized as the main driver of AMPK-dependent gene expression changes in myocytes, no such alterations were observed in cardiomyocytes with the same underlying deficiency. Further analysis of the cardiomyocyte metabolome is thus necessary to determine which metabolites or ratios evoke the diverse stress responses observed.

3.2 Identification of novel ClpXP substrates *in vitro* and *in vivo*

Mammalian mitochondria harbour >1000 proteins (Calvo et al. 2016), most of which are physically separated from the cytosol and cannot be accessed by its proteostasis machinery. They are thus mostly relying on intrinsic proteases and peptidases to ensure correct processing of imported proteins, removal of damaged or incorrectly folded proteins and adjusting the abundance of proteins with varying necessities. In the mitochondrial matrix, three ATP-dependent protease complexes are in charge of the degradation of non-functional or superfluous proteins. The mAAA and LonP1 proteases were implicated in the removal of membrane-bound and oxidatively damaged proteins, respectively (Bota and Davies 2002, Lee et al. 2017), however, little despite structure and few potential substrates is known about the ClpXP protease.

Previously, *ClpP* knockout mice (*Clpp*$^{-/-}$) were generated and a classical substrate-trapping screen was used to identify some of the first mammalian ClpXP substrates (Szczepanowska et al. 2016), however, many others are likely still unidentified and no recognition mechanism or mode of degradation has been proposed so far. To further elaborate on these shortages, the substrate screen was repeated in triplicates and an independent, unbiased approach was performed to identify N-terminal degradation products and provide further evidence for putative ClpXP substrates. Finally, conditional knockin mice were generated to enable substrate trapping screens *in vivo*.

3.2.1 Bona fide ClpXP substrate identification with N-terminome quantification

Terminal amine isotope labelling of substrates (TAILS) was used to differentially label and quantify N-termini of wild type and *Clpp*$^{-/-}$ mitochondrial proteins (Figure 3.15 A). In total, 1058 termini from 215 mitochondrial-annotated proteins could be detected. 154 of these peptides corresponded to the "expected" N-termini that are predicted to be generated after the cleavage of the mitochondrial targeting signal (MTS). The abundance of the expected N-termini correlated well with the previously published label-free quantification of wild type and CLPP-deficient heart mitochondrial proteomes (Szczepanowska et al. 2016) (Pearson correlation = 0.76), allowing for their use as protein abundance measures. All other N-termini are considered as "unexpected" and reflect degradation products and intermediates. These do not correlate well with total protein abundance (Pearson correlation = 0.31), indicating that mitochondrial protein processing is indeed affected by the loss of CLPP.

Whereas increased abundance in total protein content (LFQ) or expected N-termini in the *Clpp*$^{-/-}$ knockout can be indicative of putative ClpXP substrates, unexpected N-termini have to be interpreted in the opposite direction. If unexpected N-termini are less abundant in the absence of CLPP, they are potentially generated by ClpXP-mediated proteolysis. Sequence logo analysis of these N-termini, revealed a surprising congestion of Arg at the P1 position (Figure 3.15 C). On the other hand, unexpected N-termini that were less abundant in *Clpp*$^{-/-}$ knockout mitochondria did not show any amino acid preference within the cleavage window.

Using differentially abundant N-termini, potential ClpXP substrates can be identified. This approach is not restricted to expected N-termini, however, as unexpected N-termini without the Arg motif can represent ClpXP-independent quality control proteolysis and thus indicate total protein abundance. In agreement with the LFQ approach, increased N-termini abundance of HSPA9, LONP1, MRPS22 and OAT were detected in CLPP-deficient mitochondria (Figure 3.15 B). To verify these putative ClpXP substrates, steady state protein abundance and stability were analysed with western blots and cycloheximide chase experiments, respectively. Whereas three proteins showed strong accumulation in the knockout background on western blots (HSPA9, LONP1 and OAT) (Figure 3.15 D), HSPA9 was also clearly stabilised when

protein synthesis was interrupted, making it the best candidate for a bona fide substrate. LonP1 was not consistently stabilised in these experiments and is mildly induced on mRNA levels (data not shown). Although this does not rule out a protease-substrate relationship, the finding merits further investigation.

Mitochondrial LonP1 (Rendon and Shoubridge 2018), as well as bacterial homologues of ClpXP (Vass and Chien 2013) can process certain substrates at the N-terminus. The suggested mechanisms vary greatly, however, the TAILS dataset was examined for potential signs of substrate processing. No large-scale loss of processed N-termini were detected in CLPP-deficient mitochondria, although PDHA1 N-termini are a promising indication. The expected N-terminus- (like the LFQ) abundance was unaltered in the absence of CLPP, however a second N-terminus 15 amino acids further into the protein was almost absent in the *Clpp*$^{-/-}$ knockout (FC log2(KO/WT): -2.42) (Figure 3.15 E). Unfortunately, the resulting truncated protein could not be detected on western blots, as the size difference is likely too small to be distinguished from the full-length proteoform. Nevertheless, the strong difference in its fold-change suggests that more of low-abundant, and thus undetected mitochondrial proteins could be processed in a ClpXP-dependent manner.

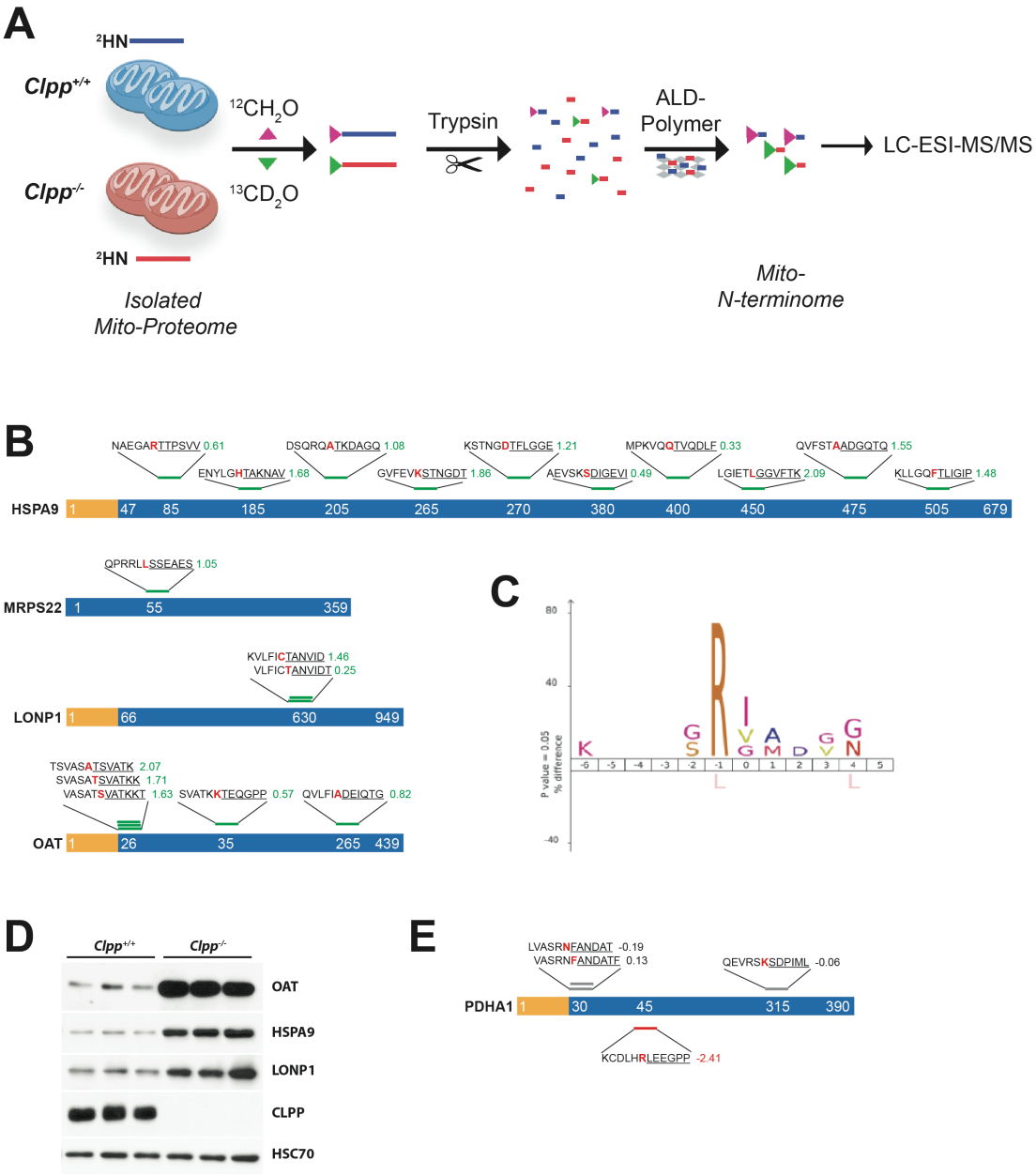

Figure 3.15 TAILS identifies novel ClpXP substrates and a possible cleavage motif
(A) Strategy for TAILS in CLPP-deficient mitochondria. Wild type and knockout mitochondrial proteins were labelled with light and heavy formaldehyde, respectively and digested with trypsin. Internal peptides were removed with an ALD-polymer and labelled peptides were prepared for mass spectrometry quantification. (B) N-termini spectrum of potential ClpXP substrates with increased (green) N-termini. The approximate position within the proteins are indicated by amino acid numbers. The yellow bar represents the MTS and the blue bar the mature protein. Cleavage windows are described for all N-termini detected, with the P1 position highlighted in red and the detected sequence being underlined. Fold-changes (KO/WT) are indicated next to the sequences. (C) Ice-logo of cleavage windows from N-termini significantly less abundant in *Clpp*$^{-/-}$ mitochondria. (D) Western blot analysis of CLPP-deficient heart lysates. Antibodies against CLPP and putative substrates were used as indicated. HSC70 was used as loading control. (E) PDHA1 N-termini spectrum with unchanged (grey) and decreased N-termini (red) in CLPP-deficient mitochondria.

3.2.2 Quantitative substrate trapping in *Clpp*$^{-/-}$ MEFs

The initial substrate trapping screen in mouse embryonic fibroblasts served as a proof of concept for the approach and already resulted in several confirmed ClpXP substrates (Szczepanowska et al. 2016). To further limit the proteins to the most promising substrates candidates, the screen was repeated in triplicates that allowed for a quantitative evaluation (Figure 3.16).

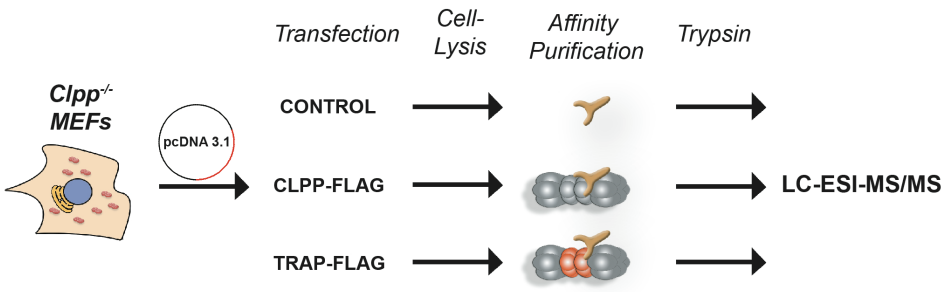

Figure 3.16 Substrate trapping strategy with FLAG-tagged CLPP variants
Three replicates of *Clpp*$^{-/-}$ MEFs were each transfected with plasmids containing control, CLPP-FLAG or TRAP-FLAG for transient expression. Cells were lysed and CLPP-FLAG was affinity purified with a-FLAG M2 bound magnetic beads. Samples were digested with trypsin and prepared for mass spectrometry quantification.

1-10% of the lysate (L), washing (W), flow-through (FT) and elution (E) fractions were pooled and used for evaluation on western blots. As expected, the only two reported interacting proteins CLPX and C1QBP were co-purified with the protease (Figure 3.17 B), while no contamination with cytosolic (ACTIN and HSC70) or mitochondrial (TOMM20) proteins that do not share the same compartment could be detected (Figure 3.17 A and B). This allowed for mass-spectrometry analysis of the elution replicates that resulted in 14 proteins significantly enriched in the affinity purification of inactive CLPP (CLPP-TRAP) over wild type CLPP (CLPP-WT) (Table 3.2). As indicated on the control western blots, CLPX also belongs to this substrate-enrichment category. CLPX steady state protein levels were increased in the absence of CLPP, which was independent of gene expression (Szczepanowska et al. 2016) and the nature of this accumulation is currently unclear. Other potential substrates enriched with CLPP-TRAP include the proteins POLDIP2 and CHCHD2, which were reported to interact with CLPP/CLPX but were not further verified in this work.

Table 3.2 Proteins significantly enriched in CLPP-TRAP over CLPP-WT elutions

Protein name
NDUFV2
CCRN4l
FPGS
MRPL13
MRPL18
MRPL39
SDHB
CLPX
UQCRC1
C1QBP
POLDIP2
CHCHD2
NDUFV1
MRPS22

Excluding the proteins that were not detected in CLPP-WT elutions, UQCRC1 showed the highest enrichment in CLPP-TRAP elutions (FC log2(TRAP/WT): 8.23). This enrichment suggests that UQCRC1 is a strong substrate candidate, however, previous LFQ data showed no changes in protein abundance in the absence of CLPP. This came as a surprise, since increased protein abundance in the absence of the respective protease is the strongest criterium for bona fide substrates.

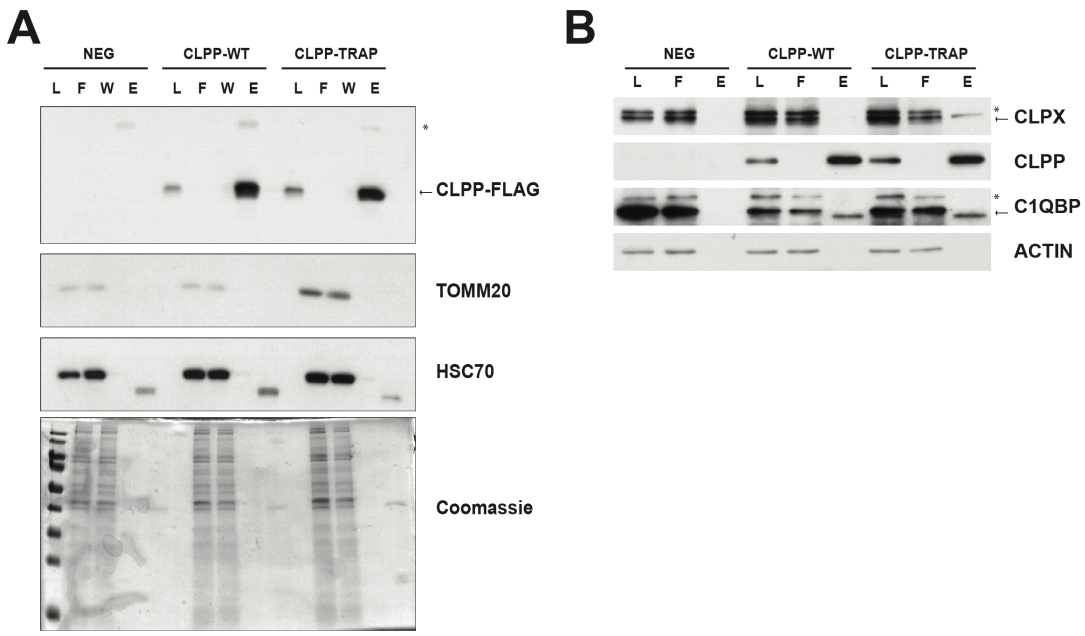

Figure 3.17 CLPP-FLAG is successfully purified from cell lysates along with known interactors
(A) Western blot analysis and Coomassie gel staining of substrate trapping fractions to determine purity and efficiency. (B) Western blot analysis of substrate trapping fractions to determine successful co-purification of CLPP-interacting proteins. Antibodies against CLPP, CLPX and C1QBP were used as indicated. TOMM20, HSC70 and ACTIN were used as controls for mitochondria and cytosolic contaminations, respectively. <- indicates correct protein bands and * represents unspecific staining of IgH from the FLAG M2 antibody in (A) or unspecific bands from CLPX/C1QBP antibodies in (B).

3.2.3 Cooperative proteolysis of UQCRC1

To better understand the underlying interaction between CLPP and UQCRC1, its N-termini abundance was closely analysed in the TAILS dataset. Not uncommon for highly abundant proteins such as subunits of the respiratory chain, 2 expected and 20 unexpected N-termini from UQCRC1 were detected. These can represent degradation intermediates as the abundance of the protein has a direct influence on the abundance of the intermediates and therefore the likelihood of their detection. However, upon close inspection, UQCRC1 N-termini revealed a non-random distribution. In agreement with LFQ data, the abundance of the expected N-termini was not affected by the absence of CLPP. Around the 40 aa, 150 aa and 190 aa position of UQCRC1, three groups of closely congested N-termini with mostly increased abundance were detected in CLPP-deficient mitochondria. These were followed by 5 N-termini with decreased abundance in *Clpp*$^{-/-}$ knockout mitochondria. While the up-regulated N-termini cleavage windows showed no preferences for certain amino acids, all 5 down-regulated termini resulted from cleavage after Arg, as it was proposed for ClpXP earlier (Figure 3.18 A).

The accumulation of a truncated UQCRC1 proteoform in *Clpp*$^{-/-}$ mitochondria was further confirmed on western blots, proving that the detected N-termini exist *in vivo* (Figure 3.18 B). Additionally, UQCRC1 protein levels in *Clpp*$^{-/-}$ cells were stabilised in cycloheximide chase experiments, as it is expected for ClpXP substrates (Figure 3.18 C).

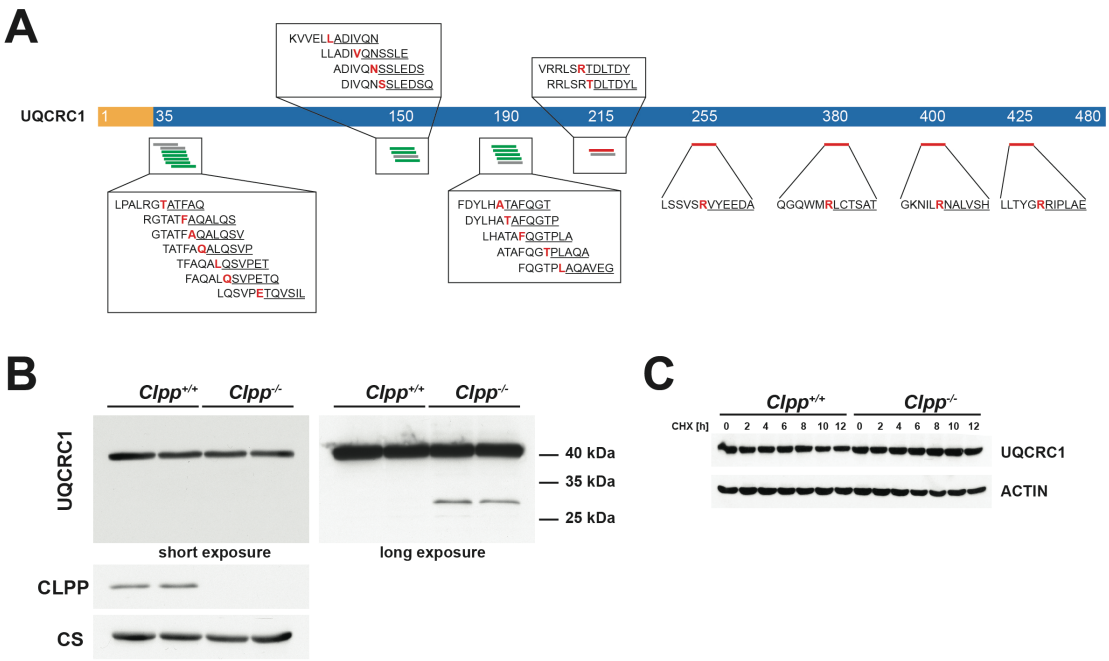

Figure 3.18 Truncated UQCRC1 becomes a substrate for ClpXP-mediated degradation
(A) UQCRC1 N-termini spectrum with increased (green), unchanged (grey) and decreased N-termini (red) in CLPP-deficient mitochondria. The approximate positions within the proteins are indicated by amino acid numbers. The yellow bar represents the MTS and the blue bar the mature protein. Cleavage windows are described for all N-termini detected, with the P1 position highlighted in red and the detected sequence being underlined. (B) Western blot analysis of *Clpp*$^{-/-}$ mitochondria performed by Dr. Karolina Szczepanowksa. (C) CHX-chase experiment for UQCRC1 stability performed by Dr. Karolina Szczepanowksa. Antibodies against CLPP and UQCRC1 were used as indicated. CS and ACTIN were used as loading controls for mitochondria and cell lysates, respectively.

3.2.4 Generation of conditional *ROSA26-CAG::CLPP-FLAG* mice

Surprisingly, the analysis of *Clpp*$^{-/-}$ livers revealed that not all substrates discovered in the heart had increased abundance in the liver and phenotypes such as the compromised mitoribosome assembly were not conserved across tissues (Becker et al. 2018). Thus, using MEFs or any other cell model for substrate trapping screens for the identification of ClpXP substrates is limited in terms of substrate expression in the investigated cell type and in its transferability to other cells or tissues. To overcome this obstacle, an *in vivo* model for substrate screens is axiomatic. To that matter, recent advances in CRIPSPR/Cas9 technologies were utilised for the generation of mice conditionally expressing CLPP-FLAG from the *ROSA26* locus under the strong CAG promoter (Figure 3.19 A). A conditional approach was chosen to overcome the possibility of detrimental effects due to the over-expression of the protease subunit. As a proof of concept, the Ckmm-Cre line was chosen to express CLPP-FLAG in the heart and the resulting mice showed a strong expression of endogenous CLPP and CLPP-FLAG protein. However, no phenotype could be observed in these mice at the age of 10 weeks and known substrates were unaltered by the expression of CLPP-FLAG (Figure 3.19 B). To investigate whether CLPP-FLAG is functionally active *in vivo*, mitochondria were isolated and functional import of the protein was confirmed (Figure 3.19 C). Furthermore, BN-PAGE analysis of these mitochondria revealed that oligomers corresponding to the tetradecameric chamber $CLPP_{14n}$ assembled *in vivo* (Figure 3.19 D). Further experiments, however, are necessary to confirm activity and to identify the underlying mechanism for the lack of substrate processing in the heart.

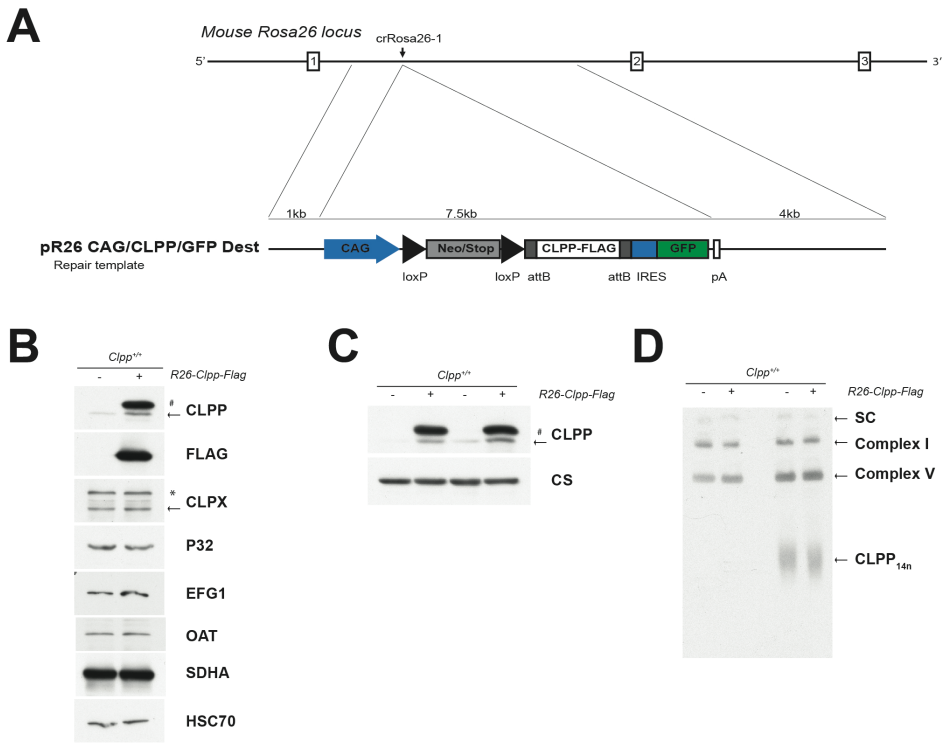

Figure 3.19 Conditional CLPP-FLAG expression *in vivo*
(A) Knockin of a *CAG::CLPP-FLAG-IRES-eGFP* cassette into the *ROSA26* locus for the generation of mice conditionally expressing CLPP-FLAG. (B) Western blot analysis of heart lysates expressing CLPP-FLAG. (C) Western blot analysis of heart mitochondrial extracts expressing CLPP-FLAG. (D) BN-PAGE analysis of heart mitochondrial extracts expressing CLPP-FLAG. Antibodies against CLPP/FLAG, known ClpXP substrates and respiratory chain subunits were used as indicated. <- indicates endogenous CLPP/CLPX, # represents CLPP-FLAG fusion protein and * indicates unspecific CLPX signal.

Together, the proteomic approaches performed further verified multiple substrate candidates suggested before and provided several novel putative substrates of mammalian ClpXP. Additionally, ClpXP was found to participate in cooperative degradation *in vivo* and a novel cleavage site was proposed for mouse CLPP.

Finally, the generation of a mouse model conditionally expressing CLPP-FLAG proved the concept of a potential *in vivo* substrate screen to elaborate on tissue-specific ClpXP function.

4 Discussion

4.1 Loss of SDHA causes energy crisis and triggers tissue-specific stress responses

Mitochondrial (energy) metabolism is essential for almost all eukaryotic cells. *Monocercomonoides sp*. is the only discovered species that adopted a cytosolic iron-sulphur cluster (ISC) synthesis pathway and therefore can also lack mitochondria-related organelles (Karnkowska et al. 2016). All multi-cellular organisms, though, contain some form of mitochondrial organelles, highlighting their importance, even if ATP production is of secondary function. In most cells and especially in tissues of mammalian organisms, these functions cannot be considered independent of each other and mitochondrial disorders may affect metabolic pathways or respiration alike. To further understand how perturbations in mitochondrial energy metabolism affect tissues with different metabolism, conditional knockouts of the succinate dehydrogenase subunit A were developed and analysed with regard to mitochondrial function and stress adaptations/responses. Numerous mouse models that affect different mitochondrial proteins in multiple tissues have been developed in recent years. However, in most cases secondary effects of altered respiration on metabolism and vice versa cannot be ruled out and are therefore indistinguishable. As a TCA cycle enzyme and part of the respiratory chain, SDHA is intimately connected with both respiration and metabolism. If these processes cannot be fully uncoupled, a simultaneous loss of both and its consequences on tissue function is left as the most promising approach to address the issue.

4.1.1 Loss of SDHA causes muscle energy crisis without triggering the ISR

Phenotypically, $Sdha^{MKO}$ mice show the expected signs of mitochondrial dysfunction in skeletal muscles with muscle loss, growth retardation and eventually lethality that was described for many mouse models using muscle-specific mitochondrial perturbations. These include muscle-specific knockouts of COX10, COX15 and TFAM (Wredenberg et al. 2002, Viscomi et al. 2011, Tezze et al. 2017, Peralta et al. 2018). With the exception of muscle-specific OPA1 deletion, that is lethal within 10 days after birth, $Sdha^{MKO}$ mice die earlier than the aforementioned cytochrome c oxidase- or TFAM-depleting models. The poor survival of $Opa1^{MKO}$ mice,

however, might stem from a much shorter protein half-life, as SDHA protein levels are never completely lost even at death. This indicates that the loss of SDHA cannot be compensated for as long as the loss of complex IV, possibly due to a quicker depletion of ATP and energy-storages. An even longer half-life of cytochrome c oxidase subunits seems unlikely, however, cannot be fully excluded as no data at 4 weeks of age or younger were presented for these knockout mice.

The induction of muscle atrophy is very common in all of these mouse models, independent of the studied protein. It was observed upon loss of COX10 or COX15 (Diaz et al. 2005, Civiletto et al. 2015), other mitochondrial proteins such as the mitochondrial calcium uniporter (MCU) (Gherardi et al. 2019) and cytosolic proteins without a direct relevance to mitochondria like in Titin-deficient muscles (Peng et al. 2005). Furthermore, muscle atrophy is also induced by prolonged starvation in the absence of genetic manipulation (Bonaldo and Sandri 2013).

Markedly different, however, is the absence of centralized nuclei in *Sdha*^{MKO} muscles. Centralized nuclei are a hallmark of myopathies and result from satellite cell activation and subsequent fusion of myoblasts with damaged fibres. Central nuclei are thus strictly speaking a sign of muscle regeneration, which is induced by degenerating muscle fibres. This process, however, requires extensive protein translation and cell proliferation (Karalaki et al. 2009), both of which are very energy-demanding processes and attenuated in *Sdha*^{MKO} muscles. Thus, muscle regeneration might not be initiated in these mice. *Acta1*, the gene of which the promoter was used for the muscle-specific *SDHA* knockout, is expressed early during development, but not in satellite cells (Chal and Pourquie 2017). The muscle stem cells themselves should therefore not be directly affected in *Sdha*^{MKO} mice. Nevertheless, a secondary loss of satellite cells was also observed in *Pax7* mutant mice, which lack an important myocyte differentiation marker that is not expressed in satellite cells (Oustanina et al. 2004).

A role for inflammation in the suppression of muscle regeneration (Mourkioti and Rosenthal 2005) cannot be excluded as well, however, no signs of increased immune cell infiltration was observed during histological examination.

Additionally, it is possible that the prolonged hypoglycaemia in *Sdha*^{MKO} mice causes changes in IGF-1 signalling, which is known to restrict muscle regeneration (Winn et al. 2002).

Upon various cellular stresses like ER-stress, mitochondrial stress, or nutrient stress, eukaryotic cells elicit the integrated stress response (ISR), a common signalling cascade that leads to global changes in gene expression in favour of cell survival (Figure 4.1).

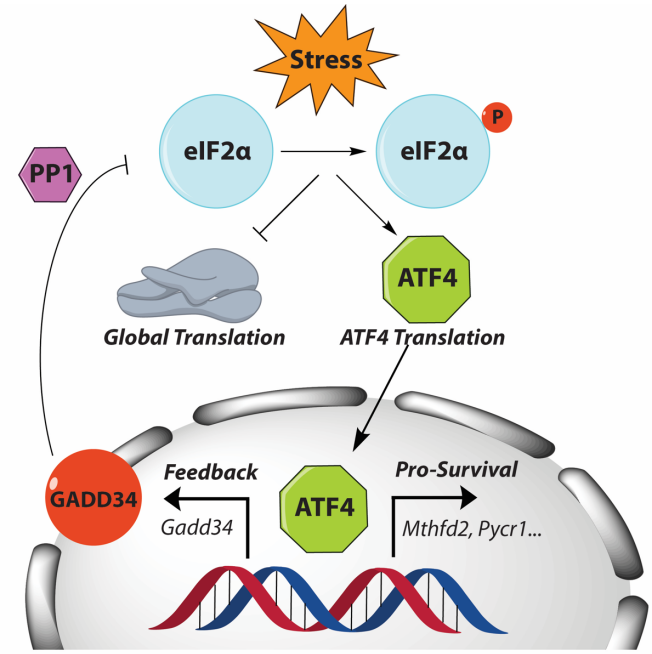

Figure 4.1 Simplified model of the integrated stress response (ISR)
Various stresses, such as nutrient or unfolded protein stress causes the phosphorylation of eIF2α by multiple kinases (not shown). Phosphorylated eIF2α inhibits 5'Cap-dependent protein translation and favours the translation of *ATF4*. Together with co-activators (not shown), ATF4 mediates the transcription of pro-survival genes. The induction of the ISR is self-regulated via GADD34, which inhibits eIF2α phosphorylation together with PP1. Pathway adopted from (Pakos-Zebrucka et al. 2016)

At the core of the ISR is the eukaryotic initiation factor eIF2 with eIF2α as the main regulatory subunit. Under normal conditions, eIF2 plays a main role in the initiation of cytosolic translation. Upon stress, however, eIF2α phosphorylation by various kinases hinders the formation of the initiation complex and therefore halts 5'Cap-dependent translation, while in turn favouring 5'Cap-independent translation. This translation initiation depends on short open reading frames within the 5'UTR that are also present in the mRNAs of the transcription factor ATF4 and one of its co-activators CHOP (Hinnebusch 2011, Palam et al. 2011). These transcription factors in turn

regulate many pro-survival processes like autophagy (B'chir et al. 2013) and proteostasis (Harding et al. 2000). Although it is currently unclear which kinase(s) are responsible for the transmission of mitochondrial stresses, the phosphorylation of eIF2α and the downstream consequences are typically observed in mouse- and cell models that affect mitochondrial function. An increased expression of *Fgf21*, for example, was observed in DARS2- or CLPP-deficient cardiomyocytes and in skeletal muscles of Twinkle- or OPA1-deficent mice. Furthermore, the induction appears to be independent of cell type, age of the animal or severity of the phenotype (Dogan et al. 2014, Khan et al. 2017, Kuhl et al. 2017, Tezze et al. 2017) and it is possible that an overactive or unstopped ISR plays a role in the described pathologies.

Surprisingly, levels of phosphorylated eIF2α were unaltered in $Sdha^{MKO}$ muscles and consequently, ATF4 protein amount was unchanged as well. A possible explanation for the lack of eIF2α phosphorylation might be that the inherent negative feedback loop through GADD34 and the protein phosphatase 1 complex (Novoa et al. 2001) favours its de-phosphorylation in $Sdha^{MKO}$ muscles. Nevertheless, it would still remain unclear as to why this feedback loop does not stop eIF2α phosphorylation in e.g. DARS2- (Dogan et al. 2014) and SDHA-deficient hearts or skeletal muscles with OPA1- or Twinkle deficiency (Khan et al. 2017, Tezze et al. 2017).

While this part of the integrated stress response cannot be explained without further data, the decreased expression of *Mthfd2* and especially *Pycr1* might be the result of altered c-MYC activity and will be discussed further in section 4.1.2.

4.1.2 The AMPK-SIRT axis possibly drives adaptations in *Sdha^{MKO}* muscles

Sdha^{MKO} muscles show clear signs of energy crisis already at the age of 3 weeks. Although detailed metabolic analyses of other time points are lacking at the moment, it can be assumed that the observed depletion of ATP and amino acids is progressing with age and peaks at death. The low energy charge causes the activation of AMPK allosterically through AMP-binding, as well as via increased phosphorylation of α-Thr172 of the γ subunit, an adaptation to low nutrient supply and energy deficits that is almost universal to eukaryotic cells (Hardie 2011). Despite its ubiquitous presence, the activity of the hetero-trimer is in part regulated by the expression of tissue-specific isoforms and phosphatase/kinase activities (Mounier et al. 2015).

In skeletal muscles, AMPK activation, e.g. during starvation, triggers a chain of events to increase the energy status and restore muscle function. Notably, one of the earliest responses is the phosphorylation of TBC1D1 by AMPK, which causes GLUT4 translocation to the sarcolemma in order to increase glucose uptake in muscle fibres (Chavez et al. 2008). Continued glucose supply into muscles is provided by hepatic gluconeogenesis through glycogenolysis and the glucose-alanine cycle. However, during prolonged fasting, this supply is not able to cover the requirements of muscle cells, leading to hypoglycaemia (Bujak et al. 2015). This is a possible explanation for the reduced blood glucose and liver glycogen levels in *Sdha^{MKO}* mice, as these mice most likely have a continuous lack of ATP in the muscles.

In order for the liver to provide enough glucose, AMPK-activated muscle atrophy further generates alanine that is deaminated in the liver (glucose-alanine cycle). During muscle atrophy, AMPK phosphorylates the transcription factor FOXO3A, which in turn increases the expression of the ubiquitin ligases Atrogin-1 (FBXO32) (Sandri et al. 2004) and MuRF-1 (TRIM63) (Senf et al. 2010) that target muscle proteins for proteasomal degradation. Both genes are highly expressed in *Sdha^{MKO}* muscles and could be the main drivers of muscle atrophy (Figure 4.2).

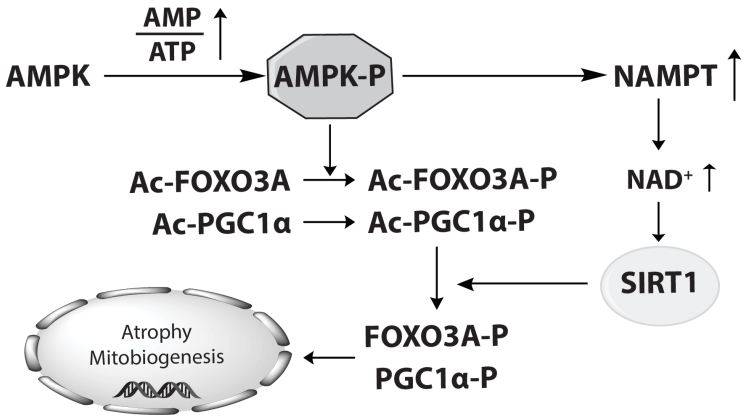

Figure 4.2 AMPK/SIRT1-regulated activation of FOXO3A and PGC1α
Energy crisis in cells is sensed through AMPK phosphorylation and its binding to AMP. These processes activate AMPK, which in turn phosphorylates the transcription factor FOXO3A and the transcriptional co-activator PGC1α. Additionally, AMPK increases the expression of NAMPT, a key enzyme of *de novo* NAD^+ synthesis. NAD^+ is as mandatory cofactor of SIRT1, that preferentially deacetylates phosphorylated FOXO3A/PGC1α. This fully activates their transcriptional activity, causing the induction of atrophy and mitochondrial biogenesis, respectively. Pathway adopted from (Canto et al. 2009).

In addition, an ATF4-mediated atrophy program (Adams et al. 2017) is also activated despite the absence of Eif2α phosphorylation or an increase in ATF4 steady state levels. The observed expression of the ATF4 targets *4Ebp1* and *Cdkn1a* in $Sdha^{MKO}$ muscles are milder in comparison to the expression of *Atrogin-1/ MuRF-1* and could result from increased nuclear ATF4 localization that does not require increased protein levels.

At 4 weeks of age, the expression of all analysed atrophy-related genes was blunted, although the underlying defect was ongoing and the energy deficit likely worsened. This could be a safe-guard mechanism within muscle tissue, as continued atrophy would result in the complete loss of muscles at this point. However, a more detailed analysis of FOXO3A and AMPK activity at this age is required to understand whether the induction is no longer maintained or if other signals interfere with it.

In addition to the activating phosphorylation by AMPK (S412), FOXO3A can be phosphorylated by ERK1/2 (S7, S12, S283, S293, S424) and AKT (T32, S252, S314), resulting in the inhibition and degradation of the protein (Wang et al. 2017). The phosphorylation (and activation) of these two kinases is reduced at the age of 3 weeks in *Sdha*^{MKO} muscles, which should even further stabilize FOXO3A and therefore increase muscle atrophy in the knockout. Both AKT and ERK1/2 are regulated by growth hormones like IGF1 or myostatin and decreased blood levels of these hormones might be adding to the observed muscle wasting. Lower levels of IGF-1 in *Sdha*^{MKO} mice would also be in line with the whole-body growth retardation and the sustained hypoglycaemia. In addition to the effect on FOXO3A, AKT and ERK1/2 are known to increase protein translation, proliferation and cell survival (Miyazaki and Takemasa 2017, Kjobsted et al. 2018, Zou et al. 2019), which are all inhibited pathways in *Sdha*^{MKO} muscles.

Another important regulator of translation and proliferation within the cell is the mammalian target of rapamycin (mTOR). mTOR is present in two multi-protein complexes (mTORC1 and mTORC2) with mTORC1 acting as a master regulator of metabolism and protein synthesis (Laplante and Sabatini 2009). Furthermore, mTOR activity can be regulated by AMPK and AKT, resulting in a complex web of cellular signalling pathways. However, no clear effect on the activity of mTOR could be detected in *Sdha*^{MKO} muscles as target protein phosphorylation was unchanged in the knockout. Multiple feedback loops could be responsible for this observation, since amino acid starvation-induced mTOR inhibition has been described in great detail and overall amino acid levels were decreased in *Sdha*^{MKO} muscles. It is also possible that mTOR inhibition precedes the chosen time points and resumed to normal activity by 3 weeks of age.

On the other hand, mTOR activation was also observed in skeletal muscles with mitochondrial defects along with the integrated stress response (Khan et al. 2017). It is thus possible that opposite stimuli act upon mTOR, which reciprocally extenuate each other. A closer inspection of multiple mTOR targets at different time points might therefore be helpful to understand its role in *Sdha*^{MKO} muscles.

In the late stages of *Sdha*^{MKO} mice, an increase in mitochondrial proteins and especially proteins involved in FAO was observed as the third response. This is also reminiscent of the classical starvation response, as fatty acid oxidation is augmented during prolonged exercise or starvation (Goodman et al. 1974).

An increase in mitobiogenesis is often caused by the activation of the peroxisome-proliferator-activated receptor gamma coactivator 1 alpha (PGC1α), which can increase PPAR/NRF-mediated expression of mitochondrial genes. PGC1α mRNA as well as the protein are generally upregulated through the activity of AMPK (Lee et al. 2006, Jager et al. 2007, Lira et al. 2010) and its phosphorylation at T177 and S538 is essential for the activation of PGC1α. It is currently unclear why the induction of PGC1α-mediated mitobiogenesis occurs only at the very late stages. Mitobiogenesis is clearly more time-consuming than the fusion of GLUT4 vesicles with the membrane or the targeted degradation of skeletal muscle proteins. However, a correlation to the severity of the phenotype is also possible.

In addition to its role in muscle atrophy, AMPK activity was reported to augment NAD^+ *de novo* synthesis. Together with the inhibition of the TCA cycle, these processes could be responsible for the increased the NAD^+/NADH ratio in *Sdha*^{MKO} muscles. An important role for AMPK in the *Sdha*^{MKO} muscle NAD^+/NADH ratio can be assumed, because the increase in the NAD^+/NADH ratio was largely due to increased NAD^+ levels (Figure 4.2). Increased NAD^+ levels in turn activate sirtuins (Canto et al. 2009), that use NAD^+ as a cofactor for the deacetylation of numerous proteins to change cellular activity and gene expression.

Although no direct evidence for enhanced sirtuin activity in *Sdha*^{MKO} muscles was provided, it is most likely the case, since SIRT1-mediated deacetylation is important for the full activation and stabilization of PGC1α and FOXO3A. It is further a coordinated activation, as the AMPK-mediated phosphorylation primes these proteins for the subsequent deacetylation by SIRT1 (Canto and Auwerx 2009, Canto et al. 2009) (Figure 4.2). The use of antibodies specific for acetylated/phosphorylated forms of PGC1α and FOXO3A could additionally substantiate the role of sirtuins in *Sdha*^{MKO} muscles at this point.

Further indirect evidence for sirtuin activation due to increased NAD^+ levels comes from the absence of HIF1α and c-MYC signalling in *Sdha*^{MKO} muscles. HIF1α activity is inhibited directly through deacetylation via SIRT1 and indirectly through the deacetylation of histone H3 via SIRT6, which affects HIF1α-dependent gene expression (Zhong et al. 2010) (Figure 4.3). Sirtuin-dependend deacetylation additionally attenuates AKT signalling (Sundaresan et al. 2012) and might therefore further inhibit protein translation and increase FOXO3A-mediated atrophy in S*dha*^{MKO} muscles.

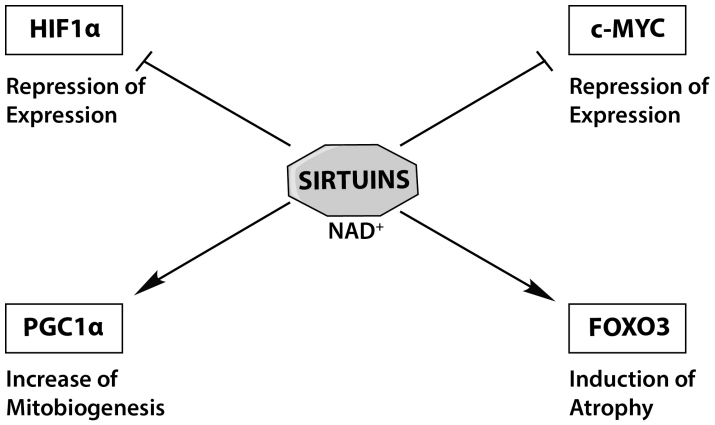

Figure 4.3 Model for sirtuin-mediated adaptations in *Sdha*^{MKO} muscles
Various cytosolic and nuclear sirtuins possibly regulate four main transcriptional pathways in SDHA-deficient muscles due to increased NAD^+ levels. Direct deacetylation of PGC1α and FOXO3A causes their activation and the induction of mitochondrial biogenesis and atrophy, respectively. Directly and indirectly, multiple sirtuins deacetylate HIF1α, c-MYC as well as histones at their respective target genes. These reactions cause the overall repression of HIF1α and c-MYC activity as observed in *Sdha*^{MKO} muscles.

c-MYC is an oncoprotein transcription factor that drives tumour transformation and induces the eIF2α/ATF4 arm of the integrated stress response (Hart et al. 2012). Additionally, it shares some of its target genes with ATF4, impeding the attribution of these genes to specific transcription factors (Kuhl et al. 2017).

The transcription of two of these genes, *Pycr1* and *Mthfd2*, is induced by both c-MYC and ATF4. This induction is observed in many models of mitochondrial dysfunction and is considered to be a hallmark of the integrated stress response (Khan et al. 2017, Kuhl et al. 2017). Surprisingly, both proteins are even reduced in abundance in *Sdha*^{MKO} muscles.

Assuming the NAD^+-dependent increase in sirtuin activity is indeed true, the deacetylation of histone H3 by SIRT6 (K9 and K56) and SIRT7 (K18) (Sebastian et al. 2012, Shin et al. 2013) and histone H4 (K16) by SIRT2 (Liu et al. 2013) consequently supress c-MYC-dependent gene expression. c-MYC is also directly regulated by SIRT1, however, it is still under debate whether this represents a positive (Menssen et al. 2012) or negative regulation (Yuan et al. 2009). Furthermore, c-MYC targets include ribosomal subunits (Sebastian et al. 2012), RNA Polymerase II (Rahl et al. 2010) and nucleotide biogenesis (Liu et al. 2008). These targets could potentially cause the decrease in cytosolic translation and nucleotide levels in *Sdha*^{MKO} muscles.

In addition to decreased mRNA translation and cell proliferation, the repression of c-MYC-dependent expression of *Pycr1* could finetune energy metabolism to conditions with low ATP and high NAD^+ levels via the proline cycle (Figure 4.4).

Cellular proline exists in a reduced (proline, Pro) and in an oxidised state (pyrroline-5-carboxylate, P5C). Oxidation and reduction of the amino acid is catalysed by proline dehydrogenase (PRODH) and P5C reductases (PYCRs), respectively. While PYCRs are located in the mitochondrial matrix (PYCR1 and 2) and in the cytosol (PYCR3), PRODH is anchored to the inner mitochondrial membrane and transfers electrons from the oxidation of proline onto ubiquinone. The cycle between oxidised and reduced state can therefore occur either within mitochondria or across the compartments, depending on which reductases are used. As an alternative energy source, proline oxidation can supply electrons to the respiratory chain and the metabolic state further dictates the place of reduction. When ATP and NAD^+ levels are low, as it is the case in e.g. complex I-deficient cells (Figure 4.4 A), reduction of P5C is performed in the matrix using NADH as the electron donor. Therefore, NADH can be oxidised in the absence of complex I, albeit at a lower efficiency due to less proton pumping. Even in the absence of major parts of the respiratory chain, such as in the mutator or *Dars2*^{HKO} mice, the proline cycle can at least replenish NAD^+ levels for nucleotide synthesis. Consequently, increased *Pycr1* expression can drive a mitochondrial proline cycle to use mitochondrial NADH in these models (Kuhl et al. 2017). On the other hand, when ATP levels are low but NAD^+ levels are high, such as in *Sdha*^{MKO} muscles (Figure 4.4 B), no additional ATP could be generated by increased *Pycr1* expression. On the contrary, low levels of PYCR1 could drive a proline cycle across the compartments using PYCR3 as the reductase, which has a higher affinity for NADPH (De Ingeniis et

al. 2012). Although NADPH could not be detected using metabolomic quantification, the global arrest of translation and anabolism in *Sdha*^{MKO} muscles argue for increased cytosolic NADPH. The cells could therefore be able to maximize ATP production, depending on the metabolic environment via sirtuin-dependent c-MYC regulation (Figure 4.4).

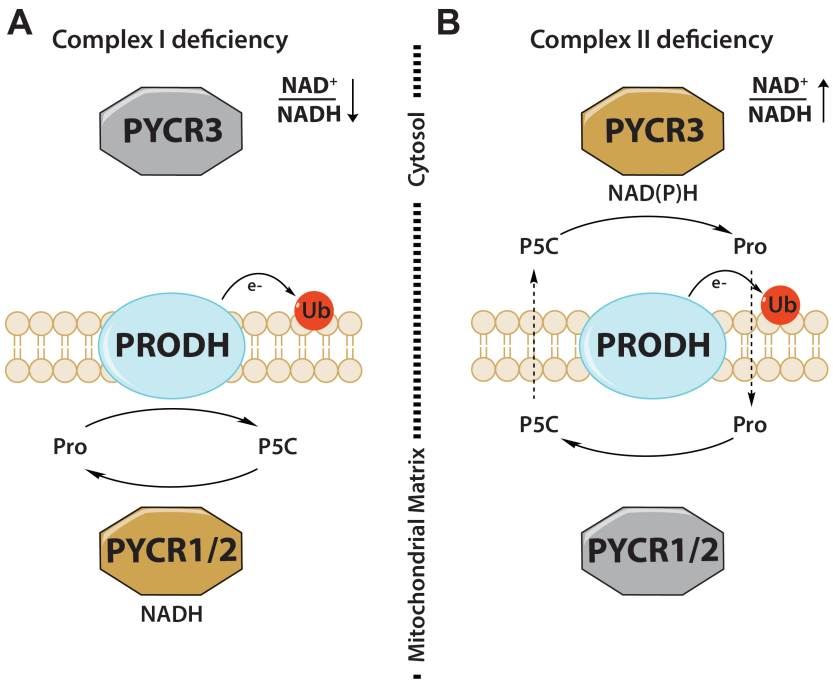

Figure 4.4 Model for proline cycle regulation during complex I and complex II deficiency
(A) During complex I deficiency, mitochondrial NADH accumulates and the mitochondrial P5C reductases (PYCR1/2) are up-regulated. This causes the proline cycle to occur preferentially in mitochondria, in which PYCR1/2 use NADH to reduce P5C into proline. Proline is oxidised by PRODH, which transfers the electrons to ubiquinone (Ub) to drive the rest of the respiratory chain. The outcome are increased respiration and NAD^+ recycling. (B) During complex II deficiency, PYCR1/2 are down-regulated, causing the proline cycle to run across the mitochondrial inner membrane. Here, cytosolic PYCR3 reduces P5C into proline using cytosolic NAD(P)H. Proline re-enters the mitochondrial matrix, where it is oxidised as in (A) into P5C, which exits the mitochondria again to complete the cycle. The outcome is a use of cytosolic reducing equivalents to increase respiration. (More) active reductases are depicted in colour. Less active or repressed reductases are shown in greyscale.

4.1.3 What is the primary deficiency in *SDHA^{MKO}* muscles?

Loss of SDHA in skeletal muscles had a profound impact on muscle and systemic physiology of the animal. Furthermore, multiple response pathways where engaged and numerous secondary effects on metabolism and gene expression could be observed. However, it is still tempting to speculate on the essential changes that occur in the tissue. Undoubtedly, the primary cause starts within the mitochondria as a clear SDH deficiency was observed, but TCA cycle function and respiration are difficult to discriminate. Nevertheless, several observations indicate that a direct role of SDH in ATP production through electron transfer is more important than its metabolic role as a TCA cycle enzyme and its production of NADH.

First of all, mitochondria are able to completely circumvent SDH *in vitro* within the TCA cycle, as long as enough pyruvate and malate are present, because oxoglutarate can be exchanged for malate, which re-enters the cycle after SDH. Thus, half of the TCA cycle can technically be skipped. Both malate and pyruvate, as well as multiple other TCA cycle metabolites were unchanged upon the loss of SDHA. It is therefore imaginable that the TCA cycle can still fulfil its function of providing metabolic intermediates and NADH.

Furthermore, NADH levels were also not affected by the knockout. Since other respiratory chain complexes were equally present and able to respire *in vitro*, it would be difficult to understand why the available NADH is not oxidised through complex I, especially upon ATP depletion.

A possible explanation for this discrepancy could be that complex I-dependent respiration is indeed working normally in the absence of SDH. *In vitro*, wild type muscle mitochondria had an increase of about 40% in respiration when succinate was added to complex I-dependent respiration. Therefore, *Sdha^{MKO}* muscles should lack a substantial amount of maximal respiration, even in the presence of sufficient NADH.

It is consequently conceivable, that the electrons transferred via SDH considerably add to respiration and oxidative phosphorylation *in vivo*, to cause the observed ATP depletion in *Sdha^{MKO}* muscles and trigger the downstream responses (Figure 4.5).

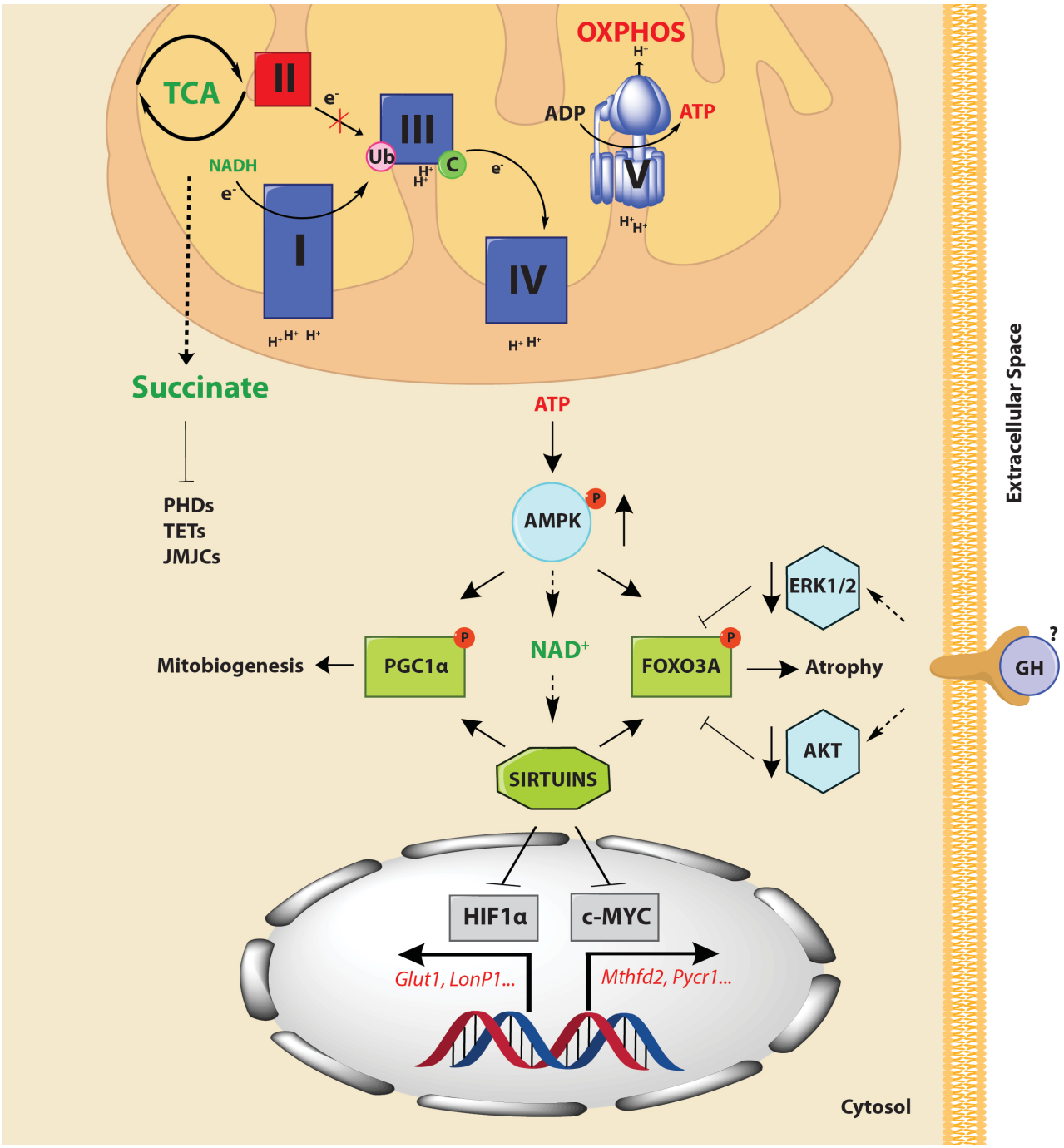

Figure 4.5 Model for ATP depletion and cellular adaptations upon SDHA deficiency in muscles
Loss of SDHA (II) results in a functional TCA cycle and normal complex I-dependent NADH oxidation, but disrupts electron flow from SDH to ubiquinone (Ub). The reduced electron transfer in turn extenuates ATP production through OXPHOS. Low ATP levels activate AMPK signalling and NAD^+ synthesis. This signalling is further enhanced by sirtuin-dependent deacetylation of PGC1α and FOXO3A, increasing mitobiogenesis and atrophy, respectively. FOXO3A is further stabilized by lower ERK1/2 and AKT activities, possibly because of reduced serum growth hormone (GH) levels. Additionally, sirtuins inhibit HIF1α and c-MYC-dependent gene expression, attenuating hypoxic induction and ISR initiation. Furthermore, loss of SDH causes succinate accumulation that represses 2-OG-dependent dioxygenases (PHDs, TETs, JMJCs).

4.1.4 Loss of SDHA in the heart triggers the ISR and pseudo-hypoxia but not AMPK activation

The striking difference between *Sdha*^{MKO} and other models for mitochondrial dysfunction prompted the question, whether the observations are unique to SDHA-deficiency or the combination of it and the investigated tissue. Although hepatic metabolism has more profound differences in comparison to myocytes, the embryonic lethality of *Sdha*^{LKO} mice even with the *Albumin* promoter-driven Cre expression excluded this model for the study. This Cre line was reported to have incomplete recombination until the age of 6 weeks (Postic and Magnuson 2000), although another study reported efficient recombination already during development (Weisend et al. 2009). In either case, the lethality of *Sdha*^{LKO} mice points towards a strong dependency of hepatocytes on SDHA early on that could be addressed using inducible knockout models.

Instead, a cardiomyocyte-specific loss of function model (*Sdha*^{HKO}) was employed, which is of similar dependency on a high ATP supply, but lacks the metabolic plasticity of skeletal muscles. Cardiomyocytes are highly dependent on fatty acid oxidation and use other nutrients only to limited extent (Grynberg and Demaison 1996). Accordingly, *Sdha*^{HKO} mice die considerably earlier than *Sdha*^{MKO} mice, with few mice reaching 3 weeks of age. Conditional knockouts with the same promoter (Ckmm) of DARS2 or TFAM survive up to 6 weeks and 10 weeks, respectively (Hansson et al. 2004, Dogan et al. 2014), while the loss of Twinkle, MTERF4 or POLRMT is lethal only after several months (Camara et al. 2011, Ruzzenente et al. 2012, Milenkovic et al. 2013). Although all models ultimately affect oxidative phosphorylation within the heart from day E13 (day of recombination) on, a straight forward comparison is not possible for multiple reasons.

Most importantly, the expression levels of each protein within the first 2 weeks of embryogenesis and their half-life after that are unknown. The development of a phenotype can therefore be determined by the time the protein is depleted from the tissue. Furthermore, the timepoint of the "functional" knockout can be varying as well. With regard to DARS2, the functional knockout appears once the loss of the protein actually affects mitochondrial protein translation and then the activity of the respiratory chain. It is conceivable, that this process takes less time compared to when the loss of mitochondrial DNA/transcription affects the same process in the TFAM

knockout, even if both proteins were lost simultaneously. Cardiac loss of SDHA complicates the comparison even further: While SDHA is a very stable housekeeping protein, SDHB was depleted rather quickly, leading to the complete inactivation of complex II already at day 11 (and possibly earlier). The importance of protein turnover is further highlighted by the finding that heart-specific TFAM knockout mice survived only 2-4 weeks of age when a different Ckmm-Cre line was used for the recombination (Wang et al. 1999). It is thus not always possible to draw conclusions about the importance of a protein from the survival of its knockout mouse.

Despite the striking difference in survival, all of the aforementioned knockouts eventually develop lethal cardiomyopathy. Furthermore, they were recently found to have a common ISR with the up-regulation of 1C-metabolism and proline conversion as common markers (Kuhl et al. 2017). Surprisingly, loss of SDHA in the heart causes the same isolated complex II deficiency as in muscles, but the ISR is only engaged in the heart.

This could be due to the lack of NAD^+-dependent c-MYC regulation, as no AMPK phosphorylation or NAD^+ accumulation was observed in *Sdha*^{HKO} hearts (Figure 4.6). Although the differences in terms of stress response could be traced back to the activation of AMPK, or the absence of it, respectively, it is unclear at this moment why the loss of SDHA in cardiomyocytes does not activate AMPK. The possibility of AMPK activation during energy depletion was reported in the heart (Coven et al. 2003) and affects glucose uptake and fatty acid oxidation. To understand the molecular reason of this discrepancy, it is inevitable to perform metabolome quantification also on *Sdha*^{HKO} hearts, since it cannot be excluded that the lack of certain metabolites, rather than ATP depletion causes the dysfunction. Another possibility for unchanged AMPK activity could be the age of the animal. Between 2 and 3 weeks of age, the mouse heart undergoes drastic remodelling that includes hypertrophic cell expansion and strongly increased mitobiogenesis (Piquereau et al. 2010), along with increased AMPK activity (Yatscoff et al. 2008). It is therefore possible that AMPK is fully phosphorylated during this time and cannot be further activated by low ATP levels.

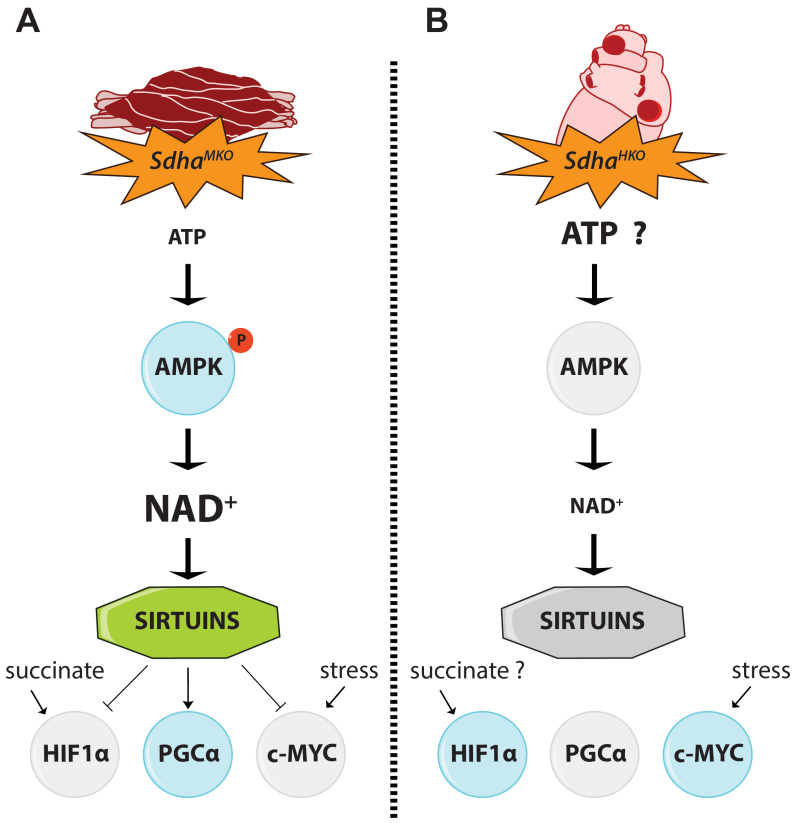

Figure 4.6 Model for tissue-specific adaptations to SDHA deficiency
(A) In skeletal muscles, loss of SDHA causes ATP depletion and AMPK phosphorylation. Increased AMPK activity triggers NAD^+ synthesis, which leads to higher sirtuin activity. Finally, sirtuins activate PGC1α, while suppressing HIF1α and c-MYC target gene expression. (B) Loss of SDHA in cardiomyocytes does not increase AMPK phosphorylation and therefore does not change NAD^+ levels or sirtuin activity. Consequently, HIF1α and c-MYC-mediated gene expression is not inhibited and PGC1α-dependent mitobiogenesis is not augmented. (More) active proteins are depicted in colour. Less active or repressed proteins are shown in greyscale.

In summary, the cellular responses towards the loss of SDHA are tissue-specific and possibly dependent on the metabolic circumstances. The example of heart and skeletal muscles shows that the alternative regulation of one pathway could already be sufficient to evoke dramatic differences in the elicited response. The extension of this work to other tissues could therefore give further insights into which metabolic changes drive the malignant transformations in SDH-deficient cells and why these are more prone to become cancer cells than others.

4.2 Proteomic approaches to identify novel ClpXP substrates *in vitro* and *in vivo*

Mitochondrial protein homeostasis is the balance between protein synthesis and protein degradation due to malfunction or overabundance and plays an important role in cell function and viability. Thus, perturbations in the protein surveillance machinery can have far-reaching consequences for human patients. Mutations in mitochondrial proteases often manifest in multisystemic phenotypes that include neurodegeneration, hearing loss or ataxia and the identification of the underlying mutations with deep sequencing methods has greatly increased the understanding of the proteostasis network. Besides the quality control function, the focus has largely shifted towards regulatory functions of mitochondrial proteases and several *in vivo* substrates have been identified for each of the ATP-dependent proteases.

The abundance of these substrates needs careful regulation and aberrations of the default state can significantly affect mitochondrial function. To date, only few such substrates have been described for the protease ClpXP and the data indicate that ClpXP has adopted functions that deviate strongly from other species such as *E. coli* or *C. elegans* (Seiferling et al. 2016). The identification of its substrates and their control is therefore of continued relevance and was the second aim of this work.

4.2.1 Identification of new bona fide ClpXP substrates

Using a classical substrate screen and the recently developed quantification of the N-terminome (TAILS), several proteins could be proposed and partially confirmed as ClpXP substrates. These proteins exhibited increased abundance on two independent proteomic quantification methods and on western blots, increasing the likelihood of true positives. This approach is particularly useful, as “omics” generate large datasets and a simple FDR cut-off analysis either retains many false positives or loses the power to detect true substrates with minor changes in abundance. Particularly, TAILS was a useful addition for the previously published LFQ data set, however, although the quantification of labelled peptides is very reproducible, it has a smaller range of identified proteins compared to label-free quantification methods. HSPA9 and OAT were identified with TAILS and confirmed with additional experiments to be ClpXP substrates. Additionally, they were also previously co-

purified with a substrate screen using a human CLPP-TRAP construct in *P. anserina* (Fischer et al. 2015). The overlap with previously suggested substrates proves the eligibility of the approach and facilitates the identification of true substrates. Furthermore, TAILS provided strong evidence for a ClpXP cleavage signature with arginine at the P1 position. This is the first description of a mouse ClpXP cleavage window that might stem from an evolutionary conserved function, as *B. subtilis* ClpCP was reported to degrade the heat shock response regulator CtsR with phosphorylated arginine (P-Arg) (Trentini et al. 2016). The phosphorylation of arginine or a corresponding kinase was not described in eukaryotes so far, thus a physiological function for P-Arg mediated degradation by ClpXP is largely speculative at this point. Although TAILS and similarly operating labelling techniques for protein N-termini have been primarily used for the description of degradation intermediates (Prudova et al. 2016, King et al. 2018), this work clearly establishes TAILS as a powerful tool to detect protease substrates along with other proteomic approaches. It is therefore very promising to perform the experiment in other tissues of *Clpp*$^{-/-}$ mice to identify tissue-specific substrates and to verify whether the cleavage motif is conserved across different cell types.

The initial substrate screen performed in MEFs provided a considerable list of putative ClpXP substrates and interacting partners, however, no confidence level could be addressed to these candidates, as an isolated experiment was performed at the time. To obtain quantitative data with a substrate trapping screen, the experiment was repeated in triplicates in MEFs. However, the experiment could only be performed using cell lysates instead of mitochondrial purifications. This allows for a manageable size and expense of the experiment, but at the cost of “diluting” low abundant mitochondrial proteins with contaminations from the cytosol. The resulting list was thus a subset of the first screen with no additional candidates, but included 14 proteins that can be suggested as ClpXP substrates with high confidence.

POLDIP2 was highly enriched in TRAP-fractions and recently identified as a ClpXP-interacting protein in a cross-linking pulldown. Independently, it was further suggested to be a CLPX-interacting protein that regulates the degradation of ACSM1 (Paredes et al. 2018, Fux et al. 2019). As the CLPP-CLPX interaction appeared to be stabilised with CLPP-TRAP proteins, it thus also inherently favours the pulldown of CLPX-interacting proteins, which would be classified as ClpXP substrates instead of protease interactors. Further investigation of the interaction is necessary as LFQ data indicated a strong accumulation of POLDIP2 in *Clpp*$^{-/-}$ hearts, which was not reported in the publication that used *Clpp* siRNA. Another protein that strongly interacted with CLPP-TRAP was Coiled-coil-helix-coiled-coil-helix domain containing 2 (CHCHD2). CHCHD2 showed a two-fold accumulation in *Clpp*$^{-/-}$ heart mitochondria (LFQ) and was reported to interact with the ClpXP interactor C1QBP (Wei et al. 2015). This report strongly suggests a ClpXP-mediated regulation and highlights the protein as a promising ClpXP substrate with potential medical implications, as CHCH protein complexes are associated with the development of neurodegenerative disorders such as Parkinson's disease (Imai et al. 2019). Other enriched proteins include subunits of the mitoribosome and therefore may result from the stabilised interaction between CLPP-TRAP and the mitoribosome, which are not necessarily true substrates. Further, several proteins are not localized to mitochondria and likely represent artefacts arising during cell lysis. However, since the interaction is nevertheless stabilised, a certain affinity for CLPP-TRAP can be cautiously postulated for the proteins. These proteins are involved in RNA or calcium binding, both of which were addressed to C1QBP (Yagi et al. 2012, Yagi et al. 2017). Although this evidence is circumstantial, it can nevertheless be useful for the identification of ClpXP substrates in the future.

4.2.2 UQCRC1, a non-canonical ClpXP substrate under cooperative degradation surveillance

In addition to the bona fide substrate candidates, the trapping screen and data on the N-terminome revealed UQCRC1 as a substrate for ClpXP with unaltered steady state protein levels in the absence of CLPP. The first and rate-limiting step of UQCRC1 degradation appears to be conducted by another protease, with LonP1 or AFG3L2 being the most likely candidates. However, ClpXP is able to eliminate the, albeit low abundant, truncated UQCRC1 proteoform (Figure 4.7). Similar mechanisms have been described in chloroplasts (Kato et al. 2012) and the cytosol (Jang et al. 2000) and are possibly also present in mitochondria. The impact of this cooperative degradation cannot be finally concluded at this point; however, the effect might be exacerbated under stress conditions, when the proteolytic system is used to full capacity or even overloaded by unfolded or damaged proteins. It therefore suggests the very interesting possibility to investigate degradation intermediates in *Clpp*$^{-/-}$ under varying conditions with TAILS, as ClpXP and other proteases can adopt additional functions under stress conditions such as heat- and oxidative stress in bacteria (Gottesman 1996, Michel et al. 2006), light stress in plants (Kato et al. 2012) or oxidative- and unfolded protein stress in mitochondria (Ngo et al. 2013, Al-Furoukh et al. 2015, Bezawork-Geleta et al. 2015, Pareek and Pallanck 2018).

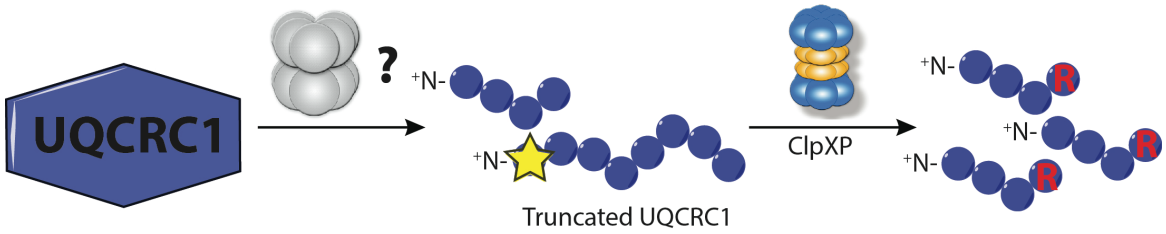

Figure 4.7 Model for cooperative degradation of UQCRC1
UQCRC1 abundance is regulated by an unknown protease, which cleaves a part of the protein from the N-terminus. This results in a truncated UQCRC1 protein, that exhibits a degron (star) for ClpXP-mediated proteolysis. Peptides released from ClpXP preferentially show arginine (R) at the P1 position.

4.2.3 Generation of mice conditionally expressing CLPP-FLAG for substrate identification *in vivo*

To date, the role of CLPP was described in the heart, liver, adipose and reproductive tissue as well as several cancer cell lines with partially contradicting results (Gispert et al. 2013, Cole et al. 2015, Seiferling et al. 2016, Szczepanowska et al. 2016, Becker et al. 2018, Bhaskaran et al. 2018, Ishizawa et al. 2019). The most plausible explanations for these results are that ClpXP has diverse regulatory substrates in these tissues or that substrate abundance/importance differs between cell types. Both possibilities result in severe limitations for the substrate identification approaches used here and by others, as the employed species and cell type will be restrictive and only partially transferable. To overcome this obstacle, mice conditionally expressing CLPP-FLAG from the *ROSA26* locus were generated with a CRISPR/Cas9-mediated knockin strategy in zygotes. Compared to the classical recombination approach in ES cells, this method has a higher success rate of germ line transmission within a drastically reduced time frame.

The first mice analysed proved a successful integration of the construct and a strong expression of CLPP-FLAG in the heart. CLPP-FLAG is imported into mitochondria, where it forms oligomeric structures as is was observed with transient expressions in MEFs. With these prerequisites met, the mouse line ought to be suitable for large-scale affinity purifications with high purity, as sufficient mitochondrial extracts from hearts are not rate-limiting. Although catalytically active CLPP is technically suitable for the identification of ClpXP substrates, the generation of CLPP-TRAP-FLAG expressing mice would further increase the efficiency and enable the discrimination between substrates and interacting proteins. However, due to a low viability of transplanted embryos, no CLPP-TRAP-FLAG expressing mice could be generated after three injections. Nevertheless, an increased *in vitro* fertilization efficiency with e.g. electroporation of the repair template into zygotes might further enhance the chances of positive integration and viability in the near future.

Despite that CLPP-FLAG is expressed at several folds of the endogenous CLPP levels, no changes were observed in substrate abundance, indicating that in heart mitochondria, CLPX or other (adaptor-) proteins are rate limiting for the recognition and/or degradation of substrates as it was proposed before (Lowth et al. 2012). This can be of advantage for substrate screens, as no detrimental effects mitigate the expression or viability, but inevitably, the mouse line cannot be used as a physiological "over-expressor" model. Unfortunately, these mice could not be further used for substrate screens and must serve as a proof of concept for the time being.

In conclusion, the combination of a substrate screen, TAILS and the verification with CLPP-deficient tissues and cells has led to the discovery or confirmation of several novel ClpXP substrates implicated in various mitochondrial processes. In addition, a putative cleavage motif for murine ClpXP and a new cooperative degradation mechanism were proposed. Finally, the development of a mouse model suitable for *in vivo* substrate screens could extent the discovery of substrates to so far unamenable tissues and surge the understanding of Perrault syndrome's unusual tissue-specificity.

References

Acin-Perez, R., I. Carrascoso, F. Baixauli, M. Roche-Molina, A. Latorre-Pellicer, P. Fernandez-Silva, M. Mittelbrunn, F. Sanchez-Madrid, A. Perez-Martos, C. A. Lowell, G. Manfredi and J. A. Enriquez (2014). "ROS-Triggered Phosphorylation of Complex II by Fgr Kinase Regulates Cellular Adaptation to Fuel Use." Cell Metabolism **19**(6): 1020-1033.

Acin-Perez, R., P. Fernandez-Silva, M. L. Peleato, A. Perez-Martos and J. A. Enriquez (2008). "Respiratory Active Mitochondrial Supercomplexes." Molecular Cell **32**(4): 529-539.

Adam, Z., I. Adamska, K. Nakabayashi, O. Ostersetzer, K. Haussuhl, A. Manuell, B. Zheng, O. Vallon, S. R. Rodermel, K. Shinozaki and A. K. Clarke (2001). "Chloroplast and mitochondrial proteases in Arabidopsis. A proposed nomenclature." Plant Physiology **125**(4): 1912-1918.

Adams, C. M., S. M. Ebert and M. C. Dyle (2017). "Role of ATF4 in skeletal muscle atrophy." Current Opinion in Clinical Nutrition and Metabolic Care **20**(3): 164-168.

Al Khazal, F., M. N. Holte, B. Bolon, T. A. White, N. LeBrasseur and L. J. Maher, 3rd (2019). "A conditional mouse model of complex II deficiency manifesting as Leigh-like syndrome." FASEB J: fj201802655RR.

Al-Furoukh, N., A. Ianni, H. Nolte, S. Holper, M. Kruger, S. Wanrooij and T. Braun (2015). "ClpX stimulates the mitochondrial unfolded protein response (UPRmt) in mammalian cells." Biochimica Et Biophysica Acta-Molecular Cell Research **1853**(10): 2580-2591.

Al-Furoukh, N., J. R. Kardon, M. Kruger, M. Szibor, T. A. Baker and T. Braun (2014). "NOA1, a Novel ClpXP Substrate, Takes an Unexpected Nuclear Detour Prior to Mitochondrial Import." Plos One **9**(7).

Allen, P. S., G. O. Matheson, G. Zhu, D. Gheorgiu, R. S. Dunlop, T. Falconer, C. Stanley and P. W. Hochachka (1997). "Simultaneous P-31 MRS of the soleus and gastrocnemius in Sherpas during graded calf muscle exercise." American Journal of Physiology-Regulatory Integrative and Comparative Physiology **273**(3): R999-R1007.

Althoff, T., D. J. Mills, J. L. Popot and W. Kuhlbrandt (2011). "Arrangement of electron transport chain components in bovine mitochondrial supercomplex I1III2IV1." Embo Journal **30**(22): 4652-4664.

Astuti, D., M. Morris, C. Krona, F. Abel, D. Gentle, T. Martinsson, P. Kogner, H. P. H. Neumann, R. Voutilainen, C. Eng, P. Rustin, F. Latif and E. R. Maher (2004). "Investigation of the role of SDHB inactivation in sporadic phaeochromocytoma and neuroblastoma." British Journal of Cancer **91**(10): 1835-1841.

B'chir, W., A. C. Maurin, V. Carraro, J. Averous, C. Jousse, Y. Muranishi, L. Parry, G. Stepien, P. Fafournoux and A. Bruhat (2013). "The eIF2 alpha/ATF4 pathway is essential for stress-induced autophagy gene expression." Nucleic Acids Research **41**(16): 7683-7699.

Baker, T. A. and R. T. Sauer (2012). "ClpXP, an ATP-powered unfolding and protein-degradation machine." Biochimica Et Biophysica Acta-Molecular Cell Research **1823**(1): 15-28.

Barclay, C. J. (2017). "Energy demand and supply in human skeletal muscle." Journal of Muscle Research and Cell Motility **38**(2): 143-155.

Barclay, C. J., R. C. Woledge and N. A. Curtin (2007). "Energy turnover for Ca2+ cycling in skeletal muscle." J Muscle Res Cell Motil **28**(4-5): 259-274.

Bargiela, D., S. P. Burr and P. F. Chinnery (2018). "Mitochondria and Hypoxia: Metabolic Crosstalk in Cell-Fate Decisions." Trends in Endocrinology and Metabolism **29**(4): 249-259.

Bayley, J. P., I. van Minderhout, P. C. W. Hogendoorn, C. J. Cornelisse, A. van der Wal, F. A. Prins, L. Teppema, A. Dahan, P. Devilee and P. E. M. Taschner (2009). "Sdhd and Sdhd/H19 Knockout Mice Do Not Develop Paraganglioma or Pheochromocytoma." Plos One **4**(11).

Becker, C., A. Kukat, K. Szczepanowska, S. Hermans, K. Senft, C. P. Brandscheid, P. Maiti and A. Trifunovic (2018). "CLPP deficiency protects against metabolic syndrome but hinders adaptive thermogenesis." EMBO Rep **19**(5).

Bezawork-Geleta, A., E. J. Brodie, D. A. Dougan and K. N. Truscott (2015). "LON is the master protease that protects against protein aggregation in human mitochondria through direct degradation of misfolded proteins." Scientific Reports **5**.

Bezawork-Geleta, A., L. F. Dong, J. Rohlena and J. Neuzil (2016). "The Assembly Factor SDHAF2 Is Dispensable for Flavination of the Catalytic Subunit of Mitochondrial Complex II in Breast Cancer Cells." Journal of Biological Chemistry **291**(41): 21414-21420.

Bezawork-Geleta, A., J. Rohlena, L. F. Dong, K. Pacak and J. Neuzil (2017). "Mitochondrial Complex II: At the Crossroads." Trends in Biochemical Sciences **42**(4): 312-325.

Bhaskaran, S., G. Pharaoh, R. Ranjit, A. Murphy, S. Matsuzaki, B. C. Nair, B. Forbes, S. Gispert, G. Auburger, K. M. Humphries, M. Kinter, T. M. Griffin and S. S. Deepa (2018). "Loss of mitochondrial protease ClpP protects mice from diet-induced obesity and insulin resistance." Embo Reports **19**(3).

Bianchi, C., M. L. Genova, G. P. Castelli and G. Lenaz (2004). "The mitochondrial respiratory chain is partially organized in a supercomplex assembly - Kinetic evidence using flux control analysis." Journal of Biological Chemistry **279**(35): 36562-36569.

Birsoy, K., T. Wang, W. W. Chen, E. Freinkman, M. Abu-Remaileh and D. M. Sabatini (2015). "An Essential Role of the Mitochondrial Electron Transport Chain in Cell Proliferation Is to Enable Aspartate Synthesis." Cell **162**(3): 540-551.

Bonaldo, P. and M. Sandri (2013). "Cellular and molecular mechanisms of muscle atrophy." Disease Models & Mechanisms **6**(1): 25-39.

Bota, D. A. and K. J. A. Davies (2002). "Lon protease preferentially degrades oxidized mitochondrial aconitase by an ATP-stimulated mechanism." Nature Cell Biology **4**(9): 674-680.

Bujak, A. L., J. D. Crane, J. S. Lally, R. J. Ford, S. J. Kang, I. A. Rebalka, A. E. Green, B. E. Kemp, T. J. Hawke, J. D. Schertzer and G. R. Steinberg (2015). "AMPK Activation of Muscle Autophagy Prevents Fasting-Induced Hypoglycemia and Myopathy during Aging." Cell Metabolism **21**(6): 883-890.

Calvo, S. E., K. R. Clauser and V. K. Mootha (2016). "MitoCarta2.0: an updated inventory of mammalian mitochondrial proteins." Nucleic Acids Research **44**(D1): D1251-D1257.

Camara, Y., J. Asin-Cayuela, C. B. Park, M. B. Metodiev, Y. H. Shi, B. Ruzzenente, C. Kukat, B. Habermann, R. Wibom, K. Hultenby, T. Franz, H. Erdjument-Bromage, P. Tempst, B. M. Hallberg, C. M. Gustafsson and N. G. Larsson (2011). "MTERF4 Regulates Translation by Targeting the Methyltransferase NSUN4 to the Mammalian Mitochondrial Ribosome." Cell Metabolism **13**(5): 527-539.

Canto, C. and J. Auwerx (2009). "PGC-1 alpha, SIRT1 and AMPK, an energy sensing network that controls energy expenditure." Current Opinion in Lipidology **20**(2): 98-105.

Canto, C., Z. Gerhart-Hines, J. N. Feige, M. Lagouge, L. Noriega, J. C. Milne, P. J. Elliott, P. Puigserver and J. Auwerx (2009). "AMPK regulates energy expenditure by modulating NAD(+) metabolism and SIRT1 activity." Nature **458**(7241): 1056-U1140.

Chal, J. and O. Pourquie (2017). "Making muscle: skeletal myogenesis in vivo and in vitro." Development **144**(12): 2104-2122.

Chavez, J. A., W. G. Roach, S. R. Keller, W. S. Lane and G. E. Lienhard (2008). "Inhibition of GLUT4 translocation by Tbc1d1, a Rab GTPase-activating protein abundant in skeletal muscle, is partially relieved by AMP-activated protein kinase activation." Journal of Biological Chemistry **283**(14): 9187-9195.

Chu, V. T., T. Weber, R. Graf, T. Sommermann, K. Petsch, U. Sack, P. Volchkov, K. Rajewsky and R. Kuhn (2016). "Efficient generation of Rosa26 knock-in mice using CRISPR/Cas9 in C57BL/6 zygotes." BMC Biotechnol **16**: 4.

Cimen, H., M. J. Han, Y. J. Yang, Q. Tong, H. Koc and E. C. Koc (2010). "Regulation of Succinate Dehydrogenase Activity by SIRT3 in Mammalian Mitochondria." Biochemistry **49**(2): 304-311.

Civiletto, G., S. A. Dogan, R. Cerutti, G. Fagiolari, M. Moggio, C. Lamperti, C. Beninca, C. Viscomi and M. Zeviani (2018). "Rapamycin rescues mitochondrial myopathy via coordinated activation of autophagy and lysosomal biogenesis." EMBO Mol Med **10**(11).

Civiletto, G., T. Varanita, R. Cerutti, T. Gorletta, S. Barbaro, S. Marchet, C. Lamperti, C. Viscomi, L. Scorrano and M. Zeviani (2015). "Opa1 Overexpression Ameliorates the Phenotype of Two Mitochondrial Disease Mouse Models." Cell Metabolism **21**(6): 845-854.

Cole, A., Z. Z. Wang, E. Coyaud, V. Voisin, M. Gronda, Y. Jitkova, R. Mattson, R. Hurren, S. Babovic, N. Maclean, I. Restall, X. M. Wang, D. V. Jeyaraju, M. A. Sukhai, S. Prabha, S. Bashir, A. Ramakrishnan, E. Leung, Y. H. Qia, N. X. Zhang, K. R. Combes, T. Ketela, F. S. Lin, W. A. Houry, A. Aman, R. Al-awar, W. Zheng, E. Wienholds, C. J. Xu, J. Dick, J. C. Y. Wang, J. Moffat, M. D. Minden, C. J. Eaves, G. D. Bader, Z. Y. Hao, S. M. Kornblau, B. Raught and A. D. Schimmer (2015). "Inhibition of the Mitochondrial Protease ClpP as a Therapeutic Strategy for Human Acute Myeloid Leukemia." Cancer Cell **27**(6): 864-876.

Coven, D. L., X. Y. Hu, L. Cong, R. Bergeron, G. I. Shulman, D. G. Hardie and L. H. Young (2003). "Physiological role of AMP-activated protein kinase in the heart: graded activation during exercise." American Journal of Physiology-Endocrinology and Metabolism **285**(3): E629-E636.

Crane, F. L. (1989). "The Discovery of Coenzyme-Q - a Commentary on Isolation of a Quinone from Beef-Heart Mitochondria." Biochimica Et Biophysica Acta **1000**: 358-363.

Crane, F. L., Y. Hatefi, R. L. Lester and C. Widmer (1957). "Isolation of a Quinone from Beef Heart Mitochondria." Biochimica Et Biophysica Acta **25**(1): 220-221.

De Ingeniis, J., B. Ratnikov, A. D. Richardson, D. A. Scott, P. Aza-Blanc, S. K. De, M. Kazanov, M. Pellecchia, Z. Ronai, A. L. Osterman and J. W. Smith (2012). "Functional Specialization in Proline Biosynthesis of Melanoma." Plos One **7**(9).

Demir, F., S. Niedermaier, J. N. Kizhakkedathu and P. F. Huesgen (2017). "Profiling of Protein N-Termini and Their Modifications in Complex Samples." Methods Mol Biol **1574**: 35-50.

Diaz, F., C. K. Thomas, S. Garcia, D. Hernandez and C. T. Moraes (2005). "Mice lacking COX10 in skeletal muscle recapitulate the phenotype of progressive mitochondrial myopathies associated with cytochrome c oxidase deficiency." Human Molecular Genetics **14**(18): 2737-2748.

Dogan, S. A., C. Pujol, P. Maiti, A. Kukat, S. Y. Wang, S. Hermans, K. Senft, R. Wibom, E. I. Rugarli and A. Trifunovic (2014). "Tissue-Specific Loss of DARS2 Activates Stress Responses Independently of Respiratory Chain Deficiency in the Heart." Cell Metabolism **19**(3): 458-469.

Donegan, N. P., J. S. Marvin and A. L. Cheung (2014). "Role of Adaptor TrfA and ClpPC in Controlling Levels of SsrA-Tagged Proteins and Antitoxins in Staphylococcus aureus." Journal of Bacteriology **196**(23): 4140-4151.

Enriquez, J. A. (2016). "Supramolecular Organization of Respiratory Complexes." Annual Review of Physiology, Vol 78 **78**: 533-561.

Fischer, F., J. D. Langer and H. D. Osiewacz (2015). "Identification of potential mitochondrial CLPXP protease interactors and substrates suggests its central role in energy metabolism." Scientific Reports **5**.

Flynn, J. M., I. Levchenko, R. T. Sauer and T. A. Baker (2004). "Modulating substrate choice: the SspB adaptor delivers a regulator of the extracytoplasmic-stress response to the AAA plus protease ClpXP for degradation." Genes & Development **18**(18): 2292-2301.

Frezza, C., S. Cipolat and L. Scorrano (2007). "Organelle isolation: functional mitochondria from mouse liver, muscle and cultured fibroblasts." Nat Protoc **2**(2): 287-295.

Frontera, W. R. and J. Ochala (2015). "Skeletal Muscle: A Brief Review of Structure and Function." Calcified Tissue International **96**(3): 183-195.

Fukuda, R., H. F. Zhang, J. W. Kim, L. Shimoda, C. V. Dang and G. L. Semenza (2007). "HIF-1 regulates cytochrome oxidase subunits to optimize efficiency of respiration in hypoxic cells." Cell **129**(1): 111-122.

Fux, A., V. S. Korotkov, M. Schneider, I. Antes and S. A. Sieber (2019). "Chemical Cross-Linking Enables Drafting ClpXP Proximity Maps and Taking Snapshots of In Situ Interaction Networks." Cell Chemical Biology **26**(1): 48-+.

Ghai, S. J., A. Al Maawali, J. Cameron, N. Mackay, B. H. Robinson and J. Raiman (2011). "Complex II deficiency: A case report and review of literature." Molecular Genetics and Metabolism **102**(3): 291-292.

Ghebrehiwet, B., B. L. Lim, E. I. B. Peerschke, A. C. Willis and K. B. M. Reid (1994). "Isolation, Cdna Cloning, and Overexpression of a 33-Kd Cell-Surface Glycoprotein That Binds to the Globular Heads of C1q." Journal of Experimental Medicine **179**(6): 1809-1821.

Gherardi, G., L. Nogara, S. Ciciliot, G. P. Fadini, B. Blaauw, P. Braghetta, P. Bonaldo, D. De Stefani, R. Rizzuto and C. Mammucari (2019). "Loss of mitochondrial calcium uniporter rewires skeletal muscle metabolism and substrate preference." Cell Death and Differentiation **26**(2): 362-381.

Gill, A. J. (2018). "Succinate dehydrogenase (SDH)-deficient neoplasia." Histopathology **72**(1): 106-116.

Gispert, S., D. Parganlija, M. Klinkenberg, S. Drose, I. Wittig, M. Mittelbronn, P. Grzmil, S. Koob, A. Hamann, M. Walter, F. Buchel, T. Adler, M. H. de Angelis, D. H. Busch, A. Zell, A. S. Reichert, U. Brandt, H. D. Osiewacz, M. Jendrach and G. Auburger (2013). "Loss of mitochondrial peptidase Clpp leads to infertility, hearing loss plus growth retardation via accumulation of CLPX, mtDNA and inflammatory factors." Human Molecular Genetics **22**(24): 4871-4887.

Glynn, S. E. (2017). "Multifunctional Mitochondrial AAA Proteases." Frontiers in Molecular Biosciences **4**.

Goodman, M. N., M. Berger and N. B. Ruderman (1974). "Glucose-Metabolism in Rat Skeletal-Muscle at Rest Effect of Starvation, Diabetes, Ketone-Bodies and Free Fatty-Acids." Diabetes **23**(11): 881-888.

Gottesman, S. (1996). "Proteases and their targets in Escherichia coli." Annual Review of Genetics **30**: 465-506.

Greggio, C., P. Jha, S. S. Kulkarni, S. Lagarrigue, N. T. Broskey, M. Boutant, X. Wang, S. C. Alonso, E. Ofori, J. Auwerx, C. Canto and F. Amati (2017). "Enhanced Respiratory Chain Supercomplex Formation in Response to Exercise in Human Skeletal Muscle." Cell Metabolism **25**(2): 301-311.

Grynberg, A. and L. Demaison (1996). "Fatty acid oxidation in the heart." Journal of Cardiovascular Pharmacology **28**: S11-S17.

Gu, J. K., M. Wu, R. Y. Guo, K. G. Yan, J. L. Lei, N. Gao and M. J. Yang (2016). "The architecture of the mammalian respirasome." Nature **537**(7622): 639-+.

Guo, R. Y., S. Zong, M. Wu, J. K. Gu and M. J. Yang (2017). "Architecture of Human Mitochondrial Respiratory Megacomplex I2III2IV2." Cell **170**(6): 1247-1257.

Hansson, A., N. Hance, E. Dufour, A. Rantanen, K. Hultenby, D. A. Clayton, R. Wibom and N. G. Larsson (2004). "A switch in metabolism precedes increased mitochondrial biogenesis in respiratory chain-deficient mouse hearts." Proceedings of the National Academy of Sciences of the United States of America **101**(9): 3136-3141.

Hao, H. X., O. Khalimonchuk, M. Schraders, N. Dephoure, J. P. Bayley, H. Kunst, P. Devilee, C. W. R. J. Cremers, J. D. Schiffman, B. G. Bentz, S. P. Gygi, D. R. Winge, H. Kremer and J. Rutter (2009). "SDH5, a Gene Required for Flavination of Succinate Dehydrogenase, Is Mutated in Paraganglioma." Science **325**(5944): 1139-1142.

Hardie, D. G. (2011). "AMP-activated protein kinase-an energy sensor that regulates all aspects of cell function." Genes & Development **25**(18): 1895-1908.

Harding, H. P., Y. H. Zhang, A. Bertolotti, H. Q. Zeng and D. Ron (2000). "Perk is essential for translational regulation and cell survival during the unfolded protein response." Molecular Cell **5**(5): 897-904.

Hart, L. S., J. T. Cunningham, T. Datta, S. Dey, F. Tameire, S. L. Lehman, B. Qiu, H. Y. Zhang, G. Cerniglia, M. X. Bi, Y. Li, Y. Gao, H. Y. Liu, C. H. Li, A. Maity, A. Thomas-Tikhonenko, A. E. Perl, A. Koong, S. Y. Fuchs, J. A. Diehl, I. G. Mills, D. Ruggero and C. Koumenis (2012). "ER stress-mediated autophagy promotes Myc-dependent transformation and tumor growth." Journal of Clinical Investigation **122**(12): 4621-4634.

Haynes, C. M., K. Petrova, C. Benedetti, Y. Yang and D. Ron (2007). "ClpP mediates activation of a mitochondrial unfolded protein response in C-elegans." Developmental Cell **13**(4): 467-480.

Haynes, C. M., Y. Yang, S. P. Blais, T. A. Neubert and D. Ron (2010). "The Matrix Peptide Exporter HAF-1 Signals a Mitochondrial UPR by Activating the Transcription Factor ZC376.7 in C. elegans." Molecular Cell **37**(4): 529-540.

Hearris, M. A., K. M. Hammond, J. M. Fell and J. P. Morton (2018). "Regulation of Muscle Glycogen Metabolism during Exercise: Implications for Endurance Performance and Training Adaptations." Nutrients **10**(3).

Hinnebusch, A. G. (2011). "Molecular Mechanism of Scanning and Start Codon Selection in Eukaryotes." Microbiology and Molecular Biology Reviews **75**(3): 434-467.

Hong, X. B., Z. L. Yu, Z. L. Chen, H. Y. Jiang, Y. D. Niu and Z. Q. Huang (2018). "High molecular weight fibroblast growth factor 2 induces apoptosis by interacting with

complement component 1 Q subcomponent-binding protein in vitro." Journal of Cellular Biochemistry **119**(11): 8807-8817.

Hopkins, F. G. and E. J. Morgan (1938). "The influence of thiol-groups in the activity of dehydrogenases." Biochem J **32**(3): 611-620.

Horvath, R., A. Abicht, E. Holinski-Feder, A. Laner, K. Gempel, H. Prokisch, H. Lochmuller, T. Klopstock and M. Jaksch (2006). "Leigh syndrome caused by mutations in the flavoprotein (Fp) subunit of succinate dehydrogenase (SDHA)." Journal of Neurology Neurosurgery and Psychiatry **77**(1): 74-76.

Hubley, M. J., R. C. Rosanske and T. S. Moerland (1995). "Diffusion-Coefficients of Atp and Creatine-Phosphate in Isolated Muscle - Pulsed Gradient P-31 Nmr of Small Biological Samples." Nmr in Biomedicine **8**(2): 72-78.

Imai, Y., H. R. Meng, K. Shiba-Fukushima and N. Hattori (2019). "Twin CHCH Proteins, CHCHD2, and CHCHD10: Key Molecules of Parkinson's Disease, Amyotrophic Lateral Sclerosis, and Frontotemporal Dementia." International Journal of Molecular Sciences **20**(4).

Ishii, T., M. Miyazawa, A. Onodera, K. Yasuda, N. Kawabe, M. Kirinashizawa, S. Yoshimura, N. Maruyama, P. S. Hartman and N. Ishii (2011). "Mitochondrial reactive oxygen species generation by the SDHC V69E mutation causes low birth weight and neonatal growth retardation." Mitochondrion **11**(1): 155-165.

Ishizawa, J., S. F. Zarabi, R. E. Davis, O. Halgas, T. Nii, Y. Jitkova, R. Zhao, J. St-Germain, L. E. Heese, G. Egan, V. R. Ruvolo, S. H. Barghout, Y. Nishida, R. Hurren, W. C. Ma, M. Gronda, T. Link, K. Wong, M. Mabanglo, K. Kojima, G. Borthakur, N. MacLean, M. C. J. Ma, A. B. Leber, M. D. Minden, W. Houry, H. Kantarjian, M. Stogniew, B. Raught, E. F. Pai, A. D. Schimmer and M. Andreeff (2019). "Mitochondrial ClpP-Mediated Proteolysis Induces Selective Cancer Cell Lethality." Cancer Cell **35**(5): 721-+.

Jager, S., C. Handschin, J. Pierre and B. M. Spiegelman (2007). "AMP-activated protein kinase (AMPK) action in skeletal muscle via direct phosphorylation of PGC-1 alpha." Proceedings of the National Academy of Sciences of the United States of America **104**(29): 12017-12022.

Jang, J. S., B. K. Park and S. G. Hwang (2000). "Proteolytic Regulation of Retinoblastoma Family Protein p107 by Ubiquitin - proteasome Pathway." J Korean Cancer Assoc **32**(2): 417-421.

Janssen, B. D. and C. S. Hayes (2012). "THE tmRNA RIBOSOME-RESCUE SYSTEM." Advances in Protein Chemistry and Structural Biology, Vol 86 **86**: 151-191.

Kang, G., H. Yun, C. H. Sun, I. Park, S. Lee, J. Kwon, I. Do, M. E. Hong, M. Van Vrancken, J. Lee, J. O. Park, J. Cho, K. M. Kim and T. S. Sohn (2016). "Integrated genomic analyses

identify frequent gene fusion events and VHL inactivation in gastrointestinal stromal tumors." Oncotarget **7**(6): 6538-6551.

Kang, S. G., M. N. Dimitrova, J. Q. Ortega, A. Ginsburg and M. R. Maurizi (2005). "Human mitochondrial ClpP is a stable heptamer that assembles into a tetradecamer in the presence of ClpX." Journal of Biological Chemistry **280**(42): 35424-35432.

Kang, S. G., J. Ortega, S. K. Singh, N. Wang, N. N. Huang, A. C. Steven and M. R. Maurizi (2002). "Functional proteolytic complexes of the human mitochondrial ATP-dependent protease, hClpXP." Journal of Biological Chemistry **277**(23): 21095-21102.

Karalaki, M., S. Fili, A. Philippou and M. Koutsilieris (2009). "Muscle Regeneration: Cellular and Molecular Events." In Vivo **23**(5): 779-796.

Kardon, J. R., Y. Y. Yien, N. C. Huston, D. S. Branco, G. J. Hildick-Smith, K. Y. Rhee, B. H. Paw and T. A. Baker (2015). "Mitochondrial ClpX Activates a Key Enzyme for Heme Biosynthesis and Erythropoiesis." Cell **161**(4): 858-867.

Karnkowska, A., V. Vacek, Z. Zubacova, S. C. Treitli, R. Petrzelkova, L. Eme, L. Novak, V. Zarsky, L. D. Barlow, E. K. Herman, P. Soukal, M. Hroudova, P. Dolezal, C. W. Stairs, A. J. Roger, M. Elias, J. B. Dacks, C. Vlcek and V. Hampl (2016). "A Eukaryote without a Mitochondrial Organelle." Current Biology **26**(10): 1274-1284.

Kato, Y., X. W. Sun, L. X. Zhang and W. Sakamoto (2012). "Cooperative D1 Degradation in the Photosystem II Repair Mediated by Chloroplastic Proteases in Arabidopsis." Plant Physiology **159**(4): 1428-1439.

Katz, A., S. Broberg, K. Sahlin and J. Wahren (1986). "Leg Glucose-Uptake during Maximal Dynamic Exercise in Humans." American Journal of Physiology **251**(1): E65-E70.

Khan, N. A., J. Nikkanen, S. Yatsuga, C. Jackson, L. Y. Wang, S. Pradhan, R. Kivela, A. Pessia, V. Velagapudi and A. Suomalainen (2017). "mTORC1 Regulates Mitochondrial Integrated Stress Response and Mitochondrial Myopathy Progression." Cell Metabolism **26**(2): 419-+.

Kim, K., M. J. Kim, K. H. Kim, S. A. Ahn, J. H. Kim, J. Y. Cho and S. G. Yeo (2017). "C1QBP is upregulated in colon cancer and binds to apolipoprotein A-I." Experimental and Therapeutic Medicine **13**(5): 2493-2500.

King, S. L., C. K. Goth, U. Eckhard, H. J. Joshi, A. D. Haue, S. Y. Vakhrushev, K. T. Schjoldager, C. M. Overall and H. H. Wandall (2018). "TAILS N-terminomics and proteomics reveal complex regulation of proteolytic cleavage by O-glycosylation." Journal of Biological Chemistry **293**(20): 7629-7644.

Kjobsted, R., J. R. Hingst, J. Fentz, M. Foretz, M. N. Sanz, C. Pehmoller, M. Shum, A. Marette, R. Mounier, J. T. Treebak, J. F. P. Wojtaszewski, B. Viollet and L. Lantier (2018). "AMPK in skeletal muscle function and metabolism." Faseb Journal **32**(4): 1741-1777.

Kuhl, I., M. Miranda, I. Atanassov, I. Kuznetsova, Y. Hinze, A. Mourier, A. Filipovska and N. G. Larsson (2017). "Transcriptomic and proteomic landscape of mitochondrial dysfunction reveals secondary coenzyme Q deficiency in mammals." Elife **6**.

Lanner, J. T., D. K. Georgiou, A. D. Joshi and S. L. Hamilton (2010). "Ryanodine Receptors: Structure, Expression, Molecular Details, and Function in Calcium Release." Cold Spring Harbor Perspectives in Biology **2**(11).

Laurenti, G. and D. A. Tennant (2016). "Isocitrate dehydrogenase (IDH), succinate dehydrogenase (SDH), fumarate hydratase (FH): three players for one phenotype in cancer?" Biochemical Society Transactions **44**: 1111-1116.

Lee, S., H. Lee, S. Yoo and H. Kim (2017). "Molecular insights into the m-AAA protease-mediated dislocation of transmembrane helices in the mitochondrial inner membrane." Journal of Biological Chemistry **292**(49): 20058-20066.

Lee, W. J., M. Kim, H. S. Park, H. S. Kim, M. J. Jeon, K. S. Oh, E. H. Koh, J. C. Won, M. S. Kim, G. T. Oh, M. Yoon, K. U. Lee and J. Y. Park (2006). "AMPK activation increases fatty acid oxidation in skeletal muscle by activating PPAR alpha and PGC-1." Biochemical and Biophysical Research Communications **340**(1): 291-295.

Leger, C., K. Heffron, H. R. Pershad, E. Maklashina, C. Luna-Chavez, G. Cecchini, B. A. C. Ackrell and F. A. Armstrong (2001). "Enzyme electrokinetics: Energetics of succinate oxidation by fumarate reductase and succinate dehydrogenase." Biochemistry **40**(37): 11234-11245.

Lemon, P. W. R. and J. P. Mullin (1980). "Effect of Initial Muscle Glycogen Levels on Protein Catabolism during Exercise." Journal of Applied Physiology **48**(4): 624-629.

Lira, V. A., D. L. Brown, A. K. Lira, A. N. Kavazis, Q. A. Soltow, E. H. Zeanah and D. S. Criswell (2010). "Nitric oxide and AMPK cooperatively regulate PGC-1 alpha in skeletal muscle cells." Journal of Physiology-London **588**(18): 3551-3566.

Listrat, A., B. Lebret, #xe9, #xe9, dicte, I. Louveau, T. Astruc, M. Bonnet, L. Lefaucheur, B. Picard, J. Bugeon, #xe9, #xf4 and me (2016). "How Muscle Structure and Composition Influence Meat and Flesh Quality." The Scientific World Journal **2016**: 14.

Liu, P. Y., N. Xu, A. Malyukova, C. J. Scarlett, Y. T. Sun, X. D. Zhang, D. Ling, S. P. Su, C. Nelson, D. K. Chang, J. Koach, A. E. Tee, M. Haber, M. D. Norris, C. Toon, I. Rooman, C. Xue, B. B. Cheung, S. Kumar, G. M. Marshall, A. V. Biankin and T. Liu (2013). "The histone deacetylase SIRT2 stabilizes Myc oncoproteins." Cell Death and Differentiation **20**(3): 503-514.

Liu, Y. C., F. Li, J. Handler, C. R. L. Huang, Y. Xiang, N. Neretti, J. M. Sedivy, K. I. Zeller and C. V. Dang (2008). "Global Regulation of Nucleotide Biosynthetic Genes by c-Myc." Plos One **3**(7).

Lowth, B. R., J. Kirstein-Miles, T. Saiyed, H. Brotz-Oesterhelt, R. I. Morimoto, K. N. Truscott and D. A. Dougan (2012). "Substrate recognition and processing by a Walker B mutant of the human mitochondrial AAA+ protein CLPX." Journal of Structural Biology **179**(2): 193-201.

Marino, G., M. Niso-Santano, E. H. Baehrecke and G. Kroemer (2014). "Self-consumption: the interplay of autophagy and apoptosis." Nature Reviews Molecular Cell Biology **15**(2): 81-94.

Martin, A., T. A. Baker and R. T. Sauer (2008). "Diverse pore loops of the AAA plus ClpX machine mediate unassisted and adaptor-dependent recognition of ssrA-tagged substrates." Molecular Cell **29**(4): 441-450.

Matsushima, Y., Y. Goto and L. S. Kaguni (2010). "Mitochondrial Lon protease regulates mitochondrial DNA copy number and transcription by selective degradation of mitochondrial transcription factor A (TFAM)." Proceedings of the National Academy of Sciences of the United States of America **107**(43): 18410-18415.

Matsushima, Y., Y. Hirofuji, M. Aihara, S. Yue, T. Uchiumi, L. S. Kaguni and D. C. Kang (2017). "Drosophila protease ClpXP specifically degrades DmLRPPRC1 controlling mitochondrial mRNA and translation." Scientific Reports **7**.

Mcgee, A. M. and C. P. Baines (2011). "Complement 1q-binding protein inhibits the mitochondrial permeability transition pore and protects against oxidative stress-induced death." Biochemical Journal **433**: 119-125.

Menssen, A., P. Hydbring, K. Kapelle, J. Vervoorts, J. Diebold, B. Luscher, L. G. Larsson and H. Hermeking (2012). "The c-MYC oncoprotein, the NAMPT enzyme, the SIRT1-inhibitor DBC1, and the SIRT1 deacetylase form a positive feedback loop." Proceedings of the National Academy of Sciences of the United States of America **109**(4): E187-E196.

Michel, A., F. Agerer, C. R. Hauck, M. Herrmann, J. Ullrich, J. Hacker and K. Ohlsen (2006). "Global regulatory impact of ClpP protease of Staphylococcus aureus on regulons involved in virulence, oxidative stress response, autolysis, and DNA repair." Journal of Bacteriology **188**(16): 5783-5796.

Milenkovic, D., S. Matic, I. Kuhl, B. Ruzzenente, C. Freyer, E. Jemt, C. B. Park, M. Falkenberg and N. G. Larsson (2013). "TWINKLE is an essential mitochondrial helicase required for synthesis of nascent D-loop strands and complete mtDNA replication." Human Molecular Genetics **22**(10): 1983-1993.

Millan-Ucles, A., B. Diaz-Castro, P. Garcia-Flores, A. Baez, J. A. Perez-Simon, J. Lopez-Barneo and J. I. Piruat (2014). "A Conditional Mouse Mutant in the Tumor Suppressor SdhD Gene Unveils a Link between p21(WAF1/Cip1) Induction and Mitochondrial Dysfunction." Plos One **9**(1).

Miyazaki, M. and T. Takemasa (2017). "TSC2/Rheb signaling mediates ERK-dependent regulation of mTORC1 activity in C2C12 myoblasts." Febs Open Bio **7**(3): 424-433.

Mounier, R., M. Theret, L. Lantier, M. Foretz and B. Viollet (2015). "Expanding roles for AMPK in skeletal muscle plasticity." Trends in Endocrinology and Metabolism **26**(6): 275-286.

Mourkioti, F. and N. Rosenthal (2005). "IGF-1, inflammation and stem cells: interactions during muscle regeneration." Trends in Immunology **26**(10): 535-542.

Murru, S., S. Hess, E. Barth, E. R. Almajan, D. Schatton, S. Hermans, S. Brodesser, T. Langer, P. Kloppenburg and E. I. Rugarli (2019). "Astrocyte-specific deletion of the mitochondrial m-AAA protease reveals glial contribution to neurodegeneration." Glia **67**(8): 1526-1541.

Na, U., W. D. Yu, J. Cox, D. K. Bricker, K. Brockmann, J. Rutter, C. S. Thummel and D. R. Winge (2014). "The LYR Factors SDHAF1 and SDHAF3 Mediate Maturation of the Iron-Sulfur Subunit of Succinate Dehydrogenase." Cell Metabolism **20**(2): 253-266.

Ngo, J. K., L. C. D. Pomatto and K. J. A. Davies (2013). "Upregulation of the mitochondrial Lon Protease allows adaptation to acute oxidative stress but dysregulation is associated with chronic stress, disease, and aging." Redox Biology **1**(1): 258-264.

Nielsen, J. and N. Ortenblad (2013). "Physiological aspects of the subcellular localization of glycogen in skeletal muscle." Applied Physiology Nutrition and Metabolism **38**(2): 91-99.

Novoa, I., H. Q. Zeng, H. P. Harding and D. Ron (2001). "Feedback inhibition of the unfolded protein response by GADD34-mediated dephosphorylation of eIF2 alpha." Journal of Cell Biology **153**(5): 1011-1021.

Olinares, P. D. B., J. Kim and K. J. van Wijk (2011). "The Clp protease system; a central component of the chloroplast protease network." Biochimica Et Biophysica Acta-Bioenergetics **1807**(8): 999-1011.

Olivares, A. O., H. C. Kotamarthi, B. J. Stein, R. T. Sauer and T. A. Baker (2017). "Effect of directional pulling on mechanical protein degradation by ATP-dependent proteolytic machines." Proceedings of the National Academy of Sciences of the United States of America **114**(31): E6306-E6313.

Ortenblad, N., J. Nielsen, B. Saltin and H. C. Holmberg (2011). "Role of glycogen availability in sarcoplasmic reticulum Ca2+ kinetics in human skeletal muscle." Journal of Physiology-London **589**(3): 711-725.

Ortenblad, N., H. Westerblad and J. Nielsen (2013). "Muscle glycogen stores and fatigue." Journal of Physiology-London **591**(18): 4405-4413.

Oustanina, S., G. Hause and T. Braun (2004). "Pax7 directs postnatal renewal and propagation of myogenic satellite cells but not their specification." EMBO J **23**(16): 3430-3439.

Pakos-Zebrucka, K., I. Koryga, K. Mnich, M. Ljujic, A. Samali and A. M. Gorman (2016). "The integrated stress response." Embo Reports **17**(10): 1374-1395.

Palam, L. R., T. D. Baird and R. C. Wek (2011). "Phosphorylation of eIF2 Facilitates Ribosomal Bypass of an Inhibitory Upstream ORF to Enhance CHOP Translation." Journal of Biological Chemistry **286**(13): 10939-10949.

Paredes, F., K. Sheldon, B. Lassegue, H. C. Williams, E. A. Faidley, G. A. Benavides, G. Torres, F. Sanhueza-Olivares, S. M. Yeligar, K. K. Griendling, V. Darley-Usmar and A. San Martin (2018). "Poldip2 is an oxygen-sensitive protein that controls PDH and alpha KGDH lipoylation and activation to support metabolic adaptation in hypoxia and cancer." Proceedings of the National Academy of Sciences of the United States of America **115**(8): 1789-1794.

Pareek, G. and L. J. Pallanck (2018). "Inactivation of Lon protease reveals a link between mitochondrial unfolded protein stress and mitochondrial translation inhibition." Cell Death & Disease **9**.

Park, J., Y. Chen, D. X. Tishkoff, C. Peng, M. J. Tan, L. Z. Dai, Z. Y. Xie, Y. Zhang, B. M. M. Zwaans, M. E. Skinner, D. B. Lombard and Y. M. Zhao (2013). "SIRT5-Mediated Lysine Desuccinylation Impacts Diverse Metabolic Pathways." Molecular Cell **50**(6): 919-930.

Peng, J., K. Raddatz, S. Labeit, H. Granzier and M. Gotthardt (2005). "Muscle atrophy in titin M-line deficient mice." Journal of Muscle Research and Cell Motility **26**(6-8): 381-388.

Peralta, S., S. Goffart, S. L. Williams, F. Diaz, S. Garcia, N. Nissanka, E. Area-Gomez, J. Pohjoismaki and C. T. Moraes (2018). "ATAD3 controls mitochondrial cristae structure in mouse muscle, influencing mtDNA replication and cholesterol levels." Journal of Cell Science **131**(13).

Pickles, S., P. Vigie and R. J. Youle (2018). "Mitophagy and Quality Control Mechanisms in Mitochondrial Maintenance." Current Biology **28**(4): R170-R185.

Pinti, M., L. Gibellini, M. Nasi, S. De Biasi, C. A. Bortolotti, A. Iannone and A. Cossarizza (2016). "Emerging role of Lon protease as a master regulator of mitochondrial functions." Biochimica Et Biophysica Acta-Bioenergetics **1857**(8): 1300-1306.

Piquereau, J., M. Novotova, D. Fortin, A. Garnier, R. Ventura-Clapier, V. Veksler and F. Joubert (2010). "Postnatal development of mouse heart: formation of energetic microdomains." Journal of Physiology-London **588**(13): 2443-2454.

Piruat, J. I., C. O. Pintado, P. Ortega-Saenz, M. Roche and J. Lopez-Barneo (2004). "The mitochondrial SDHD gene is required for early embryogenesis, and its partial deficiency results in persistent carotid body glomus cell activation with full responsiveness to hypoxia." Molecular and Cellular Biology **24**(24): 10933-10940.

Postic, C. and M. A. Magnuson (2000). "DNA excision in liver by an albumin-Cre transgene occurs progressively with age." Genesis **26**(2): 149-150.

Prudova, A., V. Gocheva, U. A. D. Keller, U. Eckhard, O. C. Olson, L. Akkari, G. S. Butler, N. Fortelny, P. F. Lange, J. C. Mark, J. A. Joyce and C. M. Overall (2016). "TAILS N-Terminomics and Proteomics Show Protein Degradation Dominates over Proteolytic Processing by Cathepsins in Pancreatic Tumors." Cell Reports **16**(6): 1762-1773.

Quiros, P. M., A. Goyal, P. Jha and J. Auwerx (2017). "Analysis of mtDNA/nDNA Ratio in Mice." Curr Protoc Mouse Biol **7**(1): 47-54.

Rahl, P. B., C. Y. Lin, A. C. Seila, R. A. Flynn, S. McCuine, C. B. Burge, P. A. Sharp and R. A. Young (2010). "c-Myc Regulates Transcriptional Pause Release." Cell **141**(3): 432-445.

Rednam, S. P., A. Erez, H. Druker, K. A. Janeway, J. Kamihara, W. K. Kohlmann, K. L. Nathanson, L. J. States, G. E. Tomlinson, A. Villani, S. D. Voss, J. D. Schiffman and J. D. Wasserman (2017). "Von Hippel-Lindau and Hereditary Pheochromocytoma/Paraganglioma Syndromes: Clinical Features, Genetics, and Surveillance Recommendations in Childhood." Clinical Cancer Research **23**(12): E68-E75.

Rendon, O. Z. and E. A. Shoubridge (2018). "LONP1 Is Required for Maturation of a Subset of Mitochondrial Proteins, and Its Loss Elicits an Integrated Stress Response." Molecular and Cellular Biology **38**(20).

Romijn, J. A., E. F. Coyle, L. S. Sidossis, A. Gastaldelli, J. F. Horowitz, E. Endert and R. R. Wolfe (1993). "Regulation of Endogenous Fat and Carbohydrate-Metabolism in Relation to Exercise Intensity and Duration." American Journal of Physiology **265**(3): E380-E391.

Ruzzenente, B., M. D. Metodiev, A. Wredenberg, A. Bratic, C. B. Park, Y. Camara, D. Milenkovic, V. Zickermann, R. Wibom, K. Hultenby, H. Erdjument-Bromage, P. Tempst, U. Brandt, J. B. Stewart, C. M. Gustafsson and N. G. Larsson (2012). "LRPPRC is necessary for polyadenylation and coordination of translation of mitochondrial mRNAs." Embo Journal **31**(2): 443-456.

Sahlin, K., M. Tonkonogi and K. Soderlund (1998). "Energy supply and muscle fatigue in humans." Acta Physiologica Scandinavica **162**(3): 261-266.

Salvi, M., N. A. Morrice, A. M. Brunati and A. Toninello (2007). "Identification of the flavoprotein of succinate dehydrogenase and aconitase as in vitro mitochondrial substrates of Fgr tyrosine kinase." Febs Letters **581**(29): 5579-5585.

Sandri, M., C. Sandri, A. Gilbert, C. Skurk, E. Calabria, A. Picard, K. Walsh, S. Schiaffino, S. H. Lecker and A. L. Goldberg (2004). "Foxo transcription factors induce the atrophy-related ubiquitin ligase atrogin-1 and cause skeletal muscle atrophy." Cell **117**(3): 399-412.

Schafer, E., N. A. Dencher, J. Vonck and D. N. Parcej (2007). "Three-dimensional structure of the respiratory chain supercomplex I1III2IV1 from bovine heart mitochondria." Biochemistry **46**(44): 12579-12585.

Schagger, H. and K. Pfeiffer (2000). "Supercomplexes in the respiratory chains of yeast and mammalian mitochondria." Embo Journal **19**(8): 1777-1783.

Schiaffino, S., V. Hanzlikova and S. Pierobon (1970). "Relations between Structure and Function in Rat Skeletal Muscle Fibers." Journal of Cell Biology **47**(1): 107-+.

Schiaffino, S. and C. Reggiani (2011). "Fiber Types in Mammalian Skeletal Muscles." Physiological Reviews **91**(4): 1447-1531.

Schwaiger, M., E. Rampler, G. Hermann, W. Miklos, W. Berger and G. Koellensperger (2017). "Anion-Exchange Chromatography Coupled to High-Resolution Mass Spectrometry: A Powerful Tool for Merging Targeted and Non targeted Metabolomics." Analytical Chemistry **89**(14): 7667-7674.

Sciacovelli, M., G. Guzzo, V. Morello, C. Frezza, L. Zheng, N. Nannini, F. Calabrese, G. Laudiero, F. Esposito, M. Landriscina, P. Defilippi, P. Bernardi and A. Rasola (2013). "The Mitochondrial Chaperone TRAP1 Promotes Neoplastic Growth by Inhibiting Succinate Dehydrogenase." Cell Metabolism **17**(6): 988-999.

Sebastian, C., B. M. M. Zwaans, D. M. Silberman, M. Gymrek, A. Goren, L. Zhong, O. Ram, J. Truelove, A. R. Guimaraes, D. Toiber, C. Cosentino, J. K. Greenson, A. I. MacDonald, L. McGlynn, F. Maxwell, J. Edwards, S. Giacosa, E. Guccione, R. Weissleder, B. E. Bernstein, A. Regev, P. G. Shiels, D. B. Lombard and R. Mostoslavsky (2012). "The Histone Deacetylase SIRT6 Is a Tumor Suppressor that Controls Cancer Metabolism." Cell **151**(6): 1185-1199.

Seiferling, D., K. Szczepanowska, C. Becker, K. Senft, S. Hermans, P. Maiti, T. Konig, A. Kukat and A. Trifunovic (2016). "Loss of CLPP alleviates mitochondrial cardiomyopathy without affecting the mammalian UPRmt." EMBO Rep **17**(7): 953-964.

Senf, S. M., S. L. Dodd and A. R. Judge (2010). "FOXO signaling is required for disuse muscle atrophy and is directly regulated by Hsp70." American Journal of Physiology-Cell Physiology **298**(1): C38-C45.

Shin, J. Y., M. He, Y. F. Liu, S. Paredes, L. Villanova, K. Brown, X. L. Qiu, N. Nabavi, M. Mohrin, K. Wojnoonski, P. Li, H. L. Cheng, A. J. Murphy, D. M. Valenzuela, H. Z. Luo, P. Kapahi, R. Krauss, R. Mostoslavsky, G. D. Yancopoulos, F. W. Alt, K. F. Chua and D. Chen (2013). "SIRT7 Represses Myc Activity to Suppress ER Stress and Prevent Fatty Liver Disease (vol 5, pg 654, 2013)." Cell Reports **5**(5): 1479-1479.

Skarnes, W. C., B. Rosen, A. P. West, M. Koutsourakis, W. Bushell, V. Iyer, A. O. Mujica, M. Thomas, J. Harrow, T. Cox, D. Jackson, J. Severin, P. Biggs, J. Fu, M. Nefedov, P. J. de Jong, A. F. Stewart and A. Bradley (2011). "A conditional knockout resource for the genome-wide study of mouse gene function." Nature **474**(7351): 337-342.

Smerdu, V., I. Karschmizrachi, M. Campione, L. Leinwand and S. Schiaffino (1994). "Type-Iix Myosin Heavy-Chain Transcripts Are Expressed in Type Iib Fibers of Human Skeletal-Muscle." American Journal of Physiology-Cell Physiology **267**(6): C1723-C1728.

Spinazzi, M., A. Casarin, V. Pertegato, L. Salviati and C. Angelini (2012). "Assessment of mitochondrial respiratory chain enzymatic activities on tissues and cultured cells." Nature Protocols **7**(6): 1235-1246.

Sullivan, L. B., D. Y. Gui, A. M. Hosios, L. N. Bush, E. Freinkman and M. G. Vander Heiden (2015). "Supporting Aspartate Biosynthesis Is an Essential Function of Respiration in Proliferating Cells." Cell **162**(3): 552-563.

Sun, F., X. Huo, Y. J. Zhai, A. J. Wang, J. X. Xu, D. Su, M. Bartlam and Z. H. Rao (2005). "Crystal structure of mitochondrial respiratory membrane protein complex II." Cell **121**(7): 1043-1057.

Sundaresan, N. R., P. Vasudevan, L. Zhong, G. Kim, S. Samant, V. Parekh, V. B. Pillai, P. V. Ravindra, M. Gupta, V. Jeevanandam, J. M. Cunningham, C. X. Deng, D. B. Lombard, R. Mostoslavsky and M. P. Gupta (2012). "The sirtuin SIRT6 blocks IGF-Akt signaling and development of cardiac hypertrophy by targeting c-Jun." Nature Medicine **18**(11): 1643-+.

Sweeney, H. L. (1994). "The Importance of the Creatine-Kinase Reaction - the Concept of Metabolic Capacitance." Medicine and Science in Sports and Exercise **26**(1): 30-36.

Szczepanowska, K., P. Maiti, A. Kukat, E. Hofsetz, H. Nolte, K. Senft, C. Becker, B. Ruzzenente, H. T. Hornig-Do, R. Wibom, R. J. Wiesner, M. Kruger and A. Trifunovic (2016). "CLPP coordinates mitoribosomal assembly through the regulation of ERAL1 levels." EMBO J **35**(23): 2566-2583.

Tatsuta, T. and T. Langer (2008). "Quality control of mitochondria: protection against neurodegeneration and ageing." Embo Journal **27**(2): 306-314.

Tezze, C., V. Romanello, M. A. Desbats, G. P. Fadini, M. Albiero, G. Favaro, S. Ciciliot, M. E. Soriano, V. Morbidoni, C. Cerqua, S. Loefler, H. Kern, C. Franceschi, S. Salvioli, M. Conte, B. Blaauw, S. Zampieri, L. Salviati, L. Scorrano and M. Sandri (2017). "Age-Associated Loss of OPA1 in Muscle Impacts Muscle Mass, Metabolic Homeostasis, Systemic Inflammation, and Epithelial Senescence." Cell Metabolism **25**(6): 1374-+.

Thomson, D. M. (2018). "The Role of AMPK in the Regulation of Skeletal Muscle Size, Hypertrophy, and Regeneration." International Journal of Molecular Sciences **19**(10).

Thunberg, T. (1909). "Studien über die Beeinflussung des Gasaustausches des überlebenden Froschmuskels durch verschiedene Stoffe." Skandinavisches Archiv Für Physiologie **22**(2): 430-436.

Trentini, D. B., M. J. Suskiewicz, A. Heuck, R. Kurzbauer, L. Deszcz, K. Mechtler and T. Clausen (2016). "Arginine phosphorylation marks proteins for degradation by a Clp protease." Nature **539**(7627): 48-+.

Tropeano, C. V., J. Fiori, V. Carelli, L. Caporali, F. Daldal, A. M. Ghelli and M. Rugolo (2018). "Complex II phosphorylation is triggered by unbalanced redox homeostasis in cells lacking complex III." Biochimica Et Biophysica Acta-Bioenergetics **1859**(3): 182-190.

Van Vranken, J. G., D. K. Bricker, N. Dephoure, S. P. Gygi, J. E. Cox, C. S. Thummel and J. Rutter (2014). "SDHAF4 Promotes Mitochondrial Succinate Dehydrogenase Activity and Prevents Neurodegeneration." Cell Metabolism **20**(2): 241-252.

Vass, R. H. and P. Chien (2013). "Critical clamp loader processing by an essential AAA plus protease in Caulobacter crescentus." Proceedings of the National Academy of Sciences of the United States of America **110**(45): 18138-18143.

Venkatesh, S., M. Li, T. Saito, M. M. Tong, E. Rashed, S. Mareedu, P. Y. Zhai, C. Barcena, C. Lopez-Otin, G. Yehia, J. Sadoshima and C. K. Suzuki (2019). "Mitochondrial LonP1 protects cardiomyocytes from ischemia/reperfusion injury in vivo." Journal of Molecular and Cellular Cardiology **128**: 38-50.

Viscomi, C., E. Bottani, G. Civiletto, R. Cerutti, M. Moggio, G. Fagiolari, E. A. Schon, C. Lamperti and M. Zeviani (2011). "In Vivo Correction of COX Deficiency by Activation of the AMPK/PGC-1 alpha Axis." Cell Metabolism **14**(1): 80-90.

Wang, C., Z. J. Tan, B. Niu, K. Y. Tsang, A. Tai, W. C. W. Chan, R. L. K. Lo, K. K. H. Leung, N. W. F. Dung, N. Itoh, M. Q. Zhang, D. Chan and K. S. E. Cheah (2018). "Inhibiting the integrated stress response pathway prevents aberrant chondrocyte differentiation thereby alleviating chondrodysplasia." Elife **7**.

Wang, J. M., H. Wilhelmsson, C. Graff, H. Li, A. Oldfors, P. Rustin, J. C. Bruning, C. R. Kahn, D. A. Clayton, G. S. Barsh, P. Thoren and N. G. Larsson (1999). "Dilated cardiomyopathy and atrioventricular conduction blocks induced by heart-specific inactivation of mitochondrial DNA gene expression." Nature Genetics **21**(1): 133-137.

Wang, X. W., S. J. Hu and L. Liu (2017). "Phosphorylation and acetylation modifications of FOXO3a: Independently or synergistically?" Oncology Letters **13**(5): 2867-2872.

Warburg, O., F. Wind and E. Negelein (1927). "The Metabolism of Tumors in the Body." J Gen Physiol **8**(6): 519-530.

Wei, Y. H., R. N. Vellanki, E. Coyaud, V. Ignatchenko, L. Li, J. R. Krieger, P. Taylor, J. F. Tong, N. A. Pham, G. Liu, B. Raught, B. G. Wouters, T. Kislinger, M. S. Tsao and M. F. Moran (2015). "CHCHD2 Is Coamplified with EGFR in NSCLC and Regulates Mitochondrial Function and Cell Migration." Molecular Cancer Research **13**(7): 1119-1129.

Weisend, C. M., J. A. Kundert, E. S. Suvorova, J. R. Prigge and E. E. Schmidt (2009). "Cre Activity in Fetal albCre Mouse Hepatocytes: Utility for Developmental Studies." Genesis **47**(12): 789-792.

Winn, N., A. Paul, A. Musaro and N. Rosenthal (2002). "Insulin-like growth factor isoforms in skeletal muscle aging, regeneration, and disease." Cold Spring Harbor Symposia on Quantitative Biology **67**: 507-518.

Wittig, I., H. P. Braun and H. Schagger (2006). "Blue native PAGE." Nat Protoc **1**(1): 418-428.

Wittig, I., M. Karas and H. Schagger (2007). "High resolution clear native electrophoresis for in-gel functional assays and fluorescence studies of membrane protein complexes." Mol Cell Proteomics **6**(7): 1215-1225.

Wolfe, R. R. (2006). "The underappreciated role of muscle in health and disease." American Journal of Clinical Nutrition **84**(3): 475-482.

Wredenberg, A., R. Wibom, H. Wilhelmsson, C. Graff, H. H. Wiener, S. J. Burden, A. Oldfors, H. Westerblad and N. G. Larsson (2002). "Increased mitochondrial mass in mitochondrial myopathy mice." Proceedings of the National Academy of Sciences of the United States of America **99**(23): 15066-15071.

Wu, M., J. K. Gu, R. Y. Guo, Y. S. Huang and M. J. Yang (2016). "Structure of Mammalian Respiratory Supercomplex I1III2IV1." Cell **167**(6): 1598-+.

Yagi, M., T. Uchiumi, N. Sagata, D. Setoyama, R. Amamoto, Y. Matsushima and D. Kang (2017). "Neural-specific deletion of mitochondrial p32/C1qbp leads to leukoencephalopathy due to undifferentiated oligodendrocyte and axon degeneration." Scientific Reports **7**.

Yagi, M., T. Uchiumi, S. Takazaki, B. Okuno, M. Nomura, S. Yoshida, T. Kanki and D. Kang (2012). "p32/gC1qR is indispensable for fetal development and mitochondrial translation: importance of its RNA-binding ability." Nucleic Acids Research **40**(19): 9717-9737.

Yatscoff, M. A., J. S. Jaswal, M. R. Grant, R. Greenwood, T. Lukat, D. L. Beker, I. M. Rebeyka and G. D. Lopaschuk (2008). "Myocardial Hypertrophy and the Maturation of Fatty Acid Oxidation in the Newborn Human Heart." Pediatric Research **64**(6): 643-647.

Yu, J. S. L. and W. Cui (2016). "Proliferation, survival and metabolism: the role of PI3K/AKT/mTOR signalling in pluripotency and cell fate determination." Development **143**(17): 3050-3060.

Yuan, J., K. Minter-Dykhouse and Z. K. Lou (2009). "A c-Myc-SIRT1 feedback loop regulates cell growth and transformation." Journal of Cell Biology **185**(2): 203-211.

Zhang, X. F., F. Zhang, L. Guo, Y. P. Wang, P. Zhang, R. R. Wang, N. Zhang and R. B. Chen (2013). "Interactome Analysis Reveals that C1QBP (complement component 1, q subcomponent binding protein) Is Associated with Cancer Cell Chemotaxis and Metastasis." Molecular & Cellular Proteomics **12**(11): 3199-3209.

Zhong, L., A. D'Urso, D. Toiber, C. Sebastian, R. E. Henry, D. D. Vadysirisack, A. Guimaraes, B. Marinelli, J. D. Wikstrom, T. Nir, C. B. Clish, B. Vaitheesvaran, O. Iliopoulos, I. Kurland, Y. Dor, R. Weissleder, O. S. Shirihai, L. W. Ellisen, J. M. Espinosa and R. Mostoslavsky (2010). "The Histone Deacetylase Sirt6 Regulates Glucose Homeostasis via Hif1 alpha." Cell **140**(2): 280-293.

Zou, J. R., T. T. Lei, P. Guo, J. S. Yu, Q. C. Xu, Y. F. Luo, R. Ke and D. Q. Huang (2019). "Mechanisms shaping the role of ERK1/2 in cellular senescence." Molecular Medicine Reports **19**(2): 759-770.

Acknowledgement

This thesis would not have been possible without the help and support of numerous people within and outside of the lab, before and during my time as a PhD student. It is beyond the scope of this acknowledgement to thank each and every one who affected me or my thesis during that time, but I want to highlight a few I will forever connect to this thesis.

First and foremost, I want to thank you, Prof. Dr. Aleksandra “Sandra” Trifunovic for the opportunity to work on these projects. I joined the lab 5 years ago as a young Master student and I can look back on a wonderful time, in which I was given the freedom to pursue my scientific and personal development. I truely admire your kindness, generosity and passion that you demonstrated on countless occasions.

Thank you, Prof. Dr. Thomas Langer for being a member of my thesis committee and for your valuable advise during WIPs and several yearly reports.

Thank you, Prof. Dr. Jan Riemer for being the chair of my thesis committee.

Thank you, PD Dr. Tamara Gigolashvili for your mentoring and support during the earliest steps of my scientific career.

Thank you, Alexandra “Alex” Kukat for your great help in the lab, for your constant input and feedback on my work. For the uncountable hours of lunch and coffee time that were full of laughter, joy and a bit of science talk. It was a pleasure and great support to have a like-minded scientist like you on my side.

Thank you, Sophie Kaspar for being a friend and colleague to me who always had a few minutes to discuss my projects and was never short of a good idea.

Thank you, Karolina for your mentoring during my Masters and for the time and effort you put into me and the CLPP project.

Thank you, Katha and Linda for your help around the lab and the time we had together.

Thank you, all other former and current members of the Trifunovic lab for your support, expertise and time I could spend with you. Being part of such a great lab was one of the best parts I will remember about this PhD.

Vielen Dank Mama, Papa und Hermann für eure Unterstützung. Ihr wart mein ganzes Leben lang für mich da und ich konnte immer auf euch zählen.

Und vor allem, *Cosima*.
Vielen Dank für deine Unterstützung vom ersten bis zum letzten Tag! Für deine Liebe, Geduld und Hilfe. Ich bin so glücklich darüber, dass du an meiner Seite bist und freue mich auf den nächsten Abschnitt unseres Lebens.

Erklärung

Ich versichere, dass ich die von mir vorgelegte Dissertation selbstständig angefertigt, die benutzten Quellen und Hilfsmittel vollständig angegeben und die Stellen der Arbeit – einschließlich Tabellen, Karten und Abbildungen -, die anderen Werken im Wortlaut oder dem Sinn nach entnommen sind, in jedem Einzelfall als Entlehnung kenntlich gemacht habe; dass die Dissertation noch keiner anderen Fakultät oder Universität zur Prüfung vorgelegen hat; dass sie – abgesehen von unten angegebenen Teilpublikationen – noch nicht veröffentlicht worden ist sowie, dass ich eine solche Veröffentlichung vor Abschluss des Promotionsverfahrens nicht vornehmen werde.
Die Bestimmungen der Promotionsordnung sind mir bekannt. Die von mir vorgelegte Dissertation ist von Prof. Dr. Aleksandra Trifunovic betreut worden.

Köln, den 10.01.2020

_____

Eduard Hofsetz